UNIVERSITY OF LIVERPOOL

Structure-Property Relationships in Molecular Junctions

Thesis submitted in accordance with the requirements of the University of Liverpool for the Degree of Doctor of Philosophy by

Jonathan Welsh

March 2023

Abstract

Jonathan Welsh: **Structure-Property Relationships in Molecular Junctions**

The growth of the field of molecular electronics from initial theoretical proposals for molecule-based devices to the development of experimental techniques for measuring the electrical conductance of individual molecules indicates the research interest in exploiting the unique capabilities of molecules for electronic device applications. Progress in this field is dependent on gaining knowledge and understanding of how tuning molecular structure influences charge transport behaviour to enable identification of compounds with suitable characteristics for different device functions.

This thesis investigates relationships between molecular structure and electrical properties in molecular junctions and aims to gain insight into how structural alterations in closely related molecules can lead to significant differences in charge transport behaviour. Particular emphasis is placed on exploring how molecular conductance can be controlled by quantum interference effects inherent to the small dimensions of molecules, which can lead to large changes in conductance, and anchoring groups, which control the molecule-electrode interface properties. The novel aspects of this work involve investigating the effect of changing structural features on charge transport properties in different series of molecules and explaining the behaviour observed for these compounds.

The first series of experiments focuses on the influence of interference effects on the electrical properties of pyridine-terminated molecular wires. This section explores the effect of changing the pyridyl anchoring site positions on molecular conductance. The target molecules have been synthesised via cross-coupling reactions and the experimental results compared with theoretical transmission calculations. The measurements show that changing the pyridine anchoring site positions does not lead to the large variations in conductance predicted by theory, which is attributed to the metal-molecule orbital alignment of the molecular junctions.

The second series of experiments focuses on the influence of destructive interference effects on the electrical properties of fluorene-derived molecular wires. This section explores how the addition of cross-conjugated ketone moieties to a linearly conjugated core unit affects the molecular conductance. The results indicate that the presence of cross-conjugated carbonyl groups leads to a decrease in conductance, as the cross-conjugated molecules display lower conductance values, supporting predictions of destructive interference behaviour.

The third series of experiments investigates the electrical properties of two molecules with multidentate 1,2,4-triazolyl anchoring groups. These molecules possess a simple core structure, allowing the influence of the novel bidentate anchoring moieties on the conductance properties to be assessed. The experiments indicate that 1,2,4-triazole can function as an anchoring group, as the results show that both structures form stable molecular junctions which display consistent conductance features, albeit with relatively low molecular conductance values.

Table of Contents

List of Abbreviations

CP-AFM	Conducting Probe-Atomic Force Microscopy
CQI	Constructive Quantum Interference
DBU	1,8-diazabicyclo[5.4.0]undec-7-ene
DETB	1,4-bis(3,5-diethyl-4H-1,2,4-triazol-4-yl)benzene
DFT	Density Functional Theory
DMSO	Dimethyl Sulfoxide
DMTB	1,4-bis(3,5-dimethyl-4H-1,2,4-triazol-4-yl)benzene
DOS	Density of States
DPP	Diketopyrrolopyrrole
DQI	Destructive Quantum Interference
E_F	Fermi Energy
GNP	Gold Nanoparticle
HOMO	Highest Occupied Molecular Orbital
HRMS	High Resolution Mass Spectrometry
LUMO	Lowest Unoccupied Molecular Orbital
MCBJ	Mechanically Controlled Break Junction
MMI	Monolayer Matrix Isolation
NEGF	Non-equilibrium Green's Function
NMR	Nuclear Magnetic Resonance
OPE	Oligo(phenyleneethynylene)
OPV	Oligo(phenylenevinylene)
QI	Quantum Interference
QTOF-MS	Quadrupole Time-of-Flight-Mass Spectrometry
SAM	Self-Assembled Monolayer
SPM	Scanning Probe Microscopy
STM	Scanning Tunnelling Microscopy
STM-BJ	Scanning Tunnelling Microscopy-Break Junction
TBPT	4,4′-bis(5-(methylthio)thiophen-2-yl)-1,1′-biphenyl
TDO	Thiophene-S,S-dioxide

TFA	Trifluoroacetic acid
TFLT	2,7-bis(5-(methylthio)thiophen-2-yl)-9H-fluorene
TFOT	2,7-bis(5-(methylthio)thiophen-2-yl)-9H-fluoren-9-one
TMS	Tetramethylsilane
TPDOT	2,7-bis(5-(methylthio)thiophen-2-yl)-phenanthrene-9,10-dione

Chapter 1: Introduction

1.1 Introduction to Key Concepts in Molecular Electronics

The field of molecular electronics is an interdisciplinary branch of nanotechnology which involves the use of molecules as functional components in electronic circuits. This includes the measurement of the electrical properties of individual molecules and nanoscale molecular assemblies (typically in the 1-4 nm length range) and their applications as electronic device components.[1] In this regard, molecular electronics has several similarities with the more established field of organic electronics, which also investigates the electrical properties of organic materials with the aim of utilising these materials as electronic device components.[2] However, whereas organic electronics focuses on the bulk properties of longer conductive organic polymers, which are measured and observed on the macroscopic scale, molecular electronics investigates the fundamental properties of molecules at nanoscale level. Work in this field uses a combination of experimental and theoretical approaches to determine the properties of molecular wires, with a particular emphasis on investigating the charge transport characteristics, including the energy separation between the electrode Fermi level (E_F) and the energy levels of the molecular orbitals, the molecule-electrode coupling interface and the inherent functionality of the molecules.[3] These studies are performed with the aim of utilising the properties of molecular wires attached to two or more electrodes in order to design and construct components which can perform useful functions in electronic devices.[4] The use of molecules as active electronic components is highly promising as it has the potential to not only emulate existing solid-state electronic devices but could also lead to new technological possibilities beyond the scope of current approaches.[1,5]

In 1965, less than a decade after the invention of the integrated circuit, the research director of Fairchild Semiconductor Gordon Moore predicted that the number of transistors on a microprocessor chip would approximately double every two years.[6] This forecast, widely referred to as Moore's law, provided an accurate prediction of the development of Si-based electronic devices for the majority of the next five decades and became a self-imposed target for the semiconductor industry. This enabled the continuous miniaturisation of electronic device components, which has resulted in an exponential increase in device performance and complexity. In more recent years, however, the miniaturisation of electronic devices has reached the limits of traditional Si-based circuit integration as transistor sizes have approached atomic dimensions. Further reductions in size with the present technology beyond this scale would lead to excessive loss of current in the form of heat energy via off-state leakage.[7] These limits mean there is diminishing scope for further reduction of component sizes and as a

consequence there is increasing interest in finding alternative methods of improving device performance to meet the continuing demand for increased computer processing power.

The possibility of advancing molecular electronics is therefore of great interest, particularly as the development of several experimental techniques in the late 1990s and early 2000s has made it feasible to investigate the electrical properties of small numbers of molecules at the nanometre scale.[8,9,10] These studies may be performed with a view to the potential deployment of molecules in electronic devices, which can be seen as the ultimate miniaturisation of electronic components. The use of single molecule-based electronics would represent a 'bottom up' approach which would allow the limitations of existing Si-based circuit integration methods inherent to a 'top down' approach to be overcome. The minimal size of molecules could also offer further improvements compared to existing approaches by enabling greater functionalisation of electronic devices and delivering improved device performance. The use of molecular electronic approaches could enable the development of many new functionalities which exploit the unique characteristics of molecules and cannot be achieved using existing Si-based methods, representing a significant expansion of the overall electronics 'toolkit'.[5]

Other advantages of using individual molecules as components in electronic devices include highly flexible synthetic pathways and the inherently wide range of molecular structures, as molecules represent the smallest individual units capable of displaying wide ranging structural variations. This allows a broad range of properties to be tuned and the influence of different effects to be investigated. For studies focusing on individual small molecules, this is particularly interesting, as this includes properties intrinsic to the molecular scale which are not observed in larger components. Molecular electronic devices are still in an early stage of development, and there are significant technological barriers and fundamental issues which must be overcome before the potential of molecules in electronics applications can be fully realised and their use can become widespread. Most notably, in contrast to traditional Si-based semiconductor fabrication, there is currently no standard, reproducible method for molecular electronic device fabrication.[11] However, in recent decades, single molecule electronic devices have been constructed which have demonstrated similar behaviour to semiconductor-based devices, including switches,[12] transistors[13] and diodes.[14] The first commercially available molecular electronic devices became available in 2016 with the marketing of audio processing circuits incorporating components based on individual molecules.[15]

One of the most important concepts in molecular electronics is the metal-molecule-metal junction, often referred to as a molecular junction. A single molecule junction consists of three components: the electrode contacts, the molecular wire and the molecule-electrode interface (Figure 1.1). The molecule is attached to the electrode contacts via molecular moieties known as anchoring groups, allowing the molecule to conduct electrical current between the electrodes.[16]

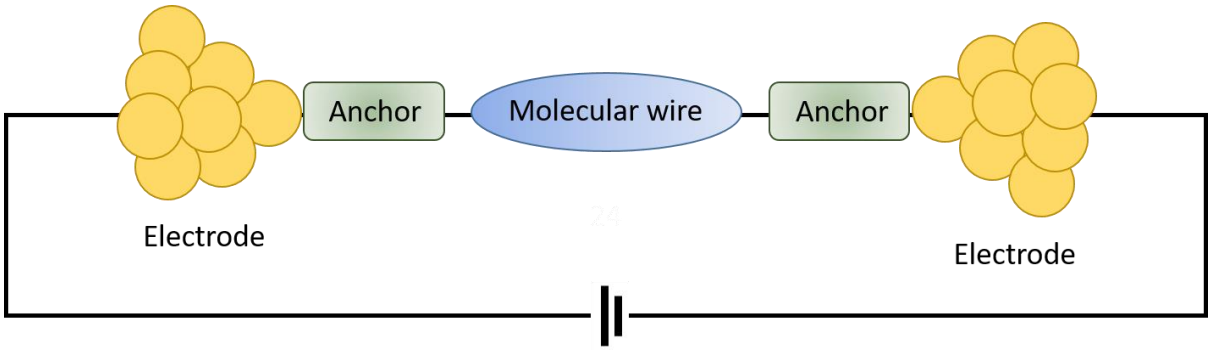

Figure 1.1. Simplified schematic showing the major components of a molecular junction, comprising the molecular wire, the metallic electrodes and the molecule-electrode interface (anchoring groups).

Obtaining a comprehensive understanding of the charge transport properties in molecular junctions and the role of structure-property relationships in determining the charge transport behaviour is of crucial importance for developing novel organic materials for applications in molecular electronic devices.[1] Metal-molecule-metal junctions provide an ideal platform for investigating these relationships as they enable precise tuning of the junction characteristics at the molecular scale, which can be used to control charge transport behaviour. However, clear rational design principles are required for the incorporation of molecular structures with appropriate features and properties in molecular junctions to enable the fabrication of practical devices which perform desirable functions with controllable behaviour. A combination of theoretical calculations and experimental studies can be used to determine the intrinsic charge transport properties of molecules in molecular junctions and establish the relationship between electronic structure and molecular conductance.[3]

The first reproducible molecular conductance study was the electrical characterisation of organic monolayers of long-chain fatty acids described by Kuhn and Mann in 1971.[17] This study used self-assembly techniques to attach the target molecules to solid substrates, thus permitting the direct measurement of charge transport through the molecules. However, the

most significant early development in this field was the Aviram-Ratner molecular diode (1974), a theoretical proposal which suggested that a molecular rectifier could be created by placing an individual molecule with distinct electron donor and acceptor groups separated by a short non-conjugated bridge between a pair of metallic electrodes.[4] It was proposed that this would allow one-way electrical conduction through the molecule when a bias voltage was applied, with the non-conjugated linker effectively preventing interaction between the energy levels of the electron donor and acceptor units. They predicted that this alignment of the molecular orbitals would lead to rectification as it would enable high current flow in the forward direction but only limited current flow in the reverse direction. This work was highly influential in popularising the idea of using molecules as electronic components and has inspired much subsequent research into exploring the possibilities of using molecules as functional components in electronic circuits.

One of the main advantages of the single molecule junction approach is the inherent flexibility resulting from the extremely wide range of possible molecular structures. However, molecular electronics studies tend to focus primarily on the properties of relatively short oligomeric π-conjugated molecular wires and this is because these structures facilitate efficient charge transport through the molecular junction.[18,19] By contrast, non-conjugated structures display less efficient charge transport and hence give significantly lower conductance values compared to equivalent conjugated molecules.[20] The properties of larger molecular structures have been less widely studied as they are unlikely to be feasible candidates for applications in nanoscale electronic devices, which typically require small component sizes. Molecular wires based on a small number of repeating units, which may be accessed via flexible chemical synthesis approaches, are ideal candidates for investigating the relationships between molecular structure and charge transport behaviour.[19] This is because experimental work focusing on the influence of molecular length on charge transport behaviour through metal-molecule-metal junctions has shown that the charge transport mechanism is controlled by the molecular length.[21]

1.2 Charge Transport and Electronic Transmission

Gaining a thorough understanding of charge transport through single molecule junctions is of pivotal importance for the development of molecule-based electronic devices. Charge transport through single molecule junctions is quantum mechanical in nature and thus displays several differences from charge transport in bulk materials. Electron transport through molecular

junctions can occur via two distinct mechanisms, coherent tunnelling and sequential hopping.[1] The first mechanism is the coherent tunnelling pathway, where electron transfer occurs in a single step via propagation through an energy barrier (i.e. the gap between the electrode contacts). This behaviour violates the laws of classical mechanics, but the nanoscale dimensions and wave-particle duality of electrons permit quantum tunnelling of the electron through the barrier without overcoming the energy barrier. In this mechanism, the electron does not localise on the molecule and therefore maintains phase information during transport. The tunnelling pathway is typically observed in short molecules (length < 5 nm), is characterised by rapid charge transport and the molecular conductance is independent of temperature.[22] The second transport mechanism is the sequential hopping pathway, which is an incoherent process where electron transfer between the electrodes occurs via a series of discrete steps across the orbitals of the molecular wire. As this involves the injection and localisation of the electron on the molecular orbitals of the bridging molecule, the electron loses phase information during transport. This usually occurs in longer molecules (length > 5 nm) where charge transport is slower and the conductance increases with increasing temperature.[19] The molecular wires studied in this project have theoretically predicted lengths shorter than 2 nm and it is therefore expected that charge transport through these molecules will occur via the tunnelling pathway.

One of the most fundamental properties of a molecule in a molecular junction is the conductance (G), which describes the ability of the molecule to conduct an electrical current. The molecular conductance is recorded by directly measuring the current (I) through the molecule as a function of the voltage (V) applied between the two electrodes and can be expressed by the equation:

$$G(V) = \frac{I(V)}{V} \quad (1)$$

The scaling of conductance with molecular length is considered a fundamental property of a molecular wire and provides insight into the charge transport mechanism. For molecular wires which transport charge via the coherent tunnelling pathway, the conductance decreases exponentially with increasing molecular length, as described by the relationship:

$$G = A\, exp(-\beta_N L) \quad (2)$$

A is a constant describing the molecule-electrode contact resistance, L is the molecular length and β_N is the tunnelling decay constant, a measure of the electron transport efficiency of the molecule (the value of β_N is dependent on the molecular structure, with smaller values

indicating more efficient transport). This relationship agrees with the experimental observation that increasing the length of the molecular wire leads to a decrease in charge transport efficiency across the molecular junction and in turn lowers the molecular conductance.[23]

The conductance also displays a negative correlation with molecular length for molecules which conduct via the sequential hopping pathway. However, the length dependence of the hopping charge transport mechanism is weaker as the decrease in conductance with increasing length is linear rather than exponential. The relationships between molecular length and conductance for the two charge transport mechanisms are consistent with results from experimental conductance measurements, which have shown that shorter molecular wires (which conduct via the tunnelling mechanism) display highly length dependent charge transport behaviour, whereas charge transport in longer molecules (which conduct via the hopping mechanism) is weakly length dependent.[24]

In addition to the different relationships between molecular length and conductance decay, the temperature dependence represents another significant difference between the two charge transport mechanisms. It is also significant that the incoherent hopping mechanism is thermally activated and the conductance of molecules which conduct via this pathway is therefore temperature dependent. The temperature dependence of the molecular conductance in the hopping charge transport mechanism follows an Arrhenius relationship and is described by the equation:

$$G \propto exp\left(\frac{-E_A}{K_B T}\right) \quad (3)$$

In this equation, E_A represents hopping activation energy, K_B represents the Boltzmann constant and T represents temperature. The most significant implication of this relationship is that for molecules which conduct via the hopping mechanism the molecular conductance is expected to increase with increasing temperature, in contrast to the temperature independent coherent tunnelling mechanism. This has been supported by experimental measurements which show that the conductance of longer molecular wires increases on raising the temperature, as it has been demonstrated that molecules which conduct via the hopping mechanism can display higher conductance values at elevated temperatures compared to analogous shorter molecules which conduct via the tunnelling mechanism. This differs from the behaviour observed at lower temperatures where the hopping charge transport pathway is less efficient and therefore the longer molecules which conduct via the hopping mechanism give lower conductance values.[24]

For a single molecule junction with a molecular wire bound to one dimensional electrode leads in the weak coupling limit, the molecular conductance can also be expressed by the following relationship:

$$G \propto \frac{2e^2}{h} T_L T_R T_{mol} \quad (4)$$

In this equation, e is the electron charge, h represents Planck's constant, while T_L, T_R and T_{mol} denote electronic transmission through the left molecule-electrode interface, right molecule-electrode interface and molecular wire, respectively. This formula can be simplified by grouping T_L, T_R and T_{mol} together to give $T(E_F)$, known as the transmission coefficient. This term refers to the electronic transmission function at the electrode Fermi Energy (E_F) and represents the probability of the transmission of electrons from one electrode to the other via the molecular junction. At the nanoscale, the conductance is quantised, which allows the quantum mechanical constants e and h to be combined to give the term G_0. This term is known as the conductance quantum and can be used in place of $2e^2/h$. In this form, this equation is called the Landauer formula:

$$G = G_0 T(E_F) \quad (5)$$

If the coupling between the leads and molecule is not too strong, then if E_F is close to a molecular energy level E_0, the transmission coefficient can be described using the single level model, which models a molecule-electrode contact as a single electronic level according to the equation:

$$T(E_F) = \frac{4\Gamma_L \Gamma_R}{(E_F - E_0)^2 + (\Gamma_L + \Gamma_R)^2} \quad (6)$$

Γ_L and Γ_R denote the strength of the coupling between the molecule and the left and right electrodes, and E_0 is the energy of the single level. The above equations illustrate that several factors can affect the conductance of a molecular junction. The influence of these factors on the molecular conductance is explained in further detail in the next section.

1.3 Factors Influencing Single Molecule Conductance

The ability to gain reliable and quantitative insight into structure-property relationships in single molecule junctions is of fundamental importance to the field of molecular electronics. The electronic conductance of a molecular junction is known to be affected by a number of

molecular features, including the extent of conjugation,[25] the anchoring groups[20] and the conformation of the molecule in the molecular junction.[26] However, one significant implication of the equation for determining the transmission coefficient (Equation 6) is that the conductance of a molecular junction is dependent on the properties of the electrode materials and the molecule-electrode interface in addition to the intrinsic properties of the molecular wire.[27] This means that variations in the electrode-anchoring group binding geometry and the strength of coupling between the molecule and electrodes can cause a molecular junction to display different conductance values. Therefore, in order to accurately measure the charge transport properties of molecules in molecular junctions, molecular conductance measurements must be performed in a well-defined environment (in air or in solution) to minimise the impact of external conditions on the electrical properties of the molecule. This section explores the influence of various features of a metal-molecule-metal junction on the overall conductance of the molecular junction.

1.3.1 Influence of Electrodes on Molecular Conductance

One of the most significant implications of the Landauer formula (Equation 5) for molecular junction design is that the choice of electrode material influences the molecular conductance. This is important because the Landauer formula indicates that electronic transmission is strongly dependent on the height of the tunnelling barrier between the electrode E_F and the molecular energy levels, and charge transport efficiency decreases as the energy separation between the molecular energy levels and the metallic E_F increases.[28] This means that the position of the metallic E_F plays an important role in determining the molecular conductance.

The most widely used electrode material in single molecule conductance studies is the noble metal gold (Au), which is favoured as it is malleable, an excellent electrical conductor and insensitive to oxidation under ambient conditions, making it highly suitable for obtaining reproducible conductance measurements.[8,9,10] The inertness of Au is a major advantage as the formation of oxide layers on electrode surfaces can prevent molecular junction formation. However, other transition metals have also been employed as electrode materials in single molecule conductance experiments, including Cu,[29] Ag,[29] Pd[30] and Pt.[31] These studies have shown that changing the metal used in metal-molecule-metal junctions provides a method of adjusting the energy level alignment between the metal E_F and frontier molecular orbitals. This is because different metals have different work functions and this in turn affects the contact resistance and the strength of molecule-electrode coupling.[31,32] For example, Kim *et al*. reported that molecular junctions with Au electrodes display higher conductance values than

equivalent junctions with Ag electrodes for both oligophenyl and alkane molecules. This is consistent with the higher work function of Au compared to Ag and is supported by theoretical transmission calculations which predict a higher contact resistance and weaker molecule-electrode coupling for junctions with Ag electrodes than with Au electrodes.[33]

Changing the electrode material also affects the density of states (DOS) of the metallic electrode at E_F, which has significant implications as experimental conductance measurements have demonstrated that the electrode DOS strongly influences the molecular junction conductance. For example, the measured conductance of 4,4′-bipyridine has been reported to be an order of magnitude higher in molecular junctions with Au electrodes compared to junctions with Ag electrodes. This difference is explained by the larger density of d-electron states of Au electrodes at energy values close to E_F compared to Ag electrodes in the same energy range, which leads to stronger molecule-electrode coupling and therefore enhances electronic transmission through the molecular junction for Au-molecule-Au junctions.[34] Using different electrode materials also influences the formation and evolution of molecular junctions. It has been demonstrated that molecular junctions formed with Ag electrodes can be elongated by longer distances than junctions with Au electrodes, which has been attributed to the smaller initial gap formed between the electrodes in Ag-molecule-Ag junctions. Also, the molecule-electrode coupling in molecular junctions with Ag electrodes is more sensitive to the binding geometry, resulting in a broader range of conductance values than for analogous junctions with Au electrodes.[33]

Additionally, the application of a bias voltage across the molecular junction electrodes provides another approach for changing the position of the electrode E_F relative to the molecular orbitals. This influences the probability of charge transport through the junction, resulting in a change in molecular conductance. The observed response is dependent on whether the applied bias causes the molecular orbitals to move closer in energy to E_F, which increases the conductance, or further away from E_F, which lowers the conductance.[35] This illustrates that the alignment of the metallic E_F with the molecular orbitals also plays a significant role in controlling electronic transmission through molecular junctions. This leads on to the influence of the molecule-electrode interface on the molecular conductance, which is discussed in the following section.

1.3.2 Influence of Anchoring Groups on Molecular Conductance

An anchoring group (also referred to as a contact group) can be defined as the atoms or functional groups at the end of the molecular wire which bind the molecule to the electrodes.

Molecular anchoring groups have two primary functions, one of which is to enable molecules to be reproducibly wired into nanoscale metal-molecule-metal junctions with high mechanical stability. In addition to providing a platform for strong molecule-electrode binding, however, the anchoring groups are also responsible for electronically coupling molecular wires with metallic electrodes and thus allowing charge transport through the junction. This is important because the anchoring groups also influence the energy levels of the frontier molecular orbitals (the highest occupied molecular orbital (HOMO) or lowest unoccupied molecular orbital (LUMO)). As the metallic electrode E_F is typically located in the HOMO-LUMO gap of a molecular junction, the molecule-electrode coupling efficiency is directly affected by the position of the frontier molecular orbital energy levels relative to the metallic E_F. This means that the electronic transmission efficiency is dependent on the molecule-electrode coupling strength and as a consequence the single molecule conductance is controlled by the alignment of the frontier orbitals with the electrodes.[36]

The single level model (equation 6) also assumes that electronic transmission through the molecular junction predominantly occurs via a single energy level. Transmission through molecular junctions is typically dominated by the frontier molecular orbitals (HOMO and LUMO) with transmission preferentially occurring via the orbital closest in energy to the electrode E_F. In molecules with HOMO-dominated transmission pathways, holes are the main charge carriers, whereas in structures with LUMO-dominated transmission pathways electrons are the primary charge carriers. The energy separation between the dominant conducting frontier orbital and E_F, sometimes referred to as the injection energy, has significant implications for the design of molecular wires. The anchoring groups play a key role in determining the primary charge transport pathway through the molecular wire because the molecule-electrode contact groups present a significant barrier to charge injection into the molecular junction. This implies that changing the anchoring group can fundamentally alter the electronic structure and properties of the molecular junction. This has been demonstrated by Tan *et al*., who measured the electric and thermoelectric properties of a series of closely related aromatic molecules with either thiol or isonitrile terminal groups. They found that the thiol-terminated molecules displayed hole-dominated charge transport via the HOMO, whereas the isonitrile-terminated compounds displayed electron-dominated charge transport via the LUMO.[37] This showed that changing the anchoring group can cause the main conductance pathway to switch from HOMO transport to LUMO transport (or vice versa) in analogous molecular wires.

In a molecular junction, high electronic transmission is dependent on strong, well-defined coupling between the molecule and electrodes and the conductance of the molecular junction is therefore correlated with the strength of the molecule-electrode coupling.[20] This implies that anchoring groups play an important role in determining the overall electrical conductance of the junction. The significance of the contacting groups in molecular junctions is reflected in the wide range of anchoring moieties that have been used in molecular electronics studies (Scheme 1.1), including functional groups such as thiols (-SH),[38] amines (-NH_2),[20] pyridines (-C_5H_5N),[39] methyl thioethers (-SCH_3),[40] methyl phosphines (-$P(CH_3)_2$),[40] nitriles (-CN),[41] isocyanides (-NC),[19] selenols (-SeH),[42] carboxylic acids (-COOH)[28] and fullerenes (-C_{60}).[43] The popularity of sulfur-based and nitrogen-based anchoring groups can be attributed to the presence of a lone pair on the central atom, which can readily bind to metallic electrodes to form stable molecular junctions.

Scheme 1.1. Examples of anchoring groups used in molecular electronics studies, where R represents the molecular core structure.

The electronegativity of the terminal groups also plays a key role in determining the dominant transmission pathway as it influences the molecule-electrode coupling and orbital alignment. On one hand, electron donating anchoring groups such as thiols and amines increase the energy of the frontier molecular orbitals relative to E_F and therefore hole transport via the HOMO is the main transmission pathway.[44] Electron withdrawing anchoring groups such as pyridine and nitrile, by contrast, lower the energy of the frontier molecular orbitals and transmission through the LUMO dominates for these molecules.[12]

In addition to the molecule-electrode coupling, the mode of molecule-electrode binding can also affect the electrical properties of the molecular junction. Anchoring groups can be divided into covalent anchors which form direct metal-molecule bonds, such as thiols, and donor-acceptor (dative) anchors which bind to metallic electrodes via coordination interactions, such as thioethers.[20] The strength of the molecule-electrode coupling is predicted to be correlated with the metal-molecule binding strength, so if molecule-electrode binding is achieved via covalent bonding, strong electronic coupling is expected, whereas the electronic coupling

associated with binding via donor-acceptor coordination, van-der-Waals interactions or aromatic π-π stacking is predicted to be significantly weaker. This suggests that substituting an anchoring group which binds to the electrodes via covalent bonding for a moiety which binds via coordinative bonding can provide another method for changing the charge transport properties of the molecular junction.

Additionally, the high binding strength provided by covalent anchoring groups is advantageous for stable molecular junction formation, as molecular junctions with covalent anchoring groups are predicted to display higher mechanical stability than analogous molecular junctions with dative anchoring moieties. This is supported by the investigation of the electromechanical properties of thiol-terminated and pyridine-terminated molecules by Xu *et al*., which showed that the force required to break the molecule-electrode contacts for (covalently bound) thiol-terminated molecules was significantly higher than the force needed to break the contacts for (datively bound) pyridine-terminated molecules.[45] On the other hand, it should be acknowledged that strong covalent bonds can lead to deformations in the metallic electrode structures, causing changes in the electrode behaviour. Arroyo *et al*. reported that covalent binding alkanedithiol molecules form multiple molecular junctions in the electrode gap and cause deformations of the metallic electrodes, which modifies the junction breaking dynamics and leads to the observation of a broad distribution of conductance values. By contrast, dative binding alkanediamines preferentially form single molecule junctions which display a narrow distribution of conductance values.[46] This indicates that molecules with amine anchoring groups give better defined and more reproducible conductance values than thiol-terminated molecules, making it easier to reliably determine their charge transport properties.

1.3.3 Influence of Molecular Structure on Molecular Conductance

Chemical modification of the molecular structure provides another method for tuning the electrical properties and conductance behaviour of molecular junctions. Much research has focused on probing structure-property relationships in molecular wires as the molecular bridge has far greater potential for chemical manipulation than the electrodes or anchoring groups.[21] In theory, any chemically feasible structure could act as a molecular wire in a metal-molecule-metal junction and the extremely broad scope of chemical synthesis means a practically infinite number of molecules can be investigated with precise control of molecular structure, allowing numerous structural parameters to be modified. This is particularly significant in the context of molecular electronics as the molecular structure determines the functionality of the electronic

device, so it is important to identify compounds which display desirable characteristics such as efficient electronic transmission and high molecular conductance.

The core of the molecular wire bridging two electrodes in a molecular junction represents the main charge transport pathway through the junction and it follows that modification of the bridge structure can significantly influence the overall electrical properties of the junction. One key factor in determining the molecular junction properties is the length of the molecular backbone. In addition to the influence of molecular length on the charge transport mechanism discussed earlier,[19] more unusual length-dependent behaviour has been reported in oligomeric thiophene-S,S-dioxide (TDO) molecular wires by Dell *et al.*, who found that the primary charge carriers switched from holes to electrons as the length of the TDO chain increased. They reported that in the shorter oligomers the electron rich thiomethyl (-SMe) anchoring groups determined the primary charge transport pathway, resulting in HOMO-dominated conductance, but increasing the length of the electron deficient TDO chain was found to lower the LUMO energy, causing charge transport to switch to the LUMO-dominated pathway. This work demonstrated that the dominant conducting orbital and charge transport pathway can be controlled by the molecular backbone as well as the anchoring groups.[47]

The length of the molecular wire also influences the molecule-electrode coupling strength, as the hybridised molecule-electrode orbitals of shorter molecules are more likely to localise on the anchoring groups whereas in longer molecules larger proportions of the hybridised orbitals tend to localise on the molecular wire. As a consequence, the molecule-electrode coupling strength is typically weaker in longer molecules and electronic transmission is less efficient, which in turn leads to a decrease in conductance as the molecular length increases (Equation 2). It is also significant that the HOMO-LUMO separation in π-conjugated molecules is lower than in equivalent σ-bonded linear molecules. This means the energy gap between the E_F and the frontier orbitals is also lower in the conjugated wires, resulting in higher transmission through molecular junctions comprising conjugated molecules than for junctions bridged by analogous linear molecular wires. Experimental work has supported these theoretical predictions, as molecular conductance measurements have indicated that there is a strong correlation between the measured conductance and the energy difference between the metallic E_F and the relevant molecular frontier orbital for aromatic compounds.[48] Likewise, measurements of series of closely related conjugated molecules have displayed the same trends, showing that the conductance decreases with increasing molecular length and increasing HOMO-LUMO energy separation.[49] Additionally, molecular wires with π-conjugated

structures display lower tunnelling decay constant values than σ-bonded analogues, which is indicative of higher charge transport efficiency through the molecular junction. This result is also attributed to the smaller energy gap between the E_F and frontier orbital energy in conjugated molecules.[25]

Other molecular features can also affect the junction conductance. For example, Chen *et al*. established that the conductance of molecular wires based on a five-membered ring core structure decreases with increasing aromaticity. They observed that the cyclopentadiene-based structure displays a higher conductance than the increasingly aromatic furan-based and thiophene-based systems.[50] However, the charge transport properties can also be influenced by the conformation of the molecular wire in the metal-molecule-metal junction. Venkataraman *et al*. measured the electrical properties of a series of biphenyl-derived molecules and found that the conductance decreased with increasing twist angle. This was attributed to reduced orbital overlap between the phenyl rings and the molecular bridge structure for compounds with higher twist angles.[26] The increase in molecular length resulting from the insertion of linking groups between the molecular core structure and anchoring groups can also exert a significant influence on the electrical properties. This was demonstrated by Danilov *et al*., who reported that the insertion of methylene groups between the molecular core unit and anchoring groups in oligo(phenylenevinylene) (OPV) molecular wires leads to a change in the charge transport mechanism from coherent tunnelling to sequential hopping, resulting in a decrease in conductance by several orders of magnitude.[51]

Additionally, substituent effects can affect the conductance of molecular junctions. By changing the chemical identity of side groups which do not have continuous σ-bonds with the core molecular bridge structure, the alignment of the frontier molecular orbitals relative to E_F can be controlled, which directly influences the molecular junction conductance.[44] This can provide a method for identifying the nature of the charge carriers (holes or electrons) involved in charge transport through the junction, providing qualitative insight into the relative energy level alignment between the molecular frontier orbitals and electrode E_F. For example, for molecules with HOMO-dominated transmission pathways, electron donating substituents such as methoxy (-OMe) groups reduce the energy separation between the HOMO and E_F, leading to increased conductance. By contrast, electron withdrawing substituents such as fluorine atoms have the opposite effect, increasing the size of the HOMO-E_F energy gap and lowering the molecular conductance.[52] However, it should be noted that varying the substituents on a molecular backbone represents only a minor modification of the electronic structure and the

influence of substituent effects on charge transport properties is minimal compared to that of the electrode materials, molecule-electrode interface and the core molecular bridge structure.[18] As a consequence, substituent effects do not usually control the preferred conductance pathway through the molecule and only exert a significant effect on the conductance when the substituted core structures are decoupled from the molecule-electrode contacts.

1.4 Techniques For Measuring Single Molecule Conductance

In order to probe the electrical properties of individual molecules, a number of experimental techniques for measuring single molecule conductance have been developed. Most of these techniques are dependent on the cleavage of metal contacts in the presence of the target molecules, allowing small numbers of molecules to be trapped between electrode contacts to repeatedly form robust electrode-molecule-electrode junctions under controlled conditions. By repeatedly measuring the junction current as a function of the separation distance or bias voltage and then recording and statistically analysing the data collected, the conductance of a single molecule can be determined. The techniques have several important similarities, although they differ in the methods used to form reproducible metal-molecule contacts and measure charge transport properties. The development of these experimental approaches has promoted the growth of the field of molecular electronics as they have provided great insight into the relationship between the structures of molecular wires and the electrical properties of the resulting molecular junctions. The most important and widely used methods, based on the formation of break junctions or the use of scanning probe microscopy (SPM) techniques, are described in detail below.

1.4.1 Mechanically Controlled Break Junctions (MCBJ)

The mechanically controlled break junction (MCBJ) technique allows the electrical properties of atomic-scale metallic constrictions and small numbers of molecular wires to be measured via the mechanical cleavage of a fine wire to form a pair of electrodes. Devised by Reed *et al*. in 1997, the MCBJ technique was the earliest modern method for studying the electrical properties of individual molecules.[8] In this experiment, a Au wire was stretched on top of a flexible support in a solution of benzene-1,4-dithiol molecules until the wire was cleaved to form a pair of Au electrodes (Figure 1.2). The counterfacing electrodes were moved towards each other until the onset of conductance, indicating the adsorption of target molecules to the electrodes to form metal-molecule-metal junctions, after which current-voltage (I-V)

measurements were recorded. This enabled the molecular conductance values and electrode separation distances to be determined, significantly improving understanding of charge transport behaviour in molecular junctions.

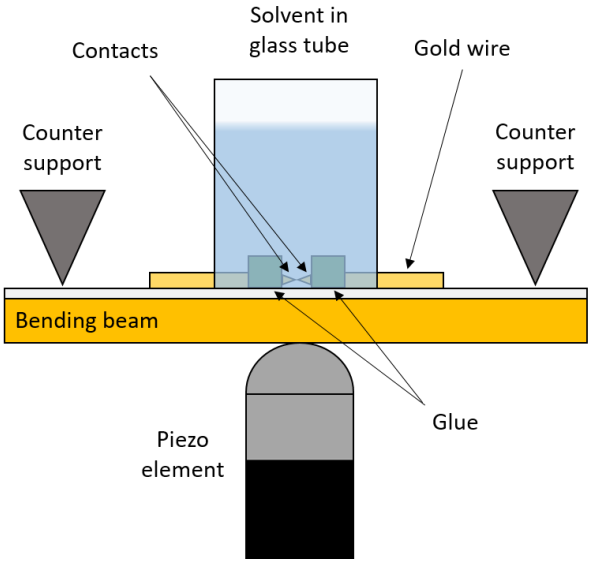

Figure 1.2. Schematic of the MCBJ technique for measuring single molecule conductance.

The high reproducibility of the I-V traces obtained from this experiment implied that the number of active molecules was very small. However, one drawback of this method is that it is not possible to define the exact number of molecular junctions formed, making it difficult to accurately determine the true single molecule conductance value.

1.4.2 Conducting Probe-Atomic Force Microscopy (CP-AFM)

The conducting probe-atomic force microscope (CP-AFM) was developed by Cui *et al*. to measure the conductance of individual molecules as part of the Monolayer Matrix Isolation (MMI) technique in 2001.[9] This SPM approach uses nanoparticles to establish electrical contact between individual molecules and the CP-AFM, allowing the electrical properties of the resulting molecular junctions to be measured. They prepared a self-assembled monolayer (SAM) of alkanethiols with alkanedithiols at high dilution on a Au substrate and attached gold nanoparticles (GNPs) to the terminal thiol moieties of the alkanedithiols. The CP-AFM tip was used to make electrical contact with the nanoparticles and the electrical properties of the molecular junctions were measured by recording current-voltage (I-V) traces, with statistical analysis performed to determine the most probable conductance value. As the electrical response was dominated by current flow through individual molecular junctions, this experiment provided the first reproducible evidence of single molecule conductance. However,

the CP-AFM approach has several significant drawbacks, as it is technically challenging to perform and the capping ligands on the GNPs can prevent direct metal-to-metal contact between the nanoparticle and tip. Another problem is observed when very small GNPs are used, as quantum charging of the GNPs results in a Coulomb blockade effect due to the finite contact resistance between the probe and nanoparticle, which distorts the I-V measurements and gives unreliable conductance values. This can be resolved by using larger GNPs, although this increases the density of dithiol molecules, resulting in a broader spread of conductance values.[53]

1.4.3 Scanning Tunnelling Microscopy (STM)

The Scanning Tunnelling Microscope (STM) is a highly versatile instrument invented by Binnig and Rohrer at IBM in the early 1980s[54] which has played a major role in the development of methods for measuring single molecule conductance. The most important feature of the STM is the metallic probe tip, which is connected to three piezoelectric transducers mounted at angles of 90° relative to each other in the x, y and z directions. This means the tip position can be controlled with fine precision, enabling the tip to be approached within nanometres of a substrate surface. The STM tip allows the substrate surface to be imaged with atomic-scale resolution, allowing it to fulfil its original and primary function of obtaining information about the surface topography. However, in addition to its imaging capabilities, the STM has also provided an ideal method for forming and characterising single molecule junctions.

The Scanning Tunnelling Microscopy-Break Junction (STM-BJ) technique, also known as the *in situ* break junction technique, is a contact-based SPM approach for constructing molecular junctions developed by Xu and Tao in 2003.[10] This method has a degree of similarity to the MCBJ technique, as it is based on the mechanical formation of break junctions, but instead uses an STM tip to mechanically form break junctions by pushing the tip into the metallic substrate to form a metal-to-metal contact between the tip and surface (Figure 1.3). One significant advantage of this SPM approach compared to the MCBJ technique is that both the tip and substrate can be easily replaced, allowing them to be changed independently. It is also experimentally convenient as it is compatible with commercially available STM instruments. In this approach, the current is continuously monitored as the tip is rapidly withdrawn from the surface and the retraction of the tip causes the junction to narrow to a single atomic point contact. As the metallic contact narrows, the current decreases in quantum steps at integer multiples of the conductance quantum, G_0 (77.48 μS), indicated by a characteristic plateau in

the current-distance (I-s) traces. Upon further tip retraction, the metallic junction is cleaved to leave an open nanogap between tip and substrate where molecular junctions can form.

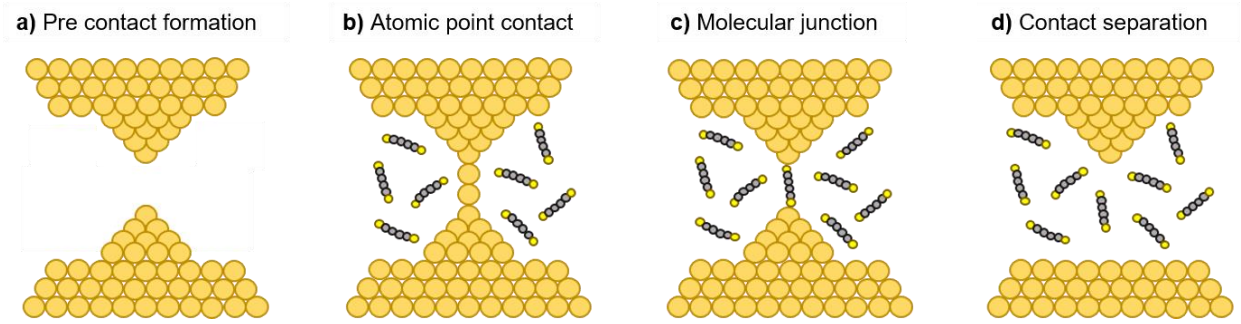

Figure 1.3. Schematic of the STM-BJ technique for measuring single molecule conductance in solution. **a)** STM tip (top) and substrate (bottom) prior to addition of solution containing the analyte molecule. **b)** After addition of the sample solution the STM tip is approached towards the substrate and makes contact with the surface, forming a Au-Au contact between tip and substrate. This contact initially comprises multiple Au atoms before narrowing to form a single atomic point contact. **c)** The tip is rapidly withdrawn from the substrate until the metallic junction is broken, leaving a nanogap which molecules can stochastically bridge to form molecular junctions. **d)** Further tip retraction leads to molecular junction cleavage, returning to the situation in (a). The atomically sharp STM tip is simplified for illustrative purposes.

If no molecules bridge the nanogap, an exponential current decay is observed during the retraction process. However, if one or more molecule(s) form molecular junctions in the metallic gap, significantly smaller decreases in current are observed as the junctions are broken. When the molecule is fully stretched, the junction will break, with junction cleavage indicated by an abrupt fall in current. The process of forming and breaking molecular junctions is repeated many times by continually approaching and withdrawing the tip and the current is measured at an applied bias voltage, allowing thousands of conductance traces to be collected. This enables the preparation of conductance histograms, which are statistically analysed to give the most probable conductance value for the molecular junction. The number of peaks observed in the conductance histograms varies, with some molecules giving a single peak and others displaying distinct high, low and medium conductance peaks, representing different molecular junction conformations or molecule-electrode contact geometries.[55] This approach allows a statistical interpretation of the structure-conductance relationship to be obtained over a series of measurements, providing insight into the properties of single molecule junctions. The collection of current-distance (I-s) traces via this method also allows the lengths of the

molecular plateaus to be determined, where the plateau length corresponds to the maximum stretching distance of the molecular junction and provides further information about the junction stability.

One significant modification of the standard technique is the electrochemical STM-BJ method, which allows nanowires of a range of metals other than Au to be electrodeposited onto the STM tip, permitting the formation of metallic clusters on the substrate surface via a jump-to-contact transfer process. An atomic-sized metallic wire can then be formed by withdrawing the tip until the metal-metal contact is broken, allowing the formation of molecular junctions in the nanogap. This approach has expanded the scope of the STM-BJ technique by enabling the use of a broader range of metals as electrode contacts in metal-molecule-metal junctions. Another advantage is the reduced noise in the current traces, which results from the significantly increased speed of tip retraction achievable using this method.[56]

A different but related STM-based approach is the I(s) technique, developed by Haiss *et al*. in 2003.[57] The I(s) method (I is current, s is tip retraction distance) is conceptually similar to the *in situ* break junction technique as it uses an STM tip to trap molecules between the tip and a metallic substrate and record electrical measurements. Where this technique differs is that molecular bridges are formed by moving the STM tip close to, but not in contact with, the metallic surface, enabling a small number of molecules (or a single molecule) to stochastically bridge the gap and form a junction between the tip and substrate. The I(s) technique is therefore a 'soft' non-contact mode of forming single molecule junctions, as no direct contact is made between the tip and substrate, in contrast to the 'hard' contact-based STM-BJ approach. As with the STM-BJ technique, the I-s plots in the absence of a molecular bridge display an exponential decay, characteristic of tunnelling through the nanogap between tip and substrate, with molecular junction formation indicated by the presence of a plateau in the I-s traces. The non-contact method of junction formation can be advantageous in some measurements, as the substrate surface is not perturbed by the STM tip, which avoids disruption to the surface, although this also means that the probability of junction formation is significantly lower. As a consequence, data selection is frequently required to exclude exponential decay traces and only include traces representing molecular junction formation in the conductance plots from I(s) experiments, which is time-consuming and increases the likelihood of errors when determining the electrical properties of the molecular wire.

Another similar ‘soft’ non-contact method for measuring the electrical properties of single molecules is the I(t) technique (I is current, t is time), which monitors molecular junction formation in the time domain.[58] In this approach, also referred to as ‘blinking’ mode, the STM tip is positioned at a constant height above the surface of a substrate coated in adsorbed molecules. This distance is set to be shorter than the length of the fully extended molecular wire, thus permitting the spontaneous formation of molecular bridges between the tip and substrate. The current is monitored as a function of time and the formation of molecular junctions is indicated by the occurrence of current jumps in the I(t) traces. As with the I(s) method, the significant advantage of this approach is that the tip does not make direct contact with the substrate and therefore disruption of the substrate is avoided. However, it shares the same major drawback, as the probability of molecular junction formation is again lower than for the contact-based STM-BJ technique.

1.5 Theory and Concepts of Quantum Interference Effects in Molecular Electronics

In recent years, there has been increasing interest in exploring the role of interference effects in controlling the properties of molecular wires. These effects can strongly influence charge transport behaviour through molecules and are therefore significant for the development of molecular electronic devices, particularly as they could permit active control of the electrical properties of molecular junctions. This would considerably broaden the scope and usefulness of molecule-based devices, overcoming the limitations of the passive length dependent conductance behaviour displayed by simple molecular wires.[59] Molecular junctions incorporating molecules which possess quasi-degenerate states (corresponding to the main conductance channels) exhibit Quantum Interference (QI) effects, as these states provide different pathways for electronic transmission through the junction. QI effects result from interference between electron waves propagating through the molecular orbitals via different pathways and arise in single molecule junctions as electron transport in single molecules is quantum phase-coherent.[60] These effects have a significant influence on the electronic transmission through the molecular junction described by the Landauer formula (Equation 5) and thus play an important role in controlling the molecular conductance.

QI effects are of significant interest in molecular electronics as they provide a flexible, *in situ* method of controlling the electrical properties of individual molecules in molecular junctions. They have no classical equivalent and therefore have the potential to enable unique and highly

desirable conductance properties, providing access to electronic device functionality which cannot be achieved using existing approaches.[59] They provide a feasible mechanism for controlling charge transport behaviour through molecular junctions that is readily accessible at room temperature and does not depend on changes in molecular length, substituent groups or redox state.[61] Also, as these effects are inherent to the small dimensions of single molecules, they are fundamentally controlled by the molecular structure. For example, cyclic molecules facilitate QI effects as their structures allow charge transport to follow multiple pathways between the electrodes.[60] Theoretical calculations also predict that molecular junctions comprising molecules which exhibit QI effects can display large modulations in conductance.[62] As a consequence, understanding the relationships between QI effects and charge transport properties is crucial for the development of design principles for molecular wires displaying QI effects, in order to provide sufficient structure-function control to maximise the potential usefulness of these molecules as electronic device components.

As the nature and type of QI effects observed for molecular wires with multiple conductance pathways depends on the molecular structure, it is possible to predict whether a molecule will display QI behaviour. The nature of the interference behaviour can be qualitatively predicted using simple diagrams depicting charge transport pathways through the molecular junction.[63] Quantitative predictions of the nature of the interference effects can be obtained by performing theoretical calculations and these calculations indicate that the patterns of QI effects in molecular junctions are dominated by the frontier molecular orbitals (HOMO and LUMO). More specifically, QI effects can be divided into constructive quantum interference (CQI) effects, which enhance the molecular conductance, and destructive quantum interference (DQI) effects, which suppress the molecular conductance. These can be identified and mapped using transmission plots, which display the probability of electronic transmission at a given energy value in the form of the transmission coefficient, which represents the efficiency of charge transport through the molecule.[62]

Constructive QI effects are caused by constructive interference between transmission through the HOMO and LUMO-mediated pathways and occur when HOMO and LUMO contributions to the conductance add up. When this occurs, the interference pattern of the electron waves has a large amplitude at both molecule-electrode contacts, resulting in an increase in the transmission probability. Clear evidence of CQI effects has been observed from conductance measurements involving double-backbone molecular junctions, which have a higher conductance than the two equivalent parallel single-backbone junctions.[64] The theoretical

transmission spectroscopy plots for molecular wires which exhibit CQI effects feature a characteristic smooth transmission curve between the HOMO and LUMO resonances.

Destructive QI effects are caused by destructive interference between transmission through the HOMO and LUMO-mediated pathways and occur when HOMO and LUMO contributions to the conductance cancel out. In this scenario, the interference pattern has a small amplitude at one or both of the molecule-electrode contacts, which decreases the electronic transmission probability. They can be identified by the presence of a sharp dip in the theoretical transmission spectroscopy plots, typically observed as an anti-resonance feature in the transmission function located within the gap between the HOMO and LUMO resonances.[62] DQI effects can also be observed in experimental differential conductance plots, indicated by a distinct conductance minimum in a V-shaped conductance vs bias voltage curve.[65] For a molecular junction with a molecule acting as a bridge between metallic electrodes, the distinctive anti-resonance feature in the transmission curve is typically observed close to the Fermi energy (E_F) of the electrodes. When the DQI anti-resonance is located close to the electrode E_F, the electronic transmission probability is significantly reduced, which means the molecular conductance can be suppressed by orders of magnitude compared to an equivalent non-DQI pathway. This can result in extremely low conductance values for molecules displaying DQI behaviour.

The benzene ring is one of the simplest molecular systems predicted to display QI effects and therefore provides an ideal model for understanding the role of these effects in controlling the conductance properties of conjugated molecular wires. Theoretical calculations predicting electronic transmission behaviour for substituted benzene molecules indicate that *para*-linked (1,4-disubstituted) benzene rings should have a molecular conductance several orders of magnitude higher than analogous *meta*-linked (1,3-disubstituted) benzene rings (Figure 1.4).[62] The large difference in conductance is attributed to DQI effects occurring near the metallic E_F in the *meta*-linked benzene structure, indicated by an anti-resonance feature in the transmission plot. These effects prevent efficient molecule-electrode coupling, leading to a sharp decrease in electronic transmission efficiency through the *meta*-linked structure compared to the *para*-linked structure, which shows a smooth transmission curve indicative of CQI effects. These findings have very useful implications for the development of molecular electronic devices, as they show that there is a strong correlation between the molecular connectivity pattern and the occurrence of QI effects in conjugated molecular wires, and that different QI behaviour can lead to a large discrepancy in conductance between molecules with similar structures.

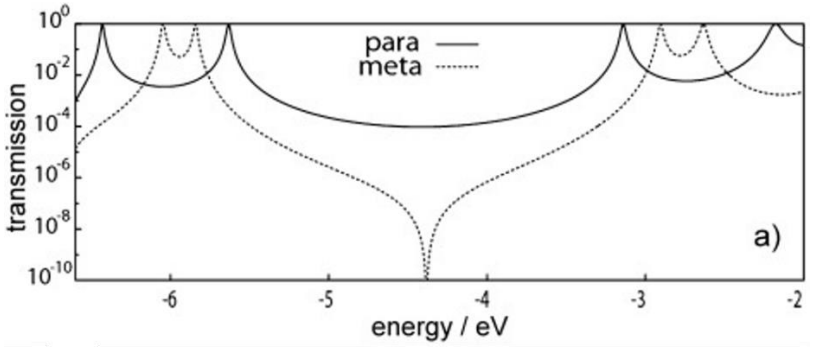

Figure 1.4. Transmission spectra depicting electronic transmission through the π-systems of molecular wires incorporating a *para*-coupled benzene ring (solid line) and a *meta*-coupled benzene ring (dotted line). The plot shows a pronounced anti-resonance feature for the *meta*-coupled benzene ring in the HOMO-LUMO gap, indicative of DQI effects, but no equivalent feature is observed for the *para*-coupled benzene ring (reproduced from reference 62).[62]

The majority of molecular electronics studies investigating QI effects have focused on DQI, as the patterns of conductance displayed by molecules exhibiting DQI effects deviate significantly from classical predictions of conductance behaviour, which may enable access to novel and unique device functions. The abrupt change in molecular conductance associated with DQI effects is potentially very useful for the development of molecular electronic devices as electronic functionality in a number of important applications, including switching, memory and sensing devices, is dependent on the ability to access distinct high and low conductance states. This means that molecules with DQI pathways may give large differences in conductance between the 'on' and 'off' state with very low conductance values in the 'off' states, which are highly desirable characteristics for many functional devices.

The occurrence of QI effects can lead to different types of resonance or anti-resonance features which can be identified in theoretical transmission plots. Three of the most notable classes of resonance that arise in molecular junctions are Breit-Wigner, Mach-Zehnder and Fano resonances.[66] Breit-Wigner resonances occur when the energy of an electron passing through a molecular wire resonates with a molecular backbone state and can be observed in simple linear molecular junctions. Mach-Zehnder resonances occur when multiple transmission pathways through a molecular junction are available and constructive interference is observed between electron waves traversing these pathways. Fano resonances result from coherent interference between direct and indirect scattering resonance pathways in the same system. In a single molecule junction, this can occur when the energy of an electron travelling through the molecule coincides with the energy of a bound state located on a pendant group, allowing the

bound state to couple to a backbone electronic state. In other words, a Fano resonance can be seen as a resonance which is attached to an anti-resonance and is indicative of destructive interference.

Fano resonances are of significant interest in molecular electronics in general and this work in particular as they provide a convenient method for controlling charge transport through molecular junctions. As this interference effect is dependent on the supply of a continuum of states from metallic electrodes, Fano resonances do not usually occur in isolated molecules but can arise in metal-molecule-metal junctions incorporating molecules with suitable pendant groups. Fano resonances can be distinguished in transmission plots by their characteristic and unique asymmetric line shape and the sharp reduction in electronic transmission associated with the anti-resonance feature.[66] The close proximity of the resonance and anti-resonance features represent a potential pathway for changing the conductance of a molecular junction by several orders of magnitude, with the resonance feature corresponding to the high conductance state and the anti-resonance corresponding to the low conductance state. This could provide a highly efficient mechanism for conductance tuning in molecular transistor or switching devices, as only a small stimulus is required to enable switching between the high and low conductance states but the predicted difference in conductance between the two states is large.

1.6 Literature Review of Quantum Interference Effects in Molecular Electronics

Quantum Interference (QI) effects in molecular electronics are a subject of increasing research interest in both theoretical and experimental studies and have become one of the most widely studied topics in the field in recent years. The tuning of QI effects is recognised as one of the major challenges in the development of molecular electronics and therefore much of this research aims to establish molecular design strategies which permit control of QI effects in molecular junctions, potentially allowing them to be exploited for use in novel functional electronic devices.[13,59,67] This section covers a number of studies investigating various aspects of QI effects and their significance in advancing the understanding of structure-property relationships in molecular junctions and the development of single molecule-based devices.

Experimental measurements performed on molecular junctions comprising molecules which are predicted to display QI effects have shown clear evidence that these effects influence the electrical properties of the molecules studied. These experiments have provided insight into the ability of DQI effects to suppress electronic transmission and control charge transport through

molecular wires. For example, Arroyo *et al*. measured the conductance of two oligo(phenylenevinylene) (OPV) derivatives where the central benzene ring was connected via either the *para*- or *meta*-positions. They observed that the conductance for the *meta*-OPV was one order of magnitude lower than the *para*-linked molecule, consistent with electronic transmission calculations predicting DQI effects for the *meta*-OPV and CQI effects for the *para*-OPV respectively.[68]

The influence of DQI effects on electrical properties is particularly apparent in measurements of molecular wires which have similar conjugated core structures but have linker groups attached to the rings in different positions. This was demonstrated by Aradhya *et al*., who measured both the molecular conductance and junction rupture force for a pair of stilbene-derived molecular wires with thiomethyl anchoring groups. They found that the *meta*-linked stilbene molecule gave a conductance value several orders of magnitude lower than the analogous *para*-linked molecule. The force measurements from this study demonstrated very similar junction cleavage behaviour for both molecules, indicating that the *para*-linked and *meta*-linked molecules formed molecular junctions with approximately the same mechanical stability. These results indicate that the large difference in conductance can be attributed to QI effects intrinsic to the *meta*-linked structure.[61] Performing force measurements is particularly useful for molecules predicted to display DQI as these experiments probe the junction mechanics independently of the conductance, providing evidence of molecular junction formation for structures which display very low conductance values.

The influence of QI effects on the electrical properties of molecules has also been investigated in molecular wires based on extended conjugated structures. For these molecules, it is very useful to understand the relative importance of the influence of the molecular core unit and anchoring groups on the nature of QI behaviour. This has been systematically investigated by Manrique *et al*. in a study measuring the conductance of a series of oligo(phenyleneethynylene) (OPE) molecular wires. They found that the conductance of an OPE molecule with a *para*-linked central ring is an order of magnitude higher than the equivalent *meta*-linked structure, irrespective of the connectivity of the anchoring groups.[69] This work indicates that the type of QI behaviour observed (constructive or destructive) in extended conjugated molecules is dependent on the connectivity of the central ring and is independent of the anchoring groups, consistent with predictions of QI behaviour determined using charge transport diagrams and electronic transmission plots.[62]

In addition to experimental measurements, the development of methods for predicting QI behaviour in molecules represents another key aspect of research into QI effects. There are several different approaches for predicting and rationalising the presence and nature of QI effects in molecular wires. These range from simple graphical methods based solely on analysis of the molecular structures to computationally demanding charge transport simulations. Graphical methods used to predict QI effects include the 'atom-counting' approach which involves drawing and analysing resonance structures to determine whether DQI effects occur in π-conjugated molecular wires.[61] Using this method, if there is a resonance structure which allows one molecule-electrode linker to be delocalised through the molecular bridge onto the opposite electrode, giving a structure with a single positive charge stabilised on one molecule-electrode linker and a single negative charge on the opposite electrode (or vice versa), CQI effects are predicted. DQI effects are predicted when there is no resonance structure which connects the metallic electrodes via a single path and it is not possible to draw a continuous path through the molecule between the left and right contacts without leaving at least one isolated site outside the conductance pathway which is not paired with any other sites.

The 'atom-counting' approach is chemically intuitive and is effective for forecasting DQI in simple molecular structures. For example, there is an unpaired site in a *meta*-linked phenyl group but no unpaired sites in a *para*-linked phenyl group, indicating that the *meta*-linked structure displays DQI effects, in good agreement with experimental conductance measurements which show that *meta*-linked benzene gives a lower conductance value than *para*-linked benzene.[62,63] However, this graphical method is qualitative and cannot be used to predict the molecular conductance value or the position of an anti-resonance feature in the corresponding transmission function. Another qualitative approach uses orbital rules derived from the phase and amplitude of the molecular frontier orbitals (HOMO and LUMO) to predict whether electronic transmission through a molecular junction is symmetry allowed or symmetry forbidden. The molecules with symmetry forbidden connections are predicted to display DQI effects which suppress the molecular conductance. Theoretical predictions from this method have been found to be in good agreement with experimentally measured conductance values for naphthalene derivatives, as molecules with symmetry allowed connections display higher conductance values than equivalent molecules with symmetry forbidden connections.[70]

The majority of studies reporting QI effects in molecular wires have focused on molecules based on core structures featuring one or more six-membered ring structures, reflecting the

popularity of substituted benzene derivatives as a model system for investigating QI behaviour.[62] More recently, however, QI effects have also been observed in molecules featuring five-membered rings, indicating that a wider range of molecular structures could potentially be used as components in electronic devices exploiting interference behaviour. This has expanded the scope of molecular electronics studies and provides another useful design strategy for tuning QI behaviour. For example, Yang *et al*. reported that the substitution of different heteroatoms in five-membered ring structures leads to a decrease in molecular conductance, which they attributed to destructive interference (Figure 1.5). They found that the conductance of asymmetric molecular junctions was significantly lower than for analogous symmetric structures, indicative of DQI effects, and the substitution of heteroatoms on the core unit allows this behaviour to be controlled *in situ* by tuning the position of the anti-resonance feature relative to the frontier orbitals.[71]

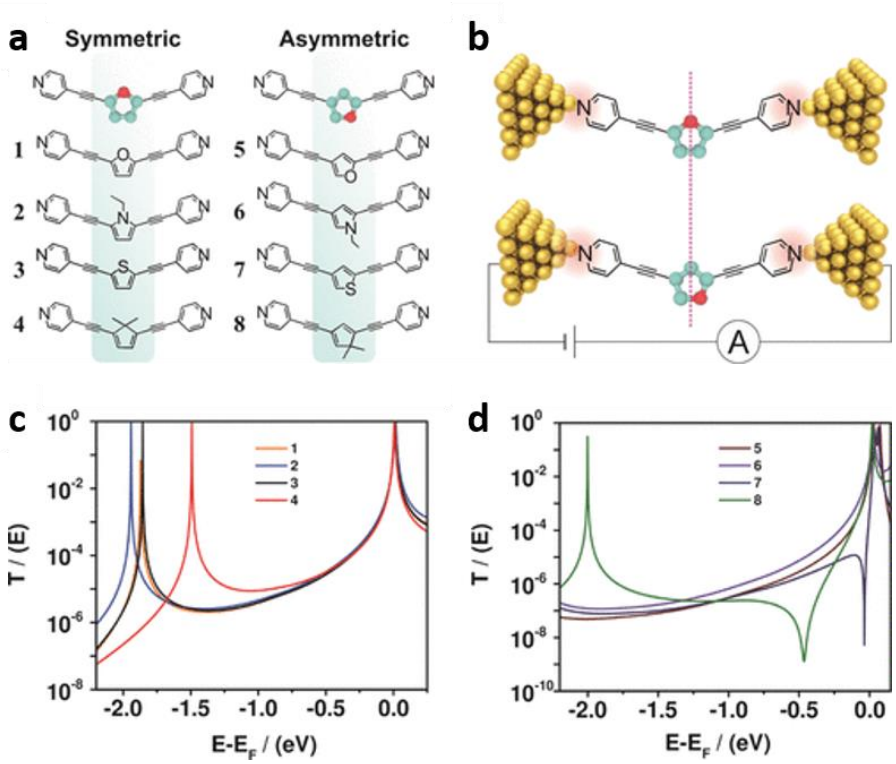

Figure 1.5. a) Molecular structures for a series of symmetric cyclopentadiene-derived molecules with different heteroatoms (1-4) and analogous asymmetric structures (5-8). **b)** Molecular junction schematic, with the dotted red line showing symmetry (top) and asymmetry (bottom) with respect to the core structure. Transmission plots calculated for **c)** symmetric cyclopentadiene derivatives and **d)** asymmetric cyclopentadiene derivatives. Note the sharp anti-resonance feature in the transmission spectrum for molecule 8, a signature of destructive QI effects (reproduced from reference 71).[71]

There is also significant interest in exploiting molecules displaying DQI effects in molecular switching devices, arising from the low conductance values associated with this behaviour. Theoretical studies have indicated that if the DQI pathway can be controllably switched, for example by applying a gate voltage to the molecular junction to switch the charge transport pathway between a constructive or non-QI pathway and a DQI pathway, the destructive pathway could provide an ideal off state for an electrical device with a large on/off ratio.[60] For switching devices, exploiting these interference effects could also improve device performance compared to devices dependent on conformational changes for shifting molecules from high to low conductance states (or vice versa), as electronic changes can be induced more rapidly than conformational changes.

One of the most widely used approaches for tuning molecular conductance is electrochemical gating, which involves changing the gate potential and investigating the response in electrical behaviour. The usefulness of electrochemical gating strategies in tuning molecular conductance has been demonstrated by Li *et al*., who found that the energy alignment between the molecular orbitals and E_F can be tuned by controlling the gate voltage. They reported that this allows the single molecule conductance of a conjugated molecular wire displaying DQI effects to be tuned by over two orders of magnitude.[72] Additionally, this work has overcome a major limitation of experiments investigating QI effects in molecular junctions, as interference features occurring away from the electrode Fermi Energy (E_F) cannot usually be exploited. This is significant because the conductance is typically measured at E_F, which implies that only interference effects close in energy to E_F can be exploited in low bias experiments. However, Li *et al*. also showed that controlling the electrochemical gate potential permits direct control of the positions of anti-resonance features corresponding to DQI effects in the transmission spectra, which provides a mechanism for tuning the positions of anti-resonances relative to the HOMO-LUMO gap.[72] This approach also enables direct observation of anti-resonance features in the transmission plots, which provides a clear signature of destructive interference behaviour and further enhances understanding of the role of QI effects in controlling the electrical properties of molecular junctions.

Further evidence of the potential usefulness of molecules displaying DQI effects in switching devices has been demonstrated by Bai *et al*. in another study showing that significant changes in conductance can be achieved by tuning the energy of the electrode E_F with the resonance state or anti-resonance state via electrochemical gating. They found that the conductance of molecular junctions incorporating a 2,4-linked thiophene-based molecular wire (2,4-TP-SMe)

displaying DQI increased by two orders of magnitude as the electrode potential was varied from -0.6 to 1.3 V, in contrast to the analogous 2,5-linked molecular junctions (2,5-TP-SMe) where the conductance increased only eight times under the same conditions (Figure 1.6).[73] This work indicates that electrochemical gating could provide a promising strategy for achieving *in situ* control of molecular conductance using anti-resonances arising from DQI effects in molecule-based devices. It also shows that the modulations in conductance for molecules displaying DQI on changing the applied bias voltage are significantly larger than for equivalent molecules which do not exhibit QI effects.

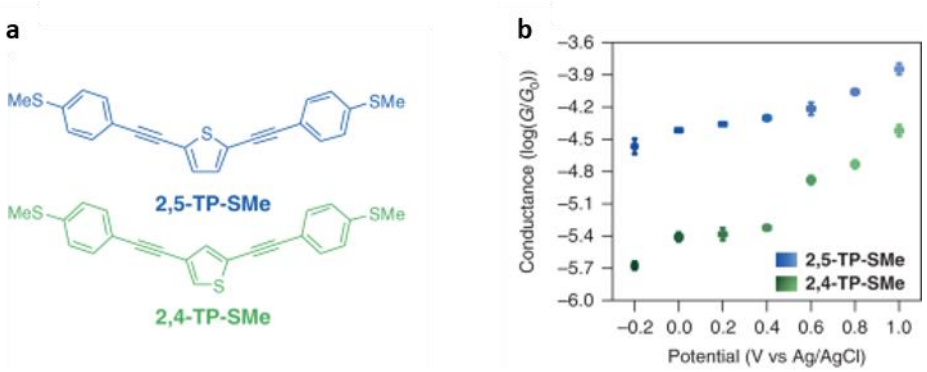

Figure 1.6. a) Molecular structures of thiophene-derived molecules with thiomethyl (-SMe) anchoring groups, 2,4-TP-SMe (green) and 2,5-TP-SMe (blue). **b)** Plots of molecular conductance for 2,4-TP-SMe and 2,5-TP-SMe versus electrode potentials varying from -0.2 to 1.0 V. It is apparent that 2,4-TP-SMe, which displays DQI effects, shows a much larger increase in conductance on raising the bias in this range than 2,5-TP-SMe. Error bars for the conductance are determined from variation of the most probable conductance values in three independent conductance measurements (reproduced from reference 73).[73]

Chemical design strategies have also been used to control switching behaviour in molecular junctions by tuning interference effects, which provides another method for achieving large modulations in molecular conductance. Greenwald *et al*. found that the conductance of oligofluorene molecular wires with benzothiadiazole core units can be tuned by over four orders of magnitude on switching the applied bias voltage. This behaviour is attributed to decoupling of the HOMO and LUMO by the core unit, as Density Functional Theory (DFT) calculations indicate that the LUMO is localised on the benzothiadiazole moiety whereas the HOMO is delocalised across the molecular wire, which suppresses CQI effects between these orbitals and enhances DQI effects between strongly coupled molecular orbitals of opposite

phase. This allows destructive interference to dominate the charge transport characteristics, resulting in a large dynamic range in molecular conductance.[74]

In experimental conductance measurements exploring the influence of DQI behaviour on the electrical properties of molecular junctions, molecules featuring cross-conjugated moieties are particularly interesting candidates for investigation. This is because theoretical transmission calculations indicate that cross-conjugated molecules display anti-resonance features in close proximity to the metallic E_F, indicative of DQI effects, and these features are expected to result in a sharp decrease in molecular conductance and, for molecules with multiple conductance states, a large discrepancy between the high and low conductance states.[75] The influence of DQI effects on the electrical properties of cross-conjugated molecules compared to analogous linearly conjugated structures has been investigated experimentally by Guédon *et al*., who observed destructive interference phenomena in anthracene-derived molecular wires (Figure 1.7). They reported that the cross-conjugated thioacetyl-terminated anthraquinone molecule, which exhibits DQI effects, displays a conductance value two orders of magnitude lower than analogous linearly conjugated anthracene molecules, which do not display this behaviour.[76]

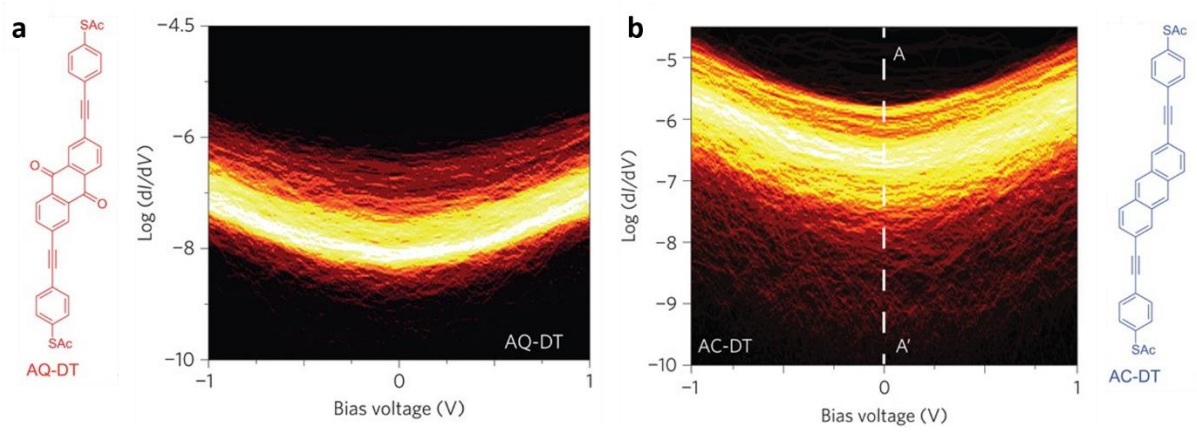

Figure 1.7. a) Experimentally measured plots of conductance (dI/dV) versus bias voltage (V) obtained for **a)** cross-conjugated anthraquinone (AQ-DT) and **b)** linearly conjugated anthracene (AC-DT) molecular structures. These plots show that the linearly conjugated AC-DT molecule has a zero bias conductance approximately two orders of magnitude higher than the cross-conjugated AQ-DT molecule (reproduced from reference 76).[76]

This study demonstrates how comparatively minor changes in molecular structure can result in QI effects which significantly affect the molecular conductance, as the two structures incorporate the same anchoring moieties and have very similar molecular lengths. Importantly, DFT calculations indicated that the two molecules also have very similar electronic energy

levels, so this large discrepancy in conductance cannot be attributed to a significant difference in the HOMO-LUMO energy separation.

The electrochemical gating approach also provides a useful method for controlling QI effects in molecular junctions comprising molecules with different redox states, allowing the molecular structure to switch between states displaying different electrical properties. Darwish *et al*. showed that the conductance of a molecular junction featuring a rigid anthraquinone core unit with norbornyl linkers can be reversibly switched between high and low conductance states under electrochemical control. They observed that, on reduction of the cross-conjugated anthraquinone form to the linearly conjugated dihydroxyanthracene form, the molecular conductance increased by approximately one order of magnitude.[13] This demonstrated that the DQI pathway could be switched on and off via a reversible redox reaction to allow the molecular junction to function as a single molecule transistor device.

Additionally, the influence of cross-conjugated moieties on the conductance of molecular wires is dependent on the position of the relevant functional groups relative to the main charge transport pathway through the molecular junction. Baghernejad *et al*. demonstrated this by using electrochemical gating to reversibly tune the conductance of two isomeric anthraquinone-derived molecules, AQ-1,4 and AQ-1,5, between the reduced and oxidised states (Figure 1.8). They observed that the discrepancy between the conductance of the reduced and oxidised forms of the AQ-1,5 molecule, where the primary charge transport pathway passes directly through the anthraquinone moiety, was significantly larger than that for the AQ-1,4 molecule, where the anthraquinone unit is attached as a side group.[77] Transmission calculations indicate that this behaviour occurs because the oxidation of the linearly conjugated reduced state of AQ-1,5 to the cross-conjugated oxidised state directly results in DQI effects which lower the electronic transmission, observed experimentally as a significant decrease in molecular conductance. By contrast, oxidation of the reduced state of AQ-1,4 only indirectly influences charge transport through the molecular wire and as a consequence the change in conductance observed at the redox potential is significantly smaller than for AQ-1,5.[77]

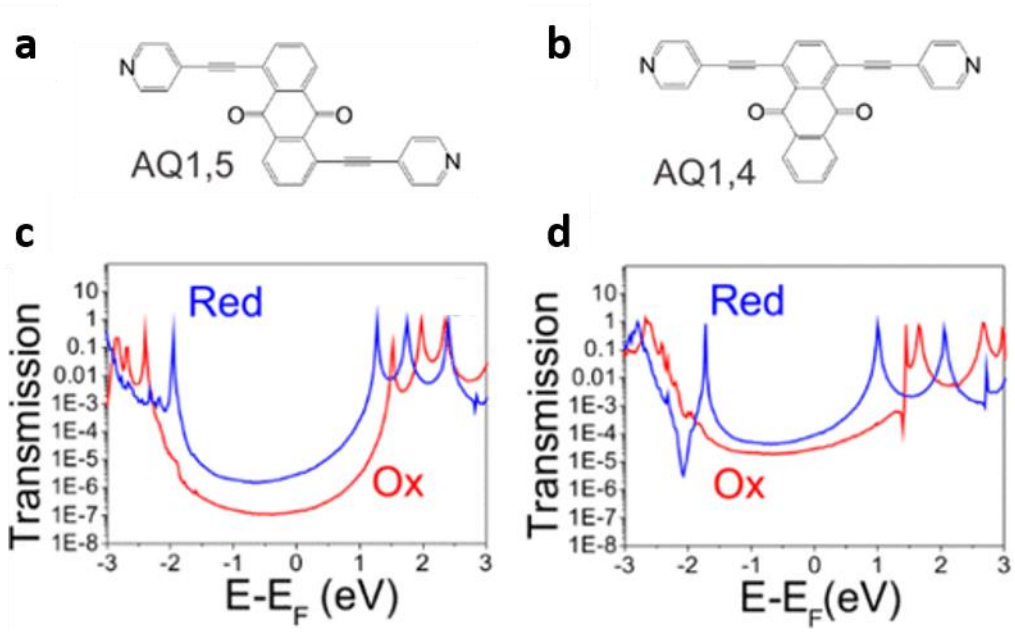

Figure 1.8. Molecular structures for the anthraquinone derivatives **a)** AQ-1,5 and **b)** AQ-1,4. Calculated transmission plots for **c)** AQ-1,5 and **d)** AQ-1,4 at energy values relative to E_F. It is apparent from these plots that there is a much greater discrepancy in electronic transmission between the reduced (blue lines) and oxidised (red lines) forms of AQ-1,5 compared to AQ-1,4 (reproduced from reference 77).[77]

The importance of measuring the electrical properties of a wide range of molecular structures and investigating structure-property relationships in the development of molecular electronics has been illustrated by surprising results observed from measurements of other cross-conjugated molecules. For example, Alanazy *et al*. found that *meta*-connected fluorene-based molecular wires give conductance values two orders of magnitude lower than analogous *para*-connected molecules, but for fluorenone-based molecular wires the difference in conductance between the *meta*- and *para*-connected structures is found to be far smaller.[78] This apparent elimination of DQI effects was unexpected as the fluorenone moiety features a cross-conjugated carbonyl group and the increase in conductance on addition of this functional group to the core structure is the opposite to the behaviour observed by Guédon *et al*. for anthraquinone-based molecules.[76]

Alternatively, atomically precise chemical gating strategies have been used to enable switching between DQI and CQI transmission pathways through single molecule junctions. Tang *et al*. found the conductance of *meta*-linked pyridine molecular wires increased by approximately one order of magnitude after the neutral pyridine was converted to positively charged pyridinium via the addition of cationic reagents, thus switching the interference pattern from

DQI to CQI.[79] Other chemical gating approaches, which are dependent on responses to acid/base stimulation, have also been employed as a means of controlling QI effects in molecular junctions. Yang *et al*. measured the electrical properties of a series of three azulene derivatives with different connectivities and found that the conductance of all three molecules increased significantly after protonation with trifluoroacetic acid (TFA) (Figure 1.9).[80] They also reported that the 5,7-linked azulene derivative (5,7-Az), which displayed destructive interference behaviour, showed a very large increase in conductance by over an order of magnitude after protonation, which is attributed to the cancellation of DQI in the protonated state. This work indicates that enhanced conductance tuning via chemical gating strategies is feasible for molecules displaying DQI effects.

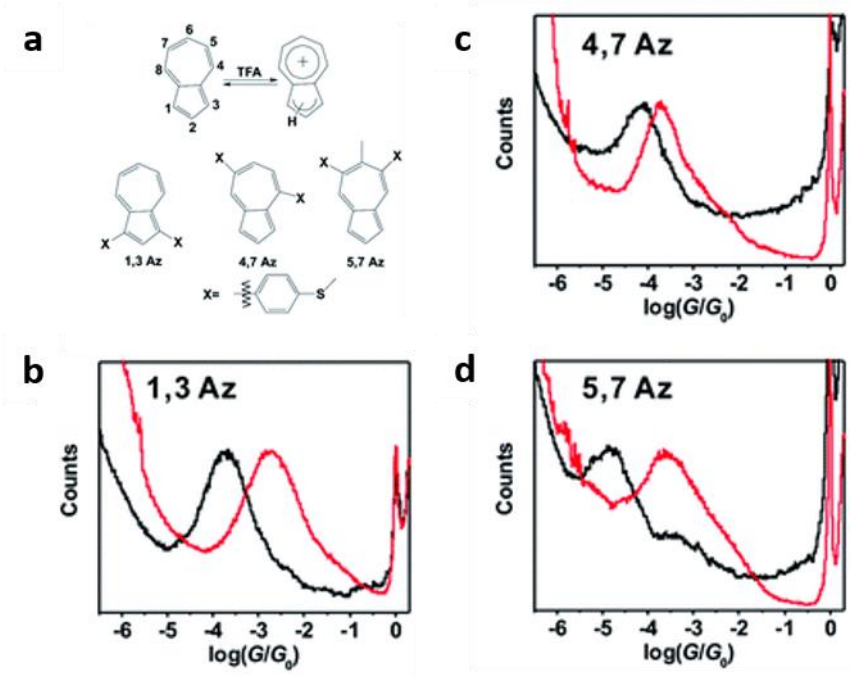

Figure 1.9. a) The protonation of azulene on addition of TFA as shown for the series of three azulene-derived molecules (1,3-Az, 4,7-Az and 5,7-Az). Conductance histograms for **b)** 1,3-Az, **c)** 4,7-Az and **d)** 5,7-Az with TFA (red) and without TFA (black). It is apparent that the conductance of all three molecules increases on protonation of the azulene core structure, with 5,7-Az displaying the largest conductance increase (reproduced from reference 80).[80]

Additionally, acid/base stimulation has been used to provide a method of distinguishing between closely related structural isomers at the single molecule level. Zhang *et al*. investigated the properties of two diketopyrrolopyrrole (DPP) isomers, known as SDPP and SPPO, before and after the introduction of acid. They found that the two DPP isomers displayed similar single molecule conductance values in their neutral states, but the conductance of SPPO was found to

decrease by one order of magnitude after addition of acid, whereas no significant change was observed for SDPP. It was determined that this discrepancy arose due to the occurrence of DQI in the protonated form of SPPO, where the dominant resonance structure is cross-conjugated, in contrast to the linearly conjugated neutral structure. It was also reported that on deprotonation of SPPO with base, the conductance was restored to a similar value to the neutral state. This work showed that the conductance of QI-based molecular devices can be reversibly switched on or off on demand via acid/base stimulation, displaying significant potential for applications in switching devices.[81]

1.7 Primary Research Objectives

Understanding the relationships between the charge transport behaviour of molecules in molecular junctions and their structural features is of great importance for the development of molecular electronic devices. In this project, single molecule conductance measurements have been performed on several different series of molecules, with the molecular wires in each series displaying variations on a common structural motif. These experiments have been performed with a particular emphasis on investigating the role of interference effects and anchoring moieties in controlling the electrical properties of molecular junctions in order to determine how these factors influence the conductance of molecules with closely related structures.

The second chapter of this work describes the synthesis of a series of three pyridine-terminated molecular wires based on the same core structure and the subsequent measurement of the electrical properties of these molecules via the STM-BJ technique. These experiments investigate the effect of changing the ring position of the N atoms on the pyridyl anchoring groups on the electronic transmission through the molecular junction and how this influences the molecular conductance. These experimental results are compared with theoretically predicted electronic transmission spectra for the relevant structures, allowing the role of interference effects in controlling the conductance properties of pyridine-terminated molecules to be determined.

The third chapter discusses the STM-BJ measurement of a series of three fluorene-derived conjugated molecular wires. The molecules studied in this series feature identical anchoring and linking groups and possess similar central conjugated units which differ in the number of cross-conjugated ketone moieties present. The introduction of ketone groups orthogonal to the primary charge transport pathway is expected to result in interference effects in the form of

Fano resonances, which have the potential to cause significant shifts in the electronic transmission through the molecular junctions. This provides a method for assessing the influence of cross-conjugation on the molecular conductance properties.

The fourth chapter focuses on the STM-BJ measurement of a pair of molecules featuring triazolyl anchoring moieties. These two molecular structures incorporate 1,2,4-triazole rings at each end of the molecular wire, with a pair of N atoms at the molecular termini which are expected to bind to metallic electrodes to form metal-molecule-metal junctions via multidentate binding. The experiments performed provide insight into the stability of molecular junctions with anchoring groups incorporating multiple heteroatoms and the influence of anchoring moieties featuring more than one binding site on the electrical properties.

The fifth chapter provides information about the experimental techniques used in this work. This section includes the general synthetic approaches used, details of the synthetic pathways used to prepare the target molecules where relevant and analysis of the sample compounds prepared in this work after synthesis. Additionally, this section includes information about the use of the STM-BJ technique to measure the electrical properties of all the molecules featured in this study.

The final section of this thesis includes an appendix featuring the results from all experimental measurements and the final conclusions from this work.

Chapter 2: Investigation of Structure-Property Relationships and Quantum Interference Effects in Pyridine-Terminated Molecular Wires

2.1 Introduction to Pyridine-Terminated Molecular Wires

In a metal-molecule-metal junction, anchoring groups play a crucial role in facilitating charge transport through the junction. Different anchoring moieties display significant variations in binding to metallic electrodes and it is therefore highly important in the development of molecular electronic devices to understand how the metal-molecule contact group affects the overall charge transport properties of the junction. This chapter focuses on the investigation of the properties of a series of molecules incorporating pyridyl anchoring groups (Scheme 2.1). These molecular wires share a common linking group and the same type of anchoring group, but the positions of the pyridyl contact groups on the aromatic rings have been varied between the *para*- and *meta*- positions relative to the amine N atom to determine how changing the positions of the anchoring sites influences electronic transmission through the molecular junction and hence controls the conductance.

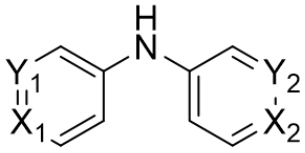

1 X_1, X_2 = N & Y_1, Y_2 = CH
2 Y_1, Y_2 = N & X_1, X_2 = CH
3 Y_1, X_2 = N & X_1, Y_2 = CH

Scheme 2.1. General structure of molecular wires based on the dipyridylamine core unit structure.

Pyridine terminal groups, which are notable for incorporating the terminal anchoring moieties into the conjugated chain as opposed to being attached as ring substituents, have been used as anchoring moieties for molecules in a number of molecular electronics studies.[10,12,39,82] These studies have shown that pyridine anchoring groups form highly stable metal-molecule contacts with metallic electrodes such as Au, with the N atoms acting as the molecular anchoring sites. The molecule-electrode contacts formed are robust but chemically selective, as the anchoring groups datively bind with high specificity to under-coordinated sites on the electrode surface, resulting in stable molecular junctions with well-defined binding geometries.[39] As a consequence, the measured conductance values for pyridine-terminated molecules are more reproducible than the values obtained for molecules with covalent anchoring groups such as thiols, which typically form junctions with a range of binding geometries.[46] This makes it easier

to determine the average conductance properties of molecular junctions comprising molecules with pyridine anchoring moieties than structures with covalent binding anchoring moieties.

In addition to its advantages relative to covalent binding groups, the properties of pyridine anchoring moieties also compare favourably to the other two widely used N-based donor-acceptor anchoring groups. Hong *et al*. measured the electrical properties of a series of four tolane molecular wires with different anchoring groups and reported that pyridine anchors display both higher stability and higher binding strength with Au electrodes than amine ($-NH_2$) and nitrile (-CN) anchoring groups.[82] This can be attributed to the incorporation of the anchoring moieties into the core of the molecular wire, with no intermediate bonds between the molecular core and electrodes, which contributes to strong Au-N interactions between the molecule and electrode. This compares favourably with Au-N interactions in nitriles, where the long, stiff molecular structure results in poor binding stability, or amines, where steric hindrance caused by H atoms bonded to the amine N atom reduces the binding strength. Likewise, combined conductance and force measurements by Frei *et al*. have demonstrated that the Au-N bond rupture force is higher for 4,4′-bipyridine than for analogous amine-terminated molecules, indicating that the Au-N binding strength is higher for structures with pyridine anchoring moieties.[83]

The combination of high stability and high binding strength results in strong molecule-electrode coupling for pyridine anchoring groups, which is expected to increase charge transport efficiency through the molecular junction and therefore explains why pyridine-terminated molecules typically display relatively high conductance values. This has been supported by research by Li *et al*. investigating the influence of anchoring groups on the molecular conductance of porphyrins. They measured the electrical properties of porphyrins with a range of seven different anchoring groups and found that molecules with pyridyl anchoring moieties displayed the highest conductance, which was again attributed to the high pyridyl N-Au binding strength.[84] Also, a more general practical advantage of using pyridine anchoring moieties is their tolerance for wide ranging reaction conditions. This eliminates the need to use protecting groups in the synthesis of the target compounds, making it easier to access a broad variety of possible molecular structures with pyridine terminal groups.

Multiple research groups have reported experimental studies which focus specifically on the electrical properties of pyridine-terminated molecular wires. In 2010, Kamenetska *et al*. measured the conductance of a series of four molecular wires with pyridine anchoring groups

using the STM-BJ technique.[39] They found that all four pyridine-terminated molecules display bistable conductance signatures, with distinct high and low conductance peaks representing different molecular junction configurations. For the three π-conjugated molecules in the study, they also performed theoretical calculations which showed that the conjugated pyridine-terminated molecules display low β (decay constant) values, indicating that charge transport through these structures predominantly occurs via the π-system. They deduced that the low conductance peak corresponds to a vertical molecular junction geometry where the Au-N bond is perpendicular to the conjugated π-system, with relatively weak coupling between the Au-N bond and π-system, whereas the high conductance feature represents a tilted junction geometry with stronger coupling between the Au-N bond and π-system. The multiple conductance states of pyridine-terminated anchoring groups, inherent to the N-Au molecule-electrode coupling, make them promising candidates for applications in nanoscale switching devices.

In addition to distinguishing distinct high and low conductance features, Kamenetska *et al*. also performed calculations which established that the LUMO pathway is favoured for charge transport through molecules with pyridine anchoring groups. This is attributed to the position of the pyridine N lone pair, which lies in the weakly conductive σ system of the molecule orthogonal to the main conductance pathway via the conjugated π-system, minimising the contribution of the lone pair to charge transport through the molecular junction. Also, the electron withdrawing pyridine group lowers the energy of the π*-antibonding orbitals towards the metallic Fermi Energy (E_F), which reduces the energy offset between these orbitals and the E_F and therefore facilitates the LUMO-dominated charge transport pathway.[39] The results reported for these pyridine-terminated molecules are consistent with theoretical electronic transmission calculations for 4,4′-bipyridine performed by Bagrets *et al*., as their work predicted that this molecule should display two distinct molecular junction geometries. They also predicted that charge transport through 4,4′-bipyridine should predominantly take place via the LUMO pathway.[85] These theoretical predictions have been experimentally verified by the simultaneous measurement of electrical and thermoelectric currents through pyridine-terminated molecular wires using the STM-BJ technique by Widawsky *et al*., which show that the thermoelectric current has a negative value for molecules with pyridyl anchoring moieties, indicative of a LUMO-dominated conductance pathway.[86]

In another study focusing on pyridine-terminated compounds, Quek *et al*. found that the conductance of molecules with pyridine anchoring groups is highly sensitive to the molecular junction geometry. They reported that at short molecule-electrode separation distances, the

high conductance state of the molecular junction dominates, with the low conductance state prevalent at longer separation distances. They also showed that the molecular junctions can rearrange between the two geometries on changing the electrode separation distance, allowing molecules with pyridine anchoring groups to be switched between the high and low conductance states through compression or elongation of the molecular junction.[12] This differs from the behaviour displayed by amine-terminated molecules, where changes in the molecular junction geometry have little effect on the conductance and mechanically induced switching is not observed.[87] This explains why the conductance histograms for pyridine-terminated molecules display two conductance peaks, whereas amine-terminated compounds give a single well-defined peak. These findings have been supported by simultaneous conductance and rupture force measurements by Aradhya *et al*., which also show that pyridine-terminated molecules form molecular junctions with two binding geometries displaying distinct high and low conductance junction configurations.[88] The ability to mechanically change the molecular junction geometry is intriguing as it provides a highly useful mechanism for switching the conductance of the junction, with significant potential for applications in molecular electronic switching devices. However, it should be noted that not all pyridine-terminated molecules display bistable conductance signatures. Tam *et al*. measured the electrical properties of a series of pyridine-terminated dithienylethene derivatives and observed a single broad conductance peak for these compounds, which they attributed to the overlap of the conductance peaks for the two molecular junction configurations.[89] This indicates that the two molecular junction geometries exhibit similar charge transport behaviour, which is less promising for applications in switching devices than molecules displaying distinct high and low conductance peaks.

In this project, the electrical properties of three isomers of dipyridylamine (compounds **1-3**) have been studied. This series of compounds utilises the ability to substitute the pyridyl N atom in different positions of the pyridine ring relative to the amine linking group, which can be accessed by making appropriate changes to the synthetic pathway (Scheme 2.2). This allows the influence of the pyridyl N anchoring site position on the electronic transmission and molecular conductance to be investigated. The 4,4′-dipyridylamine (**1**) and 3,3′-dipyridylamine (**2**) isomers have two pyridine rings with the N atom substituted in the same position relative to the amine linker, so they are collectively referred to as the symmetric dipyridylamine molecules. By contrast, in 3,4′-dipyridylamine the two pyridyl rings have N atoms in different positions, so this structure is described as asymmetric. In addition to the three dipyridylamine molecules, the conductance of dipyridylethyne (compound **4**) has also been measured to

provide a ‘control’ molecule for this series of molecular wires, as it has a broadly similar structure and incorporates the same pyridyl anchoring moieties. The charge transport properties of this molecule have been measured in several previous studies, which means this structure provides a reliable point of comparison for the conductance of the dipyridylamine molecular wires.[82,90,91]

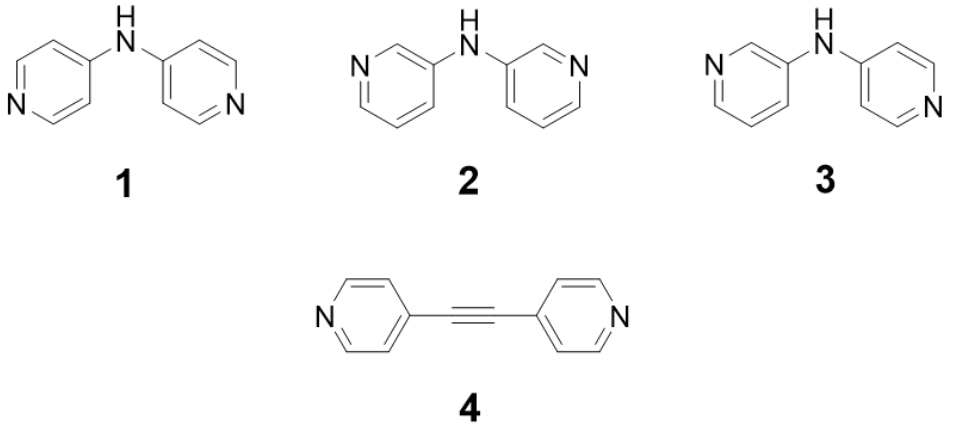

Scheme 2.2. Molecular structures of the three isomeric dipyridylamine compounds **1-3** in addition to the ‘control’ molecule **4**, 4,4′-dipyridylethyne.

The investigation of the electrical properties of the dipyridylamine isomers can be compared with an earlier study by Naghibi *et al*. involving the measurement of the conductance of a series of diazacarbazole molecules.[92] The dipyridylamine molecules have several key similarities with the carbazole-based compounds, as they have pyridine anchoring moieties and a bridging N atom possessing a lone pair of electrons between the pair of pyridyl rings. It has been proposed that the lone pair on the bridging carbazole N atom facilitates electronic coupling between the two rings to provide an efficient electronic transmission pathway through the molecule, leading to relatively high conductance values for carbazole-derived compounds.[93] It is predicted that the main charge transport pathway in the dipyridylamine molecules will pass through the bridging amine N atom, so similar behaviour is expected in this series of compounds. However, the molecules in this study differ from the diazacarbazoles as they do not have fused core structures with inter-ring C-C bonds connecting the pyridyl rings, removing this charge transport pathway through the molecular core structure. This is significant because the earlier diazacarbazole study proposes that charge transport via the pyrrolic N atom pathway (analogous to the amine N atom pathway in the dipyridylamine isomers) is more efficient than via the C-C bond pathway, where electronic transmission is suppressed by DQI effects.[92] This suggests the dipyridylamine molecules are likely to display efficient electronic transmission

and the measurements are therefore expected to display high conductance values. This should also provide greater insight into the influence of this linking group on the electrical properties of these molecules, as no alternative C-C bond charge transport pathway is available.

In this series of molecular wires, there is particular interest in the measurement of the electrical properties of the 3,3′-dipyridylamine molecule (**2**). This is because preliminary theoretical calculations investigating charge transport behaviour predict that electronic transmission through the HOMO-LUMO gap in this molecule will be significantly higher than for the other symmetric molecule, 4,4′-dipyridylamine (**1**) (Figure 2.1). The charge transport calculations for these structures were performed by Sara Sangtarash at Lancaster University using the Non-equilibrium Green's Function (NEGF) formalism in combination with the mean-field Hamiltonian determined from the converged Density Functional Theory (DFT) calculation, allowing the electronic transmission coefficient (T(E)), describing the transmission of electrons of energy E between the left and right electrodes via the molecular bridge, to be calculated using the Landauer formula. The profile of the transmission curves obtained from the calculations for the two symmetric dipyridylamine isomers is broadly similar, as there are no prominent resonance or anti-resonance features in the transmission gap between the HOMO and LUMO resonances, but transmission at the lowest point of the curve is predicted to be approximately two orders of magnitude higher for 3,3′-dipyridylamine (**2**). It has previously been reported that the insertion of heteroatoms into the core structures of aromatic molecular wires in different positions leads to changes in QI behaviour, for example by switching DQI pathways via the molecule on or off to suppress or enhance the conductance.[67] For this reason the 3,3′-dipyridylamine molecule (**2**) in this study is intriguing as it is postulated that the occurrence of CQI effects in this structure leads to significantly enhanced transmission through this molecular wire.

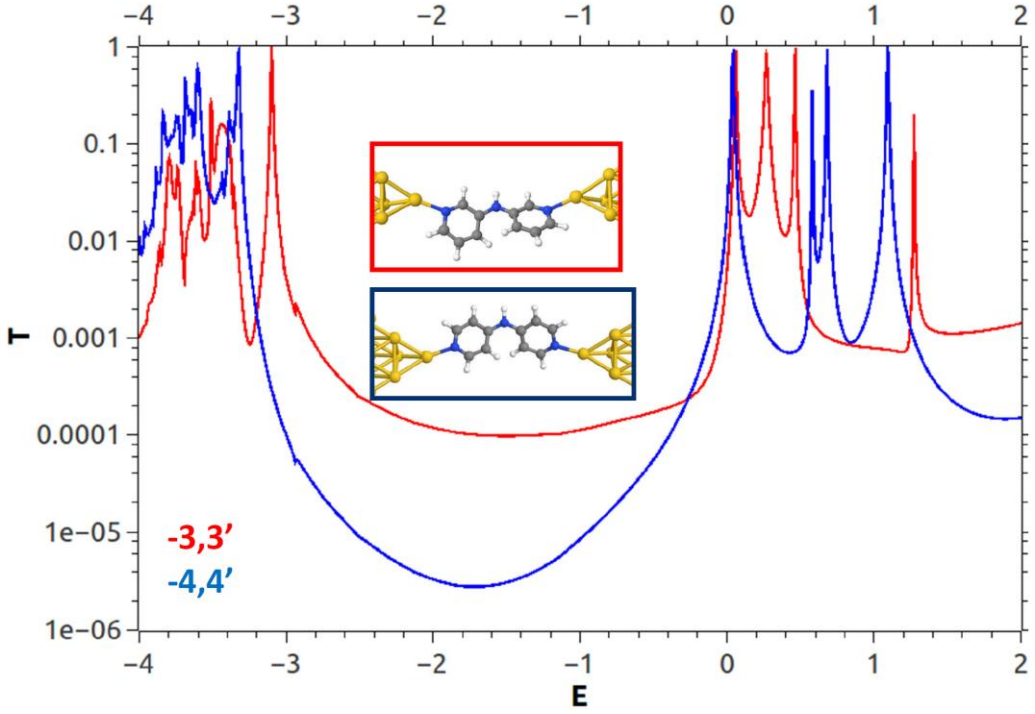

Figure 2.1. Theoretical electronic transmission plot showing electronic transmission curves as a function of energy (T(E)) for the two symmetric dipyridylamine isomers identified by the legend, 4,4′-dipyridylamine (**1**) (blue) and 3,3′-dipyridylamine (**2**) (red). Inset: Model molecular junction structures for 3,3′-dipyridylamine (**2**) (top, red) and 4,4′-dipyridylamine (**1**) (bottom, blue).

The molecular junction conductance is directly proportional to the electronic transmission, which means that if the theoretical model accurately predicts transmission through the molecular junction and the metallic E_F is located within the HOMO-LUMO gap, the experimental measurement of the 3,3′-dipyridylamine molecule (**2**) is likely to display an unusually high single molecule conductance value. Additionally, the tall peaks observed for the HOMO and LUMO resonances in the transmission spectra indicate that the interactions between the pyridyl N atoms and the electrodes are predicted to be strong. This indicates that these molecules should form stable molecular junctions with high molecule-electrode coupling strength, which is consistent with the strong molecule-electrode coupling reported for pyridine-terminated carbazole derivatives.[92] The combination of strong molecule-electrode coupling and high anchoring group-electrode binding strength is expected to contribute to high measured conductance values for all the dipyridylamine molecules, which implies that any further enhancement of the conductance for 3,3′-dipyridylamine (**2**) can be attributed to interference

effects intrinsic to the structure of that particular isomer. The experimental investigation of this series of molecules is therefore valuable in expanding the knowledge of structure-property relationships in conjugated molecular wires. It also allows the accuracy of theoretical electronic transmission calculations in predicting experimentally observed conductance in these molecules to be evaluated, thereby enhancing the overall understanding of charge transport behaviour in molecular junctions.

2.2 Synthesis and Characterisation of Pyridine-Terminated Molecular Wires

The dipyridylamine molecular wires studied in this project were synthesised, purified and characterised using common standard laboratory techniques. The target dipyridylamine molecules **2** and **3** (Scheme 2.2) featured in this study were prepared via the Buchwald-Hartwig cross-coupling of an aryl amine with an aryl halide.[94] The dipyridylamine molecule **1** was synthesised by Saman Naghibi at the University of Liverpool via the Buchwald-Hartwig cross-coupling of an aryl amine with an aryl halide. The 'control' dipyridylethyne molecule **4** was synthesised by Dr Jonathan Ward at the University of Liverpool via the Ullmann cross-coupling of an aryl halide with trimethysilylacetylene. This synthetic work was conducted in order to permit the investigation of the influence of structure-property relationships on the charge transport properties of the target molecules. The Buchwald-Hartwig cross-coupling approach was selected for the synthesis of these compounds as it is a proven method for forming C-N bonds which uses mild conditions and avoids the production of toxic by-products.

Preparation of 3,3′-Dipyridylamine

The target compound 3,3′-dipyridylamine (**2**) was prepared by a single Buchwald-Hartwig cross-coupling reaction of 3-aminopyridine and 3-bromopyridine in 31 % overall yield (Scheme 2.3). The product was fully characterised by ^{1}H and ^{13}C NMR spectroscopy, mass spectrometry and elemental microanalysis, ensuring that the compound was pure prior to performing molecular conductance measurements (refer to Chapter 5, Section 5.2.1 for full details of synthesis and characterisation).

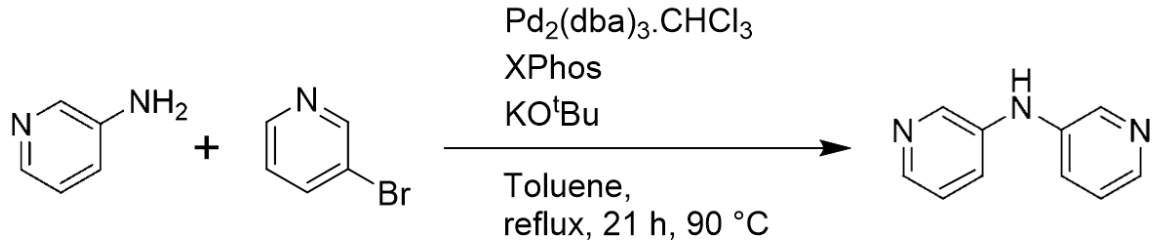

Scheme 2.3. Synthesis of 3,3′-dipyridylamine (**2**)

Preparation of 3,4′-Dipyridylamine

The target compound 3,4′-dipyridylamine (**3**) was prepared by a single Buchwald-Hartwig cross-coupling reaction of 4-aminopyridine and 3-bromopyridine in 83 % overall yield (Scheme 2.4). The product was fully characterised by ^{1}H and ^{13}C NMR spectroscopy, mass spectrometry and elemental microanalysis, ensuring that the compound was pure prior to performing molecular conductance measurements (refer to Chapter 5, Section 5.2.2 for full details of synthesis and characterisation).

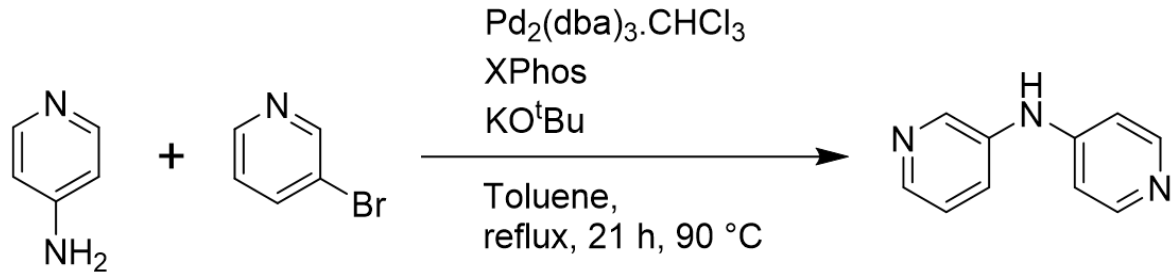

Scheme 2.4. Synthesis of 3,4′-dipyridylamine (**3**)

Preparation of 4,4′-Dipyridylethyne

The target compound 4,4′-dipyridylethyne (**4**) was prepared by a double Ullmann type cross-coupling reaction of 4-iodopyridine and trimethylsilylacetylene in 43 % overall yield (Scheme 2.5). The product was characterised by ^{1}H and ^{13}C NMR spectroscopy to confirm that the target molecule had been obtained prior to performing molecular conductance measurements (refer to Chapter 5, Section 5.2.3 for full details of synthesis and characterisation).

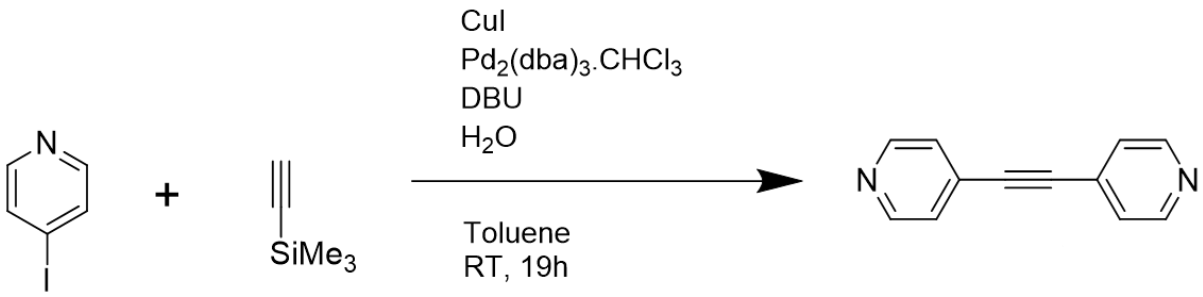

Scheme 2.5. Synthesis of 4,4′-dipyridylethyne (**4**)

2.3 STM-BJ Measurement of Pyridine-Terminated Molecular Wires

The electrical properties of the pyridine-terminated molecular wires have been measured in solution using the STM-BJ technique. For each measurement, a 10^{-3} M solution of each molecular wire was prepared by dissolving the relevant compounds (molecules **1**-**4**) in a mixed solution of mesitylene and THF (4:1). All measurements were performed at a fixed bias voltage of 200 mV. Thousands of current-distance (I-s) curves were collected from each STM-BJ experiment and all traces obtained were analysed, with no data selection methods used to construct the conductance histograms.

2.4 Experimental Results for Pyridine-Terminated Molecular Wires

The experimental results from the measurement of the electrical properties of the dipyridylamine molecular wires are presented in the form of semi-logarithmic 1-dimensional (1-D) conductance plots and 2-dimensional (2-D) conductance-distance histograms. These plots feature conductance peaks and conductance clouds which are attributed to the formation of single molecule junctions. The 1-D conductance plot obtained from the STM-BJ measurement of 4,4′-dipyridylamine (**1**) shows a sharp conductance peak at G_0, corresponding to a single atomic Au-Au point contact bridging the electrode gap. Similar peaks are also

present at higher conductance values, representing multiple atomic Au-Au contacts. More significantly, the plot also displays two distinct peaks at conductance values of $10^{-3.0}$ G_0 and $10^{-4.0}$ G_0 (Figure 2.2), several orders of magnitude lower than the single atomic point contact peak. These peaks represent two distinct molecular junction configurations with the molecule bridging the two metallic electrodes and show a marked difference in molecular conductance between the high and low conductance geometries, which are separated by one order of magnitude. The conductance values obtained for the high and low conductance junction configurations are comparatively high, with both peaks significantly higher than the noise level at approximately $10^{-6.0}$ G_0, which can be attributed to the strong molecule-electrode coupling provided by the pyridine anchoring groups incorporated into the molecular core structure.

The 2-D conductance plot obtained from the same measurement of this compound shows a conductance cloud which corresponds to the molecular conductance features observed in the 1-D plot. This histogram shows that the conductance of the molecular junction decreases as the separation between the electrodes increases and the molecule is stretched until junction cleavage occurs. This is represented by the end of the molecular conductance cloud at the maximum stretching distance. The two molecular junction configurations can be distinguished in this plot as the low conductance configuration displays a slightly longer maximum electrode separation distance at a lower molecular conductance value.

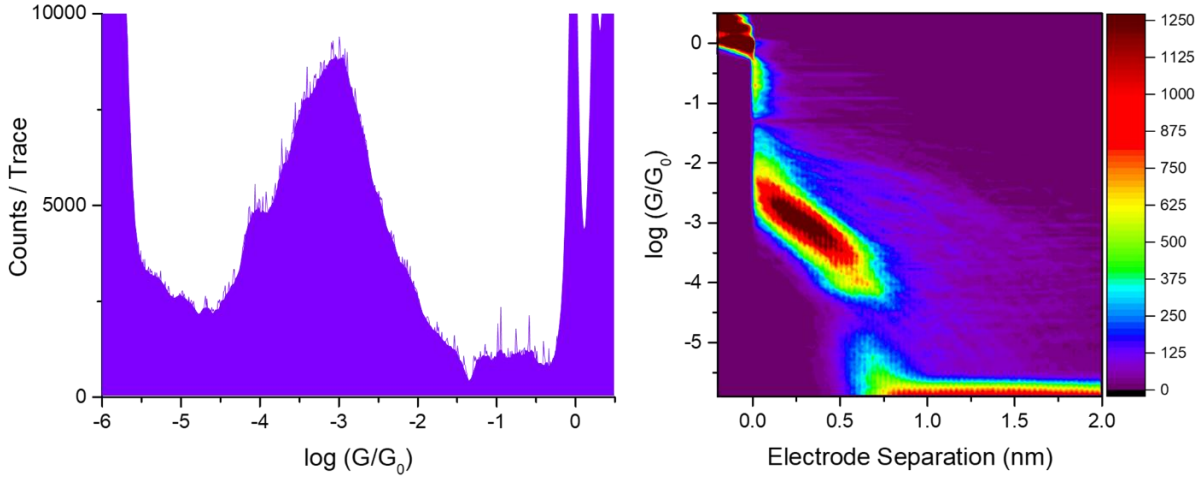

Figure 2.2. STM-BJ measurement of the molecular wire 4,4′-dipyridylamine (**1**) in solution (solvent: mesitylene/THF (4:1)) at 200 mV bias voltage.

The 1-D and 2-D conductance plots recorded for 3,3′-dipyridylamine (**2**) also display two distinct conductance features, with most probable conductance values of $10^{-3.5}$ G_0 and $10^{-3.9}$ G_0 for the high and low peaks respectively (Figure 2.3). Closer analysis of the conductance plots

for these two isomers reveals that the experimentally measured values for the low conductance peaks for 4,4′-dipyridylamine (**1**) and 3,3′-dipyridylamine (**2**) are very similar (approximately $10^{-4.0}$ G_0 for both molecules). By contrast, the measured conductance value of the high conductance peak for 4,4′-dipyridylamine (**1**) (at $10^{-3.0}$ G_0) is approximately half an order of magnitude higher than the equivalent peak for 3,3′-dipyridylamine (**2**) ($10^{-3.5}$ G_0). The similar conductance features observed for the two molecules provide strong evidence that the dipyridylamine compounds reproducibly form stable molecular junctions, particularly as the bistable conductance signatures are consistent with molecular junctions binding to the electrodes via pyridine anchoring moieties.[39]

However, it is also apparent that the observed conductance behaviour for 3,3′-dipyridylamine (**2**) differs significantly from the predictions given by theoretical electronic transmission plots, which indicated that transmission through the HOMO-LUMO gap would be approximately two orders of magnitude higher for the 3,3′-isomer (**2**). This is important because higher electronic transmission efficiency through the molecular junction is expected to result in an increase in molecular conductance. However, the experimental 1-D and 2-D conductance plots show that the low conductance geometries for the two molecules display similar conductance values, whereas 4,4′-dipyridylamine (**1**) gives a higher conductance value than the 3,3′-isomer (**2**) in the high conductance geometry. These results imply that charge transport efficiency through the 4,4′- and 3,3′-dipyridylamine molecules (**1** & **2**) in the low conductance junction configuration is similar, with more efficient transmission through the 4,4′-isomer (**1**) in the high conductance geometry, which does not match the predicted transmission behaviour.

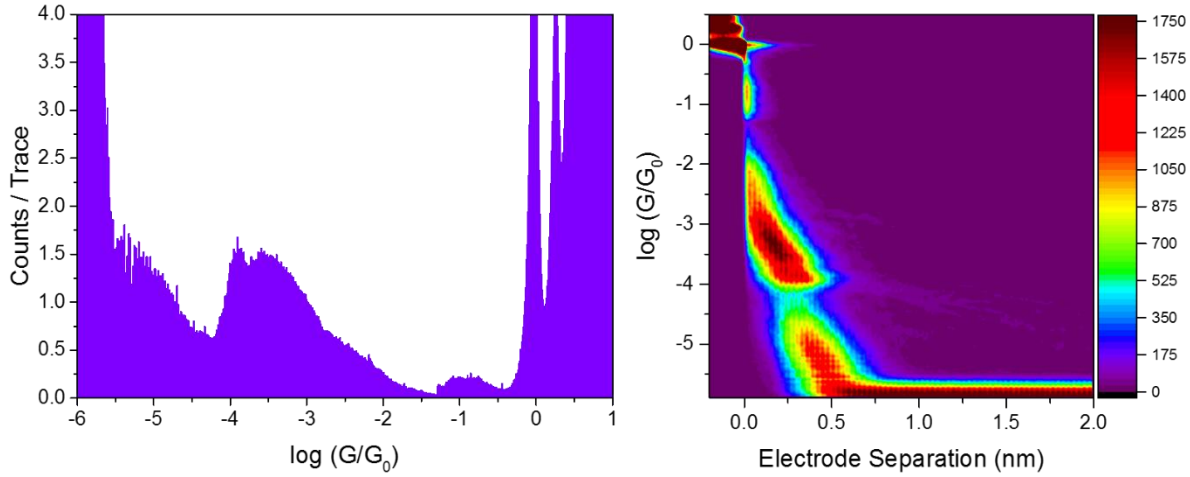

Figure 2.3. STM-BJ measurement of the molecular wire 3,3′-dipyridylamine (**2**) in solution (solvent: mesitylene/THF (4:1)) at 200 mV bias voltage.

One possible explanation for the lack of conductance variation between the two molecules is evident in the electronic transmission plot shown earlier in this chapter (Figure 2.1). This plot shows that the LUMO resonances for both molecules are very close in energy to the predicted position of the Au electrode E_F at E = 0. Also, the transmission functions for the two structures at E_F are close in value, in contrast to the large discrepancy observed closer to the centre of the HOMO-LUMO gap. This is significant because electronic transmission is highly sensitive to the position of the metallic E_F and transmission in pyridyl-terminated molecules predominantly occurs via the LUMO pathway. As a consequence, if the LUMO energy is close to the predicted E_F, the small LUMO-E_F energy separation is the dominant factor controlling transmission through the molecules rather than QI effects. This alignment of the molecule and electrode orbitals means there is expected to be only a small difference in transmission between the two structures at E_F and the two structures are therefore expected to display similar conductance values, in better agreement with the experimental results. Additionally, the proximity of the LUMO to E_F explains why 3,3′-dipyridylamine (**2**) does not display a higher conductance than the 4,4′-isomer (**1**) despite having a smaller theoretically predicted HOMO-LUMO energy gap, as the HOMO is expected to be too low in energy relative to E_F to influence charge transport behaviour. Closer inspection of the transmission plots also shows that although the transmission of 3,3′-dipyridylamine (**2**) is predicted to be two orders of magnitude higher than the 4,4′-isomer (**1**) in the centre of the HOMO-LUMO gap, at energy values slightly lower than E = 0 the predicted transmission through 4,4′-dipyridylamine (**1**) is higher than through the 3,3′-isomer (**2**). If the metallic E_F lies in this region, this would explain why the conductance value of the high conductance junction geometry for 4,4′-dipyridylamine (**1**) is higher than the conductance of the equivalent configuration for the 3,3′-isomer (**2**).

The 1-D and 2-D conductance plots for the asymmetric compound, 3,4′-dipyridylamine (**3**), also display distinct high and low conductance peaks corresponding to different molecular junction configurations (Figure 2.4). This conductance signature is in agreement with the features observed for the other two measured dipyridylamine isomers and provides further evidence that the pyridine anchoring groups permit stable molecule-electrode binding. However, the conductance values for this molecule are significantly lower than the values corresponding to the analogous peaks in the two symmetric compounds. The conductance plots obtained for the 3,4′- isomer (**3**) give a high conductance peak at $10^{-4.0}$ G_0, which has a conductance value half an order of magnitude lower than the 3,3′-dipyridylamine (**2**) high

conductance peak and one order of magnitude lower than the equivalent peak for the 4,4′-isomer (**1**). The low conductance peak for 3,4′-dipyridylamine (**3**) is found at $10^{-4.6}$ G_0, which is over half an order of magnitude lower than the analogous peaks for both symmetric molecules. These results indicate that charge transport through the 3,4′-dipyridylamine molecule (**3**) in both molecular junction configurations is significantly less efficient than through junctions comprising either the 4,4′- or 3,3′- isomers (**1** & **2**).

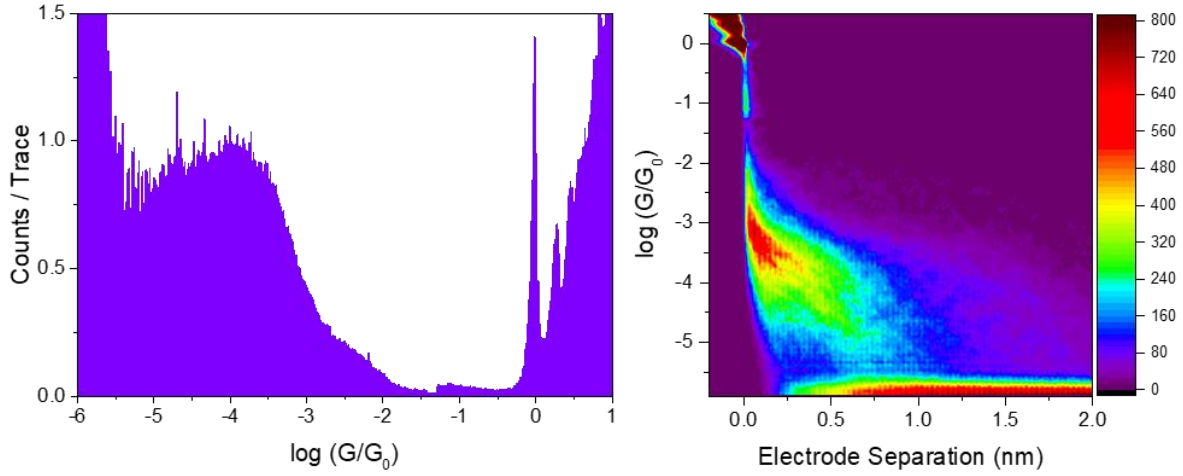

Figure 2.4. STM-BJ measurement of the molecular wire 3,4′-dipyridylamine (**3**) in solution (solvent: mesitylene/THF (4:1)) at 200 mV bias voltage.

It is possible that the lower conductance values obtained for the 3,4′-dipyridylamine molecule (**3**) relative to the symmetric molecules may be caused by DQI effects suppressing the molecular conductance through this structure. However, the decrease in conductance observed for both conductance peaks in the asymmetric isomer could instead be attributed to differences in the alignment of the molecular orbitals with the metallic E_F, with a larger energy separation between the orbitals resulting in weaker molecule-electrode coupling. This is plausible if the molecular orbitals for the symmetric dipyridylamine molecules are located close to the metallic E_F as predicted. It is also possible that the positions of the pyridyl N anchoring sites in 3,4′-dipyridylamine may lower the molecule-electrode coupling strength, leading to weaker electronic transmission through this molecule than for either the 3,3′- or 4,4′- isomers (**1** & **2**). This is significant because in pyridine-terminated molecules the conductance is sensitive to the molecular junction geometry, which means that even a relatively small difference in configuration can lead to significant changes in conductance.[12] This theory is supported by the magnitude of the conductance suppression for the two peaks relative to the equivalent peaks in 3,3′-dipyridylamine (**2**), which is not expected to display DQI effects, as the conductance

values of the high and low conductance features for the 3,4′-isomer (**3**) are both approximately half an order of magnitude lower. If DQI behaviour was responsible for the observed reduction in molecular conductance, the decrease would be expected to be larger for the high conductance peak than the low conductance peak, as DQI effects cause direct suppression of electronic transmission through the molecular wire. However, the similar decrease in conductance for both the high and low conductance peaks indicates that electronic transmission efficiency is reduced to a similar extent in both molecular junction configurations for 3,4′-dipyridylamine (**3**), suggesting this behaviour is likely to be explained by weaker molecule-electrode coupling.

The experimentally measured conductance values obtained for all molecules in this series at 200 mV bias voltage can be directly compared (Table 2.1). For all three isomeric dipyridylamine molecular wires (**1**-**3**), bistable conductance plots are observed, in agreement with the observation that pyridine-terminated molecular wires consistently display two distinct conductance peaks. For all three molecules, the two peaks represent different molecule-electrode binding geometries, so the conductance values for both the high and low conductance peaks are reported for each molecule. Comparison with previous measurements on pyridine-terminated molecules by Kamenetska *et al*. suggests it is likely that the high conductance peak corresponds to a molecular junction where the dipyridylamine molecule is bound between the tip and substrate surface at an angle. The low conductance peak is likely to correspond to an arrangement where the molecule is fully stretched between the Au electrode contacts.[39] This is because the efficiency of electronic transmission through a molecular junction decreases with increasing length and in the fully stretched configuration the charge transport pathway is longer, leading to reduced conductance compared to the configuration where the molecule is bound to the electrodes at an angle. This theory is supported by the 2-D conductance histograms observed for all three dipyridylamine molecules (**1**-**3**), as the conductance plateaus in the plots for all three molecules consistently show that molecular conductance decreases with increasing electrode separation distance. Additionally, the 2-D plots for all three molecules show that the regions of the conductance clouds corresponding to the low conductance molecular junction geometries extend to slightly longer electrode separation distances than the regions representing the high conductance junction configurations of the respective molecules, indicated by the presence of a small notch in the conductance cloud at high electrode separation distance between the features representing high and low conductance junction geometries.

This theory is also supported by work by Aradhya *et al*., who reported that pyridine-terminated molecules initially form molecular junctions in the high conductance configuration after

rupture of the metallic contact. They observed that the low conductance geometry is always preceded by the high conductance geometry, indicating that the molecular junction undergoes rearrangement to form the low conductance geometry on elongation of the molecular junction.[88] Significantly, the 2-D plots for the three molecules (**1**-**3**) reveal that the conductance features corresponding to high conductance junction geometries form at an electrode separation distance of zero, indicating that when molecular junction formation occurs the molecule binds to the electrodes in this configuration immediately after cleavage of the Au-Au point contact. By contrast, the low conductance features are not observed at zero electrode separation distance for any of these molecules and only become apparent at longer electrode separation distances, which provides further evidence that the molecular junctions do not initially form in the low conductance geometry and strongly indicates that this configuration occurs only after elongation of the molecular wire in the junction. It is therefore highly probable that molecular junctions initially bind to the tip and substrate in the more tilted high conductance junction geometry and switch to the less tilted low conductance geometry as the molecule is stretched and the electrode separation distance increases.

Table 2.1. Conductance values for molecules **1-4** (4,4′-, 3,3′- and 3,4′-dipyridylamine and 4,4′-dipyridylethyne) corresponding to high conductance (HC) and low conductance (LC) features obtained from STM-BJ measurements at 200 mV bias voltage.

Molecule	**Conductance (G) / G_0**	
	HC	**LC**
1 / 4,4′-dipyridylamine	$10^{-3.0}$	$10^{-4.0}$
2 / 3,3′-dipyridylamine	$10^{-3.5}$	$10^{-3.9}$
3 / 3,4′-dipyridylamine	$10^{-4.0}$	$10^{-4.6}$
4 / 4,4′-dipyridylethyne	$10^{-3.7}$	-

Additional evidence that the dipyridylamine molecules initially bind in the more tilted high conductance junction geometry before switching to the less tilted low conductance geometry can be found by comparing these results with work by Quek *et al*., which indicated that the conductance of pyridine-terminated molecular wires is sensitive to the orientation of the Au-N bond. They performed theoretical calculations which predicted that molecular conductance would increase with the Au-N tilt angle and this was attributed to enhanced electronic coupling between the molecule and electrode orbitals.[12] More specifically, they reported that this is

because electronic coupling is expected to be stronger for junctions where the Au-N bond is tilted relative to the pyridine ring π-system than for junctions where the Au-N bond is perpendicular to the π-system. Experimental results agreed with this prediction, as junctions with smaller electrode separation distances and larger tilt angles gave higher conductance values than junctions with larger separation distances and smaller tilt angles. This dependence of molecular conductance on the junction tilt angle explains why the conductance of the pyridine-terminated molecules in this work decreases as the molecular junction is stretched. It also explains why the dipyridylamine molecules display distinct high and low conductance peaks with a large difference in conductance, as the molecule-electrode coupling is predicted to be significantly stronger in the tilted high conductance configuration and this facilitates more efficient charge transport through molecular junctions in the tilted junction geometry.

Further information about the characteristics of the dipyridylamine molecular junctions, including the nature and strength of metal-molecule coupling via the contact groups, can also be gained from the presence of multiple peaks in the conductance plots. In a theoretical study focusing on the predicted electronic transmission behaviour of 4,4′-bipyridine, Bagrets *et al*. predicted that the pyridine anchoring group at each end of the molecule can form contacts with the Au electrode via either strong or weak coupling. As each molecule has two anchoring groups at opposite ends of the structure, three N-Au molecule-electrode coupling combinations (strong-strong, strong-weak and weak-weak) are possible for each molecular junction.[85]

Applying the same principles to the dipyridylamine molecular wires, which all possess two pyridine anchoring moieties, it is possible that the low conductance peak could correspond either to molecular junctions with strong Au-N coupling via one anchoring moiety and weak Au-N coupling via the other anchoring group, or to junctions with weak Au-N coupling at both anchoring groups. In the former scenario, the high conductance peak would represent junctions with strong Au-N coupling at both anchoring sites and the lack of a third conductance peak would be attributed to molecular junctions with weak-weak molecule-electrode coupling giving conductance values too low to practically measure (below the noise level of the instrument). However, close investigation of conductance histograms obtained from the measurement of 4,4′-bipyridine by Quek *et al*. reveals a shoulder peak attached to the high conductance peak with a slightly higher conductance which does not give a distinct measurable conductance value, in contrast to the low conductance peak which is easy to distinguish.[12] The pyridine-terminated molecules in this work display similar conductance features and from this it can be deduced that the low conductance peak is likely to correspond to molecular junctions

with weak Au-N coupling via both pyridyl anchoring groups. This also indicates that the high conductance peak represents a combination of molecular junctions with strong Au-N coupling at both anchoring groups and junctions with strong-weak Au-N coupling, as it is probable that the conductance peaks corresponding to these molecule-electrode coupling configurations overlap and cannot be individually resolved in the conductance plots.

Comparisons can be drawn between the conductance peaks observed for the three isomeric dipyridylamine molecules (**1**-**3**) and the features observed in the conductance plots for the structurally similar π-conjugated molecular wire 4,4′-dipyridylethyne (**4**). This compound provides a highly suitable 'control' molecular wire for this series of measurements as it has a broadly similar structure and incorporates a pair of pyridine anchoring groups, so it is expected to display comparable molecule-electrode binding and molecule-electrode coupling behaviour. Another reason for its suitability is that Hong *et al*. have previously measured the electrical properties of 4,4′-dipyridylethyne (**4**) using the STM-BJ technique, providing a reliable point of comparison for the measurement of the pyridine-terminated molecules in this work. In the STM-BJ measurements for this compound they observed three distinct conductance peaks, with the high conductance peak at $10^{-3.3}$ G_0 and medium conductance peak at approximately $10^{-4.0}$ G_0. These features are observed at similar values to the high and low conductance peaks reported for the symmetric dipyridylamine molecules in this work, suggesting they correspond to molecular junctions with similar charge transport characteristics. The third, low conductance peak for this compound was observed at a value of $10^{-6.0}$ G_0, which means that if the equivalent molecular junction configuration corresponding to this peak occurs for any of the dipyridylamine molecules, the resulting feature would be obscured by the noise level from the measurement.[82]

The electrical properties of the 4,4′-dipyridylethyne molecule (**4**) have been measured as part of this study using the same STM-BJ technique, sample preparation method and solvent system as for the dipyridylamine molecules (**1**-**3**) (Figure 2.5). This measurement gave a single molecular conductance peak at $10^{-3.7}$ G_0, which is lower than the experimental conductance value for the high conductance peak identified by Hong *et al*. ($10^{-3.3}$ G_0), albeit within half an order of magnitude of the value recorded in their earlier study.[82] This peak is therefore likely to correspond to a combination of molecular junctions with strong-strong Au-N coupling and strong-weak Au-N coupling, in accordance with the predicted molecule-electrode coupling behaviour for the dipyridylamine molecules (**1**-**3**). The discrepancy between the conductance value recorded in this measurement and the higher conductance value obtained by Hong *et al.*

could be attributed to a significant difference in the number of conductance-distance traces obtained between the respective experiments, as their study reports that approximately 2000 experimental conductance-distance traces were used to construct the conductance plots. In this work, a much larger number of traces (approximately 7700 traces) were used to construct the molecular conductance plots. This is significant because using a much larger data set in this experiment is expected to reduce the influence of traces displaying conductance values higher than the mean on the conductance features, which may explain the lower measured conductance value. This hypothesis is supported by the smooth conductance peak observed, which is indicative of a comparatively narrow range of conductance values for this molecule. The narrower range of recorded conductance values would also explain the lack of a distinct medium conductance feature in this measurement, particularly as the conductance value for the high conductance peak reported in this experiment is higher than that for the medium conductance peak in the earlier study ($10^{-4.0}$ G_0). However, it should be acknowledged that Hong *et al*. also report that the high conductance feature for this molecular wire extends to a minimum conductance value of $10^{-3.7}$ G_0, which is in strong agreement with the conductance value for 4,4′-dipyridylethyne (**4**) measured in this work.

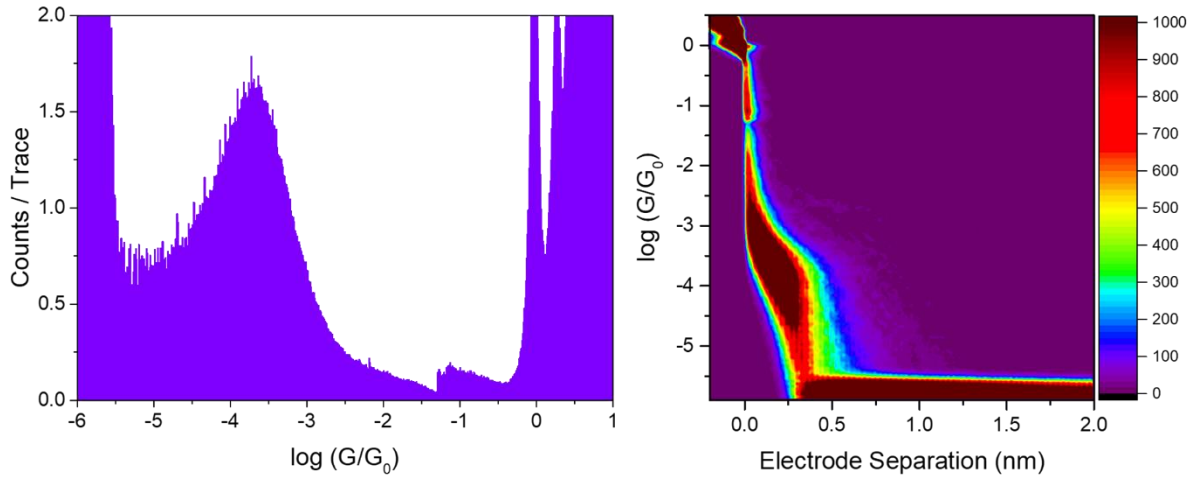

Figure 2.5. STM-BJ measurement of the molecular wire 4,4′-dipyridylethyne (**4**) in solution (solvent: mesitylene/THF (4:1)) at 200 mV bias voltage.

The absence of a low conductance peak in this plot, which is expected to correspond to molecular junctions with weak-weak Au-N coupling, can be explained as the earlier study by Hong *et al*. reported a value of $10^{-6.0}$ G_0 for this peak.[82] If the molecular junction configuration corresponding to this feature occurs for the 4,4′-dipyridylethyne (**4**) molecule in this experiment, the resulting conductance peak would be obscured by the instrument noise level,

so the formation of this junction geometry cannot be conclusively confirmed from the conductance plots. However, the clear similarities between the results obtained for the 4,4′-dipyridylamine (**1**), 3,3′-dipyridylamine (**2**) and 3,4′-dipyridylamine (**3**) molecules using the STM-BJ technique and data reported for closely related structures in other studies, in addition to the measurement of 4,4′-dipyridylethyne (**4)** as a 'control' molecule in this work, indicates that the behaviour of these three molecules is consistent with that displayed by other conjugated pyridine-terminated molecular wires.

For the three isomers of dipyridylamine featured in this work, all measured conductance values corresponding to peaks representing high conductance molecular junctions fall within approximately one order of magnitude, in the range of $10^{-3.0}$ G_0 to $10^{-4.0}$ G_0. The conductance values observed for low conductance features vary from $10^{-3.9}$ G_0 to $10^{-4.6}$ G_0, a range of less than one order of magnitude. The differences in conductance are relatively small but are sufficient to indicate that varying the positions of the pyridyl ring N atom anchoring sites does have an effect on the conductance of the molecules. However, it is unlikely that CQI or DQI effects significantly influence the conductance of the dipyridylamine molecules, because significant enhancement (CQI) or suppression (DQI) of the conductance by an order of magnitude or more would be expected on changing the anchoring site position. It is likely that the differences in conductance are caused by variations in molecule-electrode coupling on changing the anchoring site positions, as the molecular conductance for pyridine-terminated molecules is known to be sensitive to the precise junction configuration and Au-N bond tilt angle.[12] This explanation is in better agreement with the relatively small changes in conductance observed. On the other hand, these experiments show that the high and low conductance molecular junction configurations for the dipyridylamine structures display significantly different charge transport properties. The difference in conductance between the high and low conductance peaks for all three molecules ranges between approximately half an order of magnitude and a full order of magnitude. This is consistent with the formation of molecular junctions with distinctly different geometries in the high and low conductance configurations, in agreement with the measurement of other pyridine-terminated molecules.[88]

Further information about the electrical properties of the dipyridylamine isomers can be found by comparing the data from these experiments with results from conductance measurements on diazacarbazole molecular wires by Naghibi *et al*., which showed significant differences in conductance behaviour between *meta*-linked and *para*-linked diazacarbazole structures.[92] The *meta*-linked derivatives showed large modulations in conductance on chemical modification of

the core structure at the pyrrolic N atom, with conductance values varying by over one order of magnitude depending on the substituent groups. The results indicated that DQI effects suppressed the conductance of *meta*-linked carbazoles with electron donating substituents such as anisole, which decreased the electron density on the pyrrolic N atom, leading to lower charge transport efficiency and reduced conductance. These destructive effects were cancelled for *meta*-linked carbazoles with electron withdrawing substituents such as pyridine, which increased the electron density on the pyrrolic N atom, leading to higher charge transport efficiency and increased conductance. By contrast, the analogous *para*-linked carbazole derivatives displayed little variation in conductance on chemical modification of the pyrrolic N atom and no DQI behaviour was predicted or observed. Also, the *meta*-linked carbazole derivatives gave conductance plots with single broad peaks, whereas the *para*-linked carbazole derivatives displayed bistable conductance signatures with distinct high and low conductance peaks. The predicted charge transport pathway through the dipyridylamine isomers is via the amine N atom, which is analogous to the pathway via the pyrrolic N atom in the diazacarbazole compounds. From this it can be deduced that the charge transport behaviour for the dipyridylamine molecules is more similar to the *para*-linked carbazole derivatives than the *meta*-linked derivatives. This is consistent with a charge transport pathway similar to the pyrrolic N atom pathway in the carbazole derivatives as opposed to the less efficient transport pathway via the inter-ring C-C bond and is supported by the experimental conductance plots, which indicate that the three dipyridylamine molecules display bistable conductance signatures with relatively small variations in conductance on changing the structure and do not appear to exhibit DQI effects.

Another useful method for gaining quantitative information on the characteristics of molecular junctions is the determination of the length of the molecular junction plateaus. The maximum stretching distance for the junction is dependent on the interactions between the molecule and the electrodes and measuring the plateau length therefore provides information about the molecule-electrode binding strength at the anchoring sites. Also, if the junction length is recorded together with the molecular conductance value, this provides an indication of charge transport efficiency through the junction. In this work, the molecular junction lengths have been predicted by theory and measured experimentally to assess the stability of the molecular junction and the distance the molecular wire can be stretched prior to junction cleavage. Theoretical molecular junction length values for the three isomeric molecular wires were determined by performing calculations using MM2 parameters (Chem3D, Perkin Elmer).

These calculations predicted approximate molecular lengths of 0.77 nm for 4,4′-dipyridylamine (**1**), 0.57 nm for 3,3′-dipyridylamine (**2**) and 0.68 nm for 3,4′-dipyridylamine (**3**). These values represent the distance between the two pyridyl ring N atoms at the anchoring sites at opposite ends of the molecular structures, which corresponds to the length of the most probable charge transport pathway through the molecular junction.

The 2-D conductance-distance histograms obtained from this series of measurements allow the experimental molecular junction length to be determined by recording the electrode separation distance (Δs) at the end of the molecular conductance plateau. This value represents the distance the molecular junction can be stretched from the first data point giving a conductance value lower than 0.1 G_0 (defined as $\Delta s = 0$), corresponding to the cleavage of the Au-Au metallic point contact, up to the data point marking the end of the molecular conductance plateau, after which further increasing the distance between the electrodes leads to cleavage of the molecule-electrode contacts and hence molecular junction rupture. (For a more detailed explanation of how the 2-D conductance histogram is used to determine the electrode separation distance, please refer to Chapter 5, section 5.3 (STM Measurements and Sample Preparation)). Using this approach, the 2-D conductance plots give measured electrode separation distances of 0.79 nm for 4,4′-dipyridylamine (**1**), 0.51 nm for 3,3′-dipyridylamine (**2**) and 0.68 nm for 3,4′-dipyridylamine (**3**), respectively (Table 2.2). These values, also referred to as the molecular break-off distance, represent the approximate separation between tip and substrate at which junction cleavage occurs during the STM-BJ experiments. The measured electrode separation distance correlates with the length of the molecular junction, so it is significant that the measured electrode separation distances for all three molecules at 200 mV bias voltage agree well with the theoretically predicted lengths for all three structures. This agreement between theoretical and experimental lengths indicates that the molecules form stable molecular junctions where the molecule binds to the electrodes via the pyridine anchoring moieties. It also suggests that the junctions undergo stretching with increasing electrode separation until this distance approaches the maximum molecular junction length, where the gap between the electrodes becomes too large for the molecule to bridge and the junction is ruptured upon cleavage of the molecule-electrode contacts.

Table 2.2. Lengths of Molecular Junctions for molecules **1-4** (4,4′-, 3,3′- and 3,4′-dipyridylamine and 4,4′-dipyridylethyne) from Theoretical Calculations using MM2 Parameters and Experimental Measurements.

Molecule	L(MM2)[a]/ nm	Δs [b]/ nm
		200 mV
1 / 4,4′-dipyridylamine	0.77	0.79
2 / 3,3′-dipyridylamine	0.57	0.51
3 / 3,4′-dipyridylamine	0.68	0.68
4 / 4,4′-dipyridylethyne	0.92	0.49

[a]L(MM2) corresponds to the distance calculated using MM2 parameters after minimization of energy for the molecular structure between the binding N atoms on the anchoring groups at opposite ends of the molecule. [b]Values of molecular break-off distance (Δs) obtained from the relevant 2-D conductance-distance histogram.

It should be emphasised that the good agreement between the measured electrode separation distances and theoretical molecular lengths for the dipyridylamine molecules (**1-3**) provides strong evidence that the molecule-electrode binding is via the pyridyl N anchoring sites at both ends of the molecular junction. This is important because amines can also bind to Au electrodes via donor-acceptor interactions and the amine linker group bridging the pyridine rings in all three structures therefore provides a plausible alternative binding group for molecular junction formation.[20] However, junctions comprising molecules in this binding configuration would be expected to rupture at shorter electrode separation distances, as the theoretically predicted distances between either one of the two pyridyl N atoms and the bridging amine N atom are predicted to be in the region of 0.35 – 0.40 nm for all three compounds. These distances are shorter than the measured break-off distance values from the experimental measurements for all three molecules, indicating that the molecular junctions formed do not bind to the electrodes via the amine N atom. The results strongly suggest that molecule-electrode binding is via the pyridyl anchoring groups, which is consistent with earlier studies reporting that molecules with pyridine anchoring moieties have higher binding strengths and form more stable molecular junctions than analogous compounds with amine anchoring groups.[82] This is also supported by the measured conductance plots for the dipyridylamine molecules, which display distinct high and low conductance peaks in common with other pyridine-terminated molecular junctions,

rather than a single well-defined peak, which is the characteristic conductance signature of amine-terminated molecular junctions.[87]

The same theoretical calculation approaches have also been used to predict an approximate molecular length of 0.92 nm for the 'control' molecular wire, 4,4′-dipyridylethyne (**4**). The measured electrode separation distance for this molecule obtained from the 2-D conductance-distance histogram at 200 mV bias voltage was found to be 0.49 nm. If the break-off distance is the same as the electrode separation distance, this value is significantly shorter than the theoretically predicted length, in contrast to the strong agreement between theory and experiment observed for the dipyridylamine isomers (**1**-**3**). This could be because the longer ethynyl linker unit bridging the pyridine rings in this molecule leads to comparatively weak coupling between the molecular core structure and the Au electrodes relative to the dipyridylamine molecules. This would explain why the junction is cleaved before the molecule attains the full stretching distance in the junction, but this is not supported by the conductance data as weak molecule-electrode coupling is expected to lead to lower molecular conductance. The conductance value of the high conductance peak for 4,4′-dipyridylethyne (**4**) is found to be only slightly lower than the analogous peak for 3,3′-dipyridylamine (**2**) and higher than the analogous peak for 3,4′-dipyridylamine (**3**). It is unlikely that the molecule-electrode binding strength could explain this discrepancy as the dipyridylethyne molecule has the same anchoring moieties as the dipyridylamine molecules and the Au-N binding strength is likely to be comparable across all these structures. However, it is significant that 4,4′-dipyridylethyne (**4**) has a 'rod-like' structure which is expected to form longer molecular junctions than the dipyridylamine compounds. This means that the Au-Au snap-back distance, which represents the electrode separation on rupture of the metallic contact prior to molecular junction formation, may need to be added to the measured electrode separation distance to give the accurate molecular break-off distance.[82] The length of the snap-back distance for Au-molecule-Au junctions is approximately 0.5 nm and the addition of this value to the measured electrode separation distance for the 'control' molecule (**4**) gives a molecular break-off distance of 0.99 nm, which is in far stronger agreement with the theoretically predicted molecular length.

The close agreement between the theoretically calculated molecular lengths and measured electrode separation distance values for the dipyridylamine molecules **(1**-**3**) provides strong evidence that these molecules form stable molecular junctions. It should be noted that the snap-back distance is not added to the electrode separation distances for these molecules as the

measured separation distances for the three dipyridylamine isomers are similar to the theoretical molecular lengths. It is not immediately clear why this value does not need to be added to the electrode separation distances for the dipyridylamine molecules to give the accurate molecular break-off distance. It is possible that this may be explained by the short lengths of the dipyridylamine molecules, which may allow the molecules to bind in a stable molecular junction configuration in the presence of one or more Au-Au atomic contacts. This would allow the formation and stretching of molecular junctions in the gap between the electrodes prior to the rupture of the metallic contact, which is not feasible for the longer 'rod-like' dipyridylethyne molecule (**4**). This is supported by the theoretical length data, which shows that the dipyridylethyne molecule is longer than any of the dipyridylamine compounds (**1**-**3**). These results also indicate that when the molecular junction approaches its maximum stretching distance prior to junction cleavage, the molecule-electrode binding is primarily in the form of Au-N bonds via the pyridyl ring N atoms. The measured break-off distance for the 'control' molecular wire 4,4′-dipyridylethyne (**4**) obtained after addition of the snap-back length to the electrode separation distance is also similar to the theoretically predicted value. This provides further evidence that the pyridine-terminated molecules permit stable molecule-electrode binding and stretching of the molecular junction prior to rupture, with junction cleavage occurring at distances close to the theoretical molecular length.

2.5 Conclusions

In conclusion, a series of pyridine-terminated molecular wires including three isomers of dipyridylamine and the 'control' molecule 4,4′-dipyridylethyne have been synthesised for this project. The pyridine-terminated molecules have been synthesised using cross-coupling methodology and characterised prior to measurement to confirm the target compounds have been obtained with high purity. The electrical properties of these structures have been measured using the STM-BJ technique and the results compared with theoretical electronic transmission calculations. For all three dipyridylamine isomers, bistable conductance signatures are observed with distinct high and low conductance peaks representing different molecular junction configurations, consistent with the formation of stable molecular junctions for pyridine-terminated molecules. However, the enhanced conductance resulting from constructive quantum interference predicted for 3,3′-dipyridylamine from the initial theoretical calculations is not observed experimentally, as the symmetric 4,4′- and 3,3′- isomers of dipyridylamine have been found to display similar molecular conductance values. The apparent lack of agreement between theoretical transmission plots and experimentally observed conductance behaviour for 4,4′- and 3,3′-dipyridylamine is attributed to the close proximity of the metallic E_F to the LUMO resonances for the two molecules, minimising the difference in conductance between the symmetric molecules. The asymmetric 3,4′-dipyridylamine molecule, by contrast, gives a significantly lower conductance than either of the symmetric compounds, which is attributed to weaker molecule-electrode coupling for this isomer. The measured molecular junction length values provide further evidence that the compounds form stable molecular junctions as these are in good agreement with the theoretically predicted molecular lengths. Comparison with the measured electrical properties of 4,4′-dipyridylethyne and earlier experiments on diazacarbazole-based molecules indicates that the measured conductance values and features observed for the dipyridylamine molecules are similar to other pyridine-terminated molecules, confirming that the molecules form stable molecular junctions with characteristic conductance signatures. The experiments performed in this chapter have provided insight into structure-property relationships influencing charge transport through molecular wires incorporating pyridine anchoring moieties with the anchoring group N atoms in different ring positions.

Chapter 3: Investigation of Structure-Property Relationships and Quantum Interference Effects in Fluorene-Derived Molecular Wires

3.1 Introduction to Fluorene-Derived Molecular Wires

In this chapter, the main focus is on the study of the electrical properties of a series of extended molecular wires based on a conjugated fluorene core. The understanding of the role of interference effects in influencing charge transport through molecular junctions is one of the most important aspects in the development of molecular electronic devices. The influence of interference effects on the electrical properties of this series of molecular structures is observed by the addition of cross-conjugated carbonyl groups orthogonal to the main conductance pathway through the core structure. This is of significant interest as the functional groups external to the primary conductance pathway have the potential to result in DQI effects which would allow the charge transport properties and molecular conductance through the molecular wires to be controlled, with DQI behaviour lowering the conductance.

In the study of the influence of carbonyl groups on interference effects, the properties of a series of molecules based on a fluorene-derived fused central unit have been investigated (Scheme 3.1). Fluorene derivatives, in common with other molecular wires featuring fused aromatic ring systems, are particularly interesting candidates for exploring the influence of QI behaviour on molecular conductance. One reason for this is that the two aryl rings in the tricyclic structure are locked in a coplanar geometry, which means no variation in the inter-ring dihedral angle is expected between close structural analogues. Additionally, the effect of substitution in multiple positions on the fluorene core structure can be studied as chemical synthesis permits the investigation of the properties of structures displaying variations in connectivity, conjugation, substitution, aromaticity and heteroaromaticity.[92]

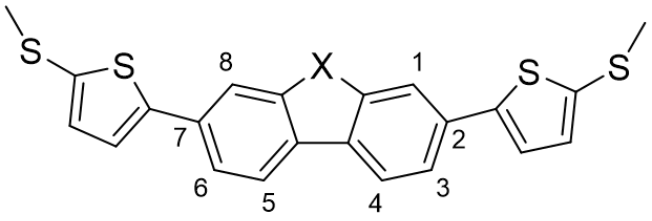

5 X = H, H **7** X = CO
6 X = CH_2 **8** X = COCO

Scheme 3.1. General structure of molecular wires based on the fluorene core unit structure (except **5**, where X = H, H represents a biphenyl-based core structure).

The electrical properties of fluorene-derived molecular wires have been studied previously by other groups. For example, Klausen *et al*. in 2014 used the STM-BJ technique to measure the

conductance properties of three fluorene derivatives. They showed that the substitution of heteroatoms (Si, O and N, respectively) in the fluorene core structure directly influences the charge transport behaviour, as they found that the carbazole derivative provides an efficient pathway for molecular conductance but the dibenzosilole and dibenzofuran derivatives do not conduct.[95] This illustrates how chemical substitution can be used as a means of controlling conductance behaviour and enhancing understanding of structure-property relationships, although these compounds differ significantly from the molecules in this work as they feature heteroatoms in place of the fluorene methylene group rather than as substituents on a fluorene core unit. A more closely related study was performed by Sagan *et al*. in 2014, who reported the measurement of the electrical properties of a series of oligofluorene molecular wires. They used the STM-BJ technique to measure the conductance of oligofluorene molecules displaying variations in the number of repeat units, anchoring moieties and substituents on the fluorene core unit.[96] However, the oligofluorene structures measured in their work possess simple alkyl side groups and it was found that these groups exert little influence on the charge transport properties of the molecular junctions, resulting in very similar molecular conductance values. The incorporation of heteroatoms in the molecular structure in this work, by contrast, is more likely to provide an effective method of modulating the charge transport properties of a molecular junction as the electronegative carbonyl O atom is expected to draw electron density away from the core structure with a much stronger inductive effect than the weakly electron donating alkyl groups, which may significantly influence electronic transmission efficiency.

Changes in electron transport behaviour on the addition of heteroatoms into the core structure have also been demonstrated in a range of molecular wires, including molecules with core structures based on five-membered and six-membered rings.[50,67] In this series of molecules, however, it is the presence of different substituents orthogonal to the main conductance pathway which changes the electronic structure of the molecule. These substituents may cause alterations in the shape or position of the QI feature, resulting in large modulations in electronic transmission which lead to an observable difference in molecular conductance. The investigation of charge transport through single molecule junctions comprising conjugated molecular wires which display QI effects therefore offers significant potential for the development of such devices. The substituents are also expected to change the positions of the frontier orbitals (HOMO and LUMO) and hence may change the width of the HOMO-LUMO energy gap, further influencing transmission through the molecular junction.

This work investigates the possible influence of interference effects on the electrical properties of three fluorene-derived molecular wires (Scheme 3.2). These molecules include a fluorene-based structure with a CH_2 bridge but no carbonyl groups in the fused core unit (TFLT, compound **6**), a similar fluorenone-based structure with one pendant carbonyl moiety (TFOT, compound **7**) and a third phenanthrene-9,10-dione-based structure with two pendant carbonyl moieties (TPDOT, compound **8**). In addition to these three fluorene derivatives, the properties of a biphenyl-based 'control' molecule (TBPT, compound **5**) with a non-fused core unit have also been investigated. All four molecules (compounds **5-8**) have thiomethyl terminal groups, with thiophene linkers separating the core unit from the anchoring groups. Thiomethyl moieties are used as the anchoring groups because previous studies have indicated that this functional group binds efficiently to Au electrodes with well-defined binding and electronically selective coupling at the anchoring sites.[40] The thiophene ring S atoms provide an alternative binding site for molecule-electrode interactions, but it is expected that the thiomethyl anchoring groups will provide the dominant binding sites for molecular junction formation. This is because the thiophene S atoms are incorporated in the aromatic ring structures and are predicted to be less electron rich than the thiomethyl S atoms, preventing efficient molecule-electrode coupling.

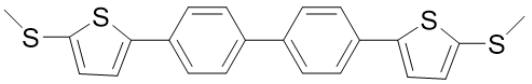

5

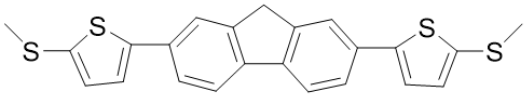

6

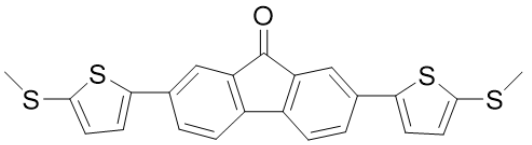

7

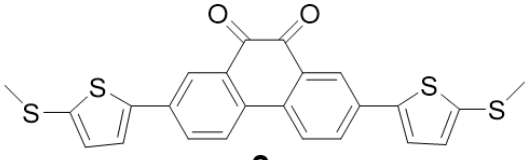

8

Scheme 3.2. Molecular structures of compounds **5-8**, TBPT, TFLT, TFOT and TPDOT.

The three molecular wires which are the primary focus of this chapter (molecules **6**-**8**) have fluorene-derived core structures based on the biphenyl core unit of the 'control' molecule (**5**). The rigid fused core units provide an ideal platform for chemically controlling the electronic properties of the molecules by allowing the number of pendant carbonyl units to be varied. The functionalised region is located away from the electrodes, which lessens the impact of electrode-linker interactions on the properties of the molecular junction and thus makes it easier to distinguish the influence of intramolecular effects on the charge transport characteristics. The highly conjugated molecular structures are advantageous for the collection of reliable data from the single molecule conductance measurements, as conjugated molecules tend to display higher conductance values and lower transport decay constants than equivalent partially or non-conjugated structures.[25] The long end-to-end molecular lengths also increase the likelihood of obtaining clean current-distance (I-s) traces with well resolved conductance peaks for these compounds, as the junction formation probability increases with increasing molecular length.[96] The combination of these two factors means that the compounds are expected to display observable molecular conductance features with reproducible conductance values.

The *para*- *para*- conjugated core units are also likely to favour efficient charge transport through the molecular junction, as *para*-linked compounds are predicted to enable more efficient electronic transmission than analogous *meta*-linked structures.[62] In addition to their primary role as anchoring groups, the incorporation of methylthioether-thiophene moieties either side of the fluorene-based core unit also enhances the solubility of the compounds in organic solvents. This represents a significant practical advantage as the STM-BJ experiments in this work are performed in solution and the formation of molecular junctions is dependent on the compounds displaying high solubility in the solvent selected. The enhanced solubility associated with these linking groups is particularly useful for the measurement of TPDOT (**8**), as the diketone moiety in the core unit is expected to lower the solubility of this structure compared to TFLT (**6**) and TFOT (**7**).

It should also be noted that the width of the HOMO-LUMO energy gap is expected to decrease as more complex moieties are introduced to the central core structure. The fluorene-derived molecules are highly conjugated and absorb wavelengths of light in the visible region of the electromagnetic spectrum. This means that the change in the HOMO-LUMO gap is indicated by the wavelength of light absorbed by each compound and hence the wavelength of light reflected. This is apparent when comparing the observed colours of these molecules, as TBPT (**5**) is pale yellow in colour, TFLT (**6**) is yellow, TFOT (**7**) is red and TPDOT (**8**) is deep purple

(Figure 3.1). This shows that the wavelength of light absorbed increases across this series of molecules and therefore the HOMO-LUMO energy separation decreases from TBPT to TPDOT (**5-8**). This is significant because earlier experimental work shows that the molecular conductance is expected to increase as the energy difference between the metallic E_F and the molecular frontier orbital closest in energy decreases.[48] However, the predicted influence of DQI effects on the charge transport characteristics of the fluorene derivatives means this trend may not be observed for this series of compounds.

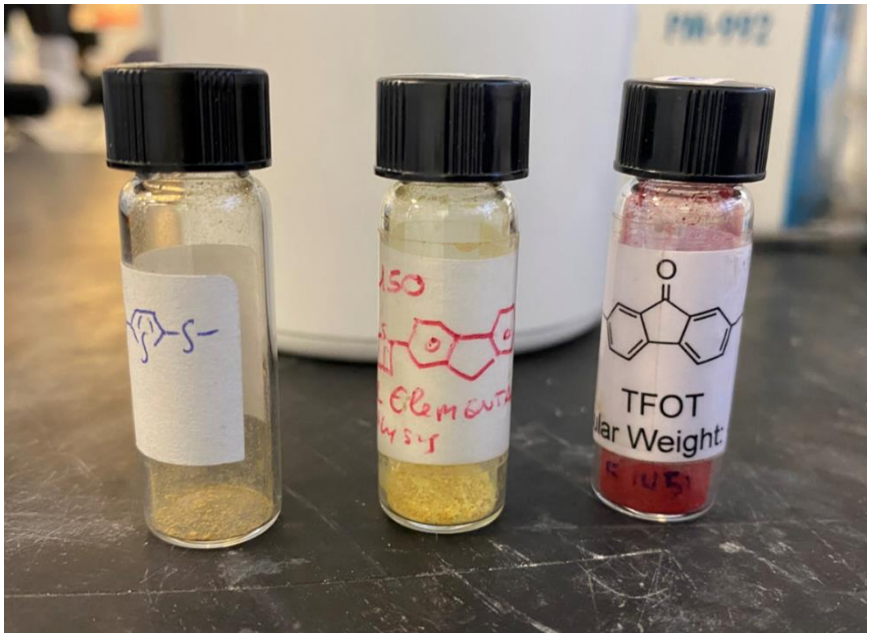

Figure 3.1. Sample vials containing compounds **5-7** (TBPT, TFLT, TFOT), showing the changes in colour associated with the change in HOMO-LUMO energy separation and the wavelength of light absorbed. Compound **8** (TPDOT) is not shown due to the low quantity of sample available in comparison to the other molecules.

This study investigates the interference effects resulting from the presence or absence of carbonyl groups in a conjugated molecular wire and their influence on the molecular conductance properties. Transport calculations have indicated that the presence of one or more carbonyl groups in the central conjugated moiety should lead to cross-conjugation. This is of particular interest for the field of molecular electronics as theoretical transmission spectra have shown that cross-conjugated molecules display distinctly different charge transport properties from linearly conjugated or non-conjugated structures and exhibit strong interference effects. This behaviour can be observed experimentally as a sharp decrease in conductance for cross-conjugated molecules compared to analogous structures.[70] The large dynamic range in conductance resulting from interference effects in cross-conjugated molecules is highly

promising for applications in a range of electronic devices, such as transistors and rectifiers.[98] Theoretical calculations also predict that the addition of any number of carbonyl groups to the molecular wire leads to the addition of an equal number of Fano resonances in the HOMO-LUMO gap. Fano resonances are observed when the energy of an electron traversing the molecule coincides with the energy of a bound state on a pendant group. As a consequence, Fano resonances are sensitive to changes in the chemical properties and structural geometry of the pendant group and this provides a means of controlling charge transport through the molecular wire.[99]

If the introduction of one or more Fano resonances occurs in close proximity to the electrode Fermi Energy (E_F), this is expected to cause a sharp increase or decrease in transmission through the molecule which in turn would result in either an increase or decrease in molecular conductance, respectively. This is because a Fano resonance comprises a resonance feature and an anti-resonance feature and therefore a comparatively small shift in the position of the resonance relative to the E_F can increase or decrease electronic transmission significantly, shifting the molecular conductance by several orders of magnitude. In order to observe this behaviour experimentally, it is necessary to adjust the alignment of the molecular frontier orbitals and the metallic E_F. Electrochemical gating provides a useful strategy for fine tuning the energy level alignment between the frontier orbitals and E_F in molecules displaying QI behaviour, as relatively small changes in the electrode potential (bias voltage) can result in large changes in the electronic transmission and molecular conductance, depending on the position of the anti-resonance feature.[100] Another advantage of this approach is that it avoids the technical challenges associated with incorporating a gate electrode in a single molecule-based junction.

In 1968, Phelan and Orchin defined cross-conjugated molecular structures as compounds possessing three unsaturated groups where two of these groups are both conjugated to another unsaturated group but not conjugated to each other.[101] It is important to acknowledge that the fluorene-derived molecules (**6**-**8**) featured in this study have a continuous pathway through the molecular core structure and therefore do not meet this strict definition. However, the structures of the molecular wires TFOT (**7**) and TPDOT (**8**) provide at least one possible non-continuous charge transport pathway incorporating the unsaturated carbonyl moieties, which can act as cross-conjugated groups relative to the anchoring groups. This is in contrast to the linearly conjugated molecule TFLT (**6**), which does not feature any carbonyl groups orthogonal to the primary conductance pathway and does not possess any non-continuous charge transport

pathways. There is significant interest in the electrical properties of cross-conjugated molecules as QI effects may dominate, resulting in significant differences in charge transport behaviour compared to similar linearly conjugated structures. These effects may cause large variations in the electronic transmission and hence the molecular conductance which cannot be predicted either from energy level diagrams or 'rules of thumb' for charge transport efficiency through molecular wires.[102]

From the perspective of this work, the most important implication of the nature of π-conjugation in the core structure is that the cross-conjugated TFOT (**7**) and TPDOT (**8**) molecules are predicted to display DQI behaviour arising from Fano resonances. It is expected that the influence of Fano resonances will be the primary factor in determining the molecular conductance rather than the width of the HOMO-LUMO energy separation. As a consequence, it is expected that electronic transmission through TFOT (**7**) and TPDOT (**8**) will be suppressed and these two molecules are predicted to give lower conductance values than the linearly conjugated TFLT molecule (**6**). This effect on charge transport is expected to be most apparent in TPDOT (**8**) as this structure possesses two cross-conjugated carbonyl moieties, with the availability of multiple cross-conjugated transport pathways leading to strong DQI effects.

3.2 STM-BJ Measurement of Fluorene-Derived Molecular Wires

The electrical properties of the three fluorene-derived molecular wires and the biphenyl-based 'control' molecule have all been measured in solution using the STM-BJ technique. Molecules **5**-**8** (Scheme 3.2) studied in this chapter were synthesised, purified and characterised using common synthetic laboratory techniques. The fluorene-derived molecules were synthesised by Dr Nicolo Ferri at the University of Liverpool. For each conductance measurement, a 10^{-3} M concentration solution (unless stated otherwise) of each molecular wire was prepared by dissolving the relevant compound in 1,2,4-trichlorobenzene and the measurements were performed at a fixed bias voltage (100 mV or 200 mV). The electrical properties of the molecules have been measured at different fixed bias voltage values to study the influence of raising the bias on the molecular conductance and interference effects observed. Thousands of current-distance (I-s) curves were collected from each STM-BJ experiment and all traces obtained were analysed, with no data selection methods used to construct the conductance histograms.

3.3 Experimental Results for Fluorene-Derived Molecular Wires

The experimental results from the measurement of the electrical properties of the fluorene-derived molecular wires and the biphenyl-based 'control' molecule are presented in the form of 1-dimensional (1-D) conductance plots and 2-dimensional (2-D) conductance-distance histograms. The 1-D conductance plot obtained from the STM-BJ measurement of the fluorene-based molecule TFLT (**6**) at 100 mV bias voltage show a sharp conductance peak at G_0, representing the conductance of a single atomic Au-Au point contact, in addition to the conductance peak corresponding to molecular junction formation (Figure 3.2). The 2-D conductance-distance histogram shows a conductance cloud with an extended plateau, which also corresponds to the molecular junction conductance. Both the 1-D and 2-D plots clearly indicate that TFLT (**6**) forms stable molecular junctions, as they display well-defined conductance features with reproducible conductance values.

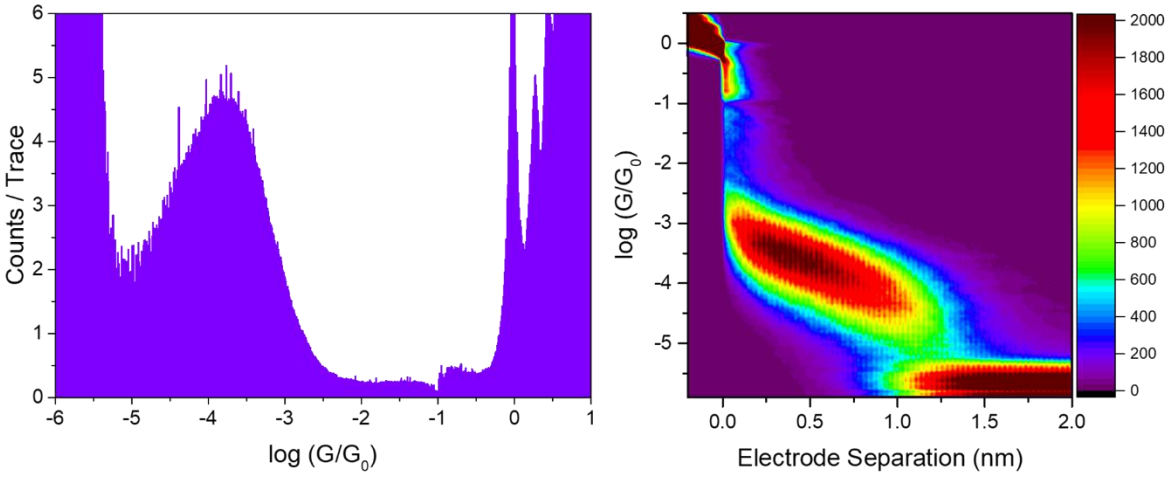

Figure 3.2. STM-BJ measurement of the molecular wire TFLT (**6**) in solution (1,2,4-trichlorobenzene) at 100 mV bias voltage.

Similar results are observed for all three fluorene-derived molecules, as clear molecular peaks with distinguishable conductance values are obtained in all measurements at 100 mV bias voltage, indicating the formation of stable molecular junctions. Comparing the conductance data for the three structures indicates that the molecular conductance decreases as the number of orthogonal carbonyl moieties incorporated into the central core unit increases (Figure 3.3). The TFLT molecular wire (**6**), which does not possess any orthogonal carbonyl groups, has the highest conductance of the three molecules at 100 mV bias ($10^{-3.8}$ G_0), with TFOT (**7**) (one carbonyl moiety) and TPDOT (**8**) (two carbonyl moieties) having the second highest ($10^{-4.0}$ G_0) and lowest ($10^{-4.2}$ G_0) conductance values respectively. The TFLT and TPDOT molecular wires

(**6** & **8**) both present sharp molecular conductance peaks, whereas the TFOT molecule (**7**) gives a slightly broader and lower conductance peak, although the peak is sufficiently sharp to enable the conductance of this molecule to be determined. In addition to the molecular conductance features, the 1-D plots for all three molecules display strong peaks at 1 G_0, representing the Au-Au atomic point contact. The clearly resolved peaks for the Au-Au contacts provide further evidence that the peaks at lower conductance values represent the formation of molecular junctions, as the features associated with the Au-Au point contact are very similar. This means the differences between the conductance values of the peaks for molecules **6**-**8** can be attributed to the intrinsic charge transport properties of the molecular junctions formed after rupture of the Au-Au contact.

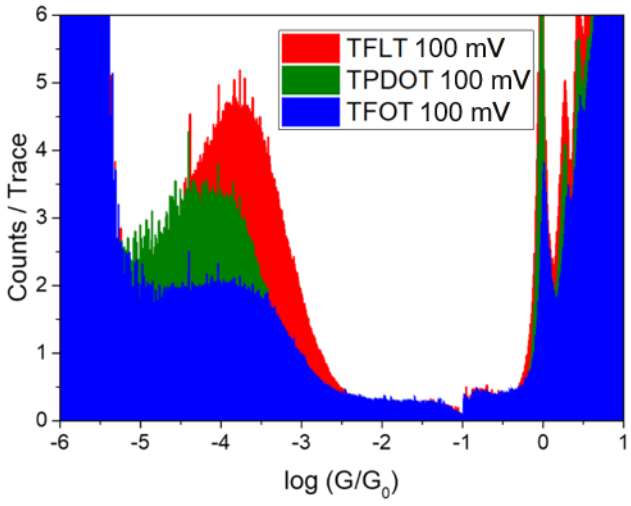

Figure 3.3. Comparison of the STM-BJ conductance measurements of molecules **6**-**8** (TFLT, TFOT and TPDOT) at 100 mV bias voltage.

The same trend in molecular conductance is observed when the bias voltage is increased to 200 mV, with the linearly conjugated TFLT (**6**) giving the highest molecular conductance ($10^{-3.6}$ G_0), TPDOT (**8**) giving the lowest conductance ($10^{-4.0}$ G_0) and TFOT (**7**) having an intermediate conductance value ($10^{-3.8}$ G_0) (Figure 3.4). This strongly supports the results from the 100 mV bias voltage experiments, as it is again found that the conductance decreases on addition of a single cross-conjugated ketone moiety to the central core unit, with a further drop in conductance observed after the addition of a second cross-conjugated carbonyl group. This is also consistent with the predicted occurrence of DQI effects in TFOT (**7**) and TPDOT (**8**).

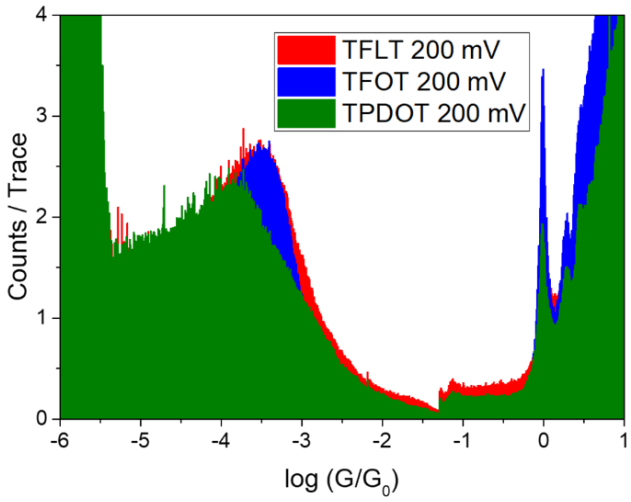

Figure 3.4. Comparison of the STM-BJ measurements of molecules **6**-**8** (TFLT, TFOT and TPDOT) at 200 mV bias voltage.

Direct comparison of the measured molecular conductance values for TFLT, TFOT and TPDOT (**6**-**8**) clearly shows that on raising the bias voltage from 100 mV to 200 mV, the conductance values of all three molecules increase (Table 3.1). The strong correlation between the applied bias and conductance is significant because the response of the molecular conductance to a change in the bias voltage indicates which molecular frontier orbital dominates charge transport. It has been shown that when the tip is biased positively relative to the substrate the conductance increases on raising the bias for molecules with HOMO-dominated conductance pathways, whereas it decreases on raising the bias for molecules with LUMO-dominated conductance pathways.[35] The increase in conductance observed for all three molecules at 200 mV bias therefore suggests that conductance preferentially occurs via the HOMO pathway for the fluorene-derived compounds. This behaviour also indicates that the expected decrease in HOMO-LUMO energy separation from TFLT to TPDOT (**6**-**8**) does not lead to a change in the primary charge transport pathway, as metal-molecule coupling is typically via the frontier orbital closer in energy to the metallic E_F. This suggests that the molecule-electrode coupling predominantly involves the HOMO, so it can be deduced that the HOMO is likely to be closer in energy to E_F than the LUMO for all three compounds.

Table 3.1. Conductance values for molecules **5-8** (TBPT, TFLT, TFOT and TPDOT) obtained from STM-BJ measurements at 100 mV and 200 mV bias voltage.

Molecule	Conductance (G) / G_0	
	100 mV	**200 mV**
5/TBPT	$10^{-3.6}$ (HC)[a] $10^{-4.4}$ (LC)	$10^{-3.5}$ (HC) $10^{-4.7}$ (LC)
6/TFLT	$10^{-3.8}$	$10^{-3.6}$
7/TFOT	$10^{-4.0}$	$10^{-3.8}$
8/TPDOT	$10^{-4.2}$	$10^{-4.0}$

[a]HC and LC denote experimentally measured high and low conductance values corresponding to distinct molecular conductance peaks in the conductance plots.

The electrical properties of the biphenyl-based molecular wire TBPT (**5**) have been measured using the same STM-BJ technique, sample preparation method and solvent as the three fluorene-derived molecules at 100 mV bias voltage (Figure 3.5). The 1-D conductance plot for this molecule shows a significant difference from the conductance features observed for the fluorene-derived compounds as two distinct conductance peaks are observed, with a high conductance peak at $10^{-3.6}$ G_0 and a low conductance peak at $10^{-4.4}$ G_0. The large discrepancy in molecular conductance (nearly one order of magnitude) between the two peaks suggest these features correspond to different molecular junction configurations. However, despite these differences, there are several key similarities between the conductance features observed for TBPT (**5**) and the fluorene-derived compounds (**6**-**8**). The peak profile for the higher of the two conductance peaks reported for TBPT (**5**) resembles the conductance signatures observed for the fluorene derivatives. This provides further evidence of stable molecular junction formation, indicating that the thiomethyl anchoring groups enable efficient molecule-electrode coupling. More significantly, the conductance value of $10^{-3.6}$ G_0 measured for TBPT (**5**) is similar to the conductance of the linearly conjugated TFLT molecule (**6**), but is higher than the conductance values obtained for TFOT (**7**) and TPDOT (**8**) at the same bias voltage. This result is consistent with the expected relationship between cross-conjugation and charge transport and therefore supports the prediction that DQI suppresses the conductance of the molecules featuring cross-conjugated carbonyl moieties.

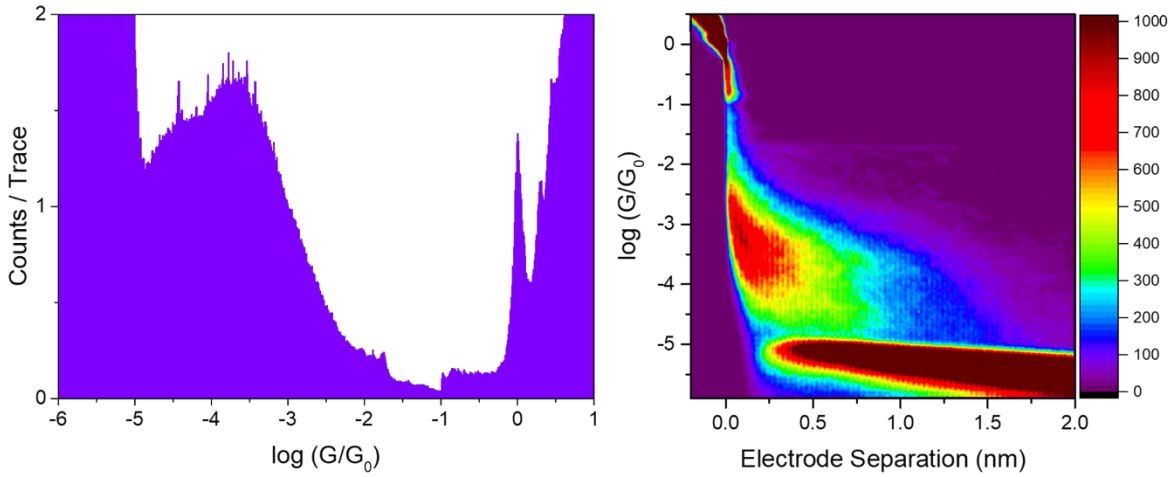

Figure 3.5. STM-BJ measurement of the molecular wire TBPT (**5**) in solution (solvent: 1,2,4-trichlorobenzene) at 100 mV bias voltage.

The observation of a second lower conductance peak for the biphenyl derivative TBPT (**5**), which is not observed for the fluorene-derived compounds (**6**-**8**), can be explained by the different electronic properties displayed by the biphenyl-based molecule, which has a non-fused molecular core structure, compared to the fluorene derivatives, which possess fused core unit structures. The second peak in TFLT (**5**) is attributed to the formation of a hemilabile molecular junction configuration where the thiophene S atom acts as a molecule-electrode binding group at one end of the molecular junction. This binding geometry can be assigned to the lower conductance peak as it is expected that the molecule-electrode binding interactions for the thiophene S binding sites incorporated in the five-membered aromatic rings are weaker than for the thiomethyl terminal groups due to the inverse relationship between aromaticity and molecular conductance.[50] It is likely that this configuration is stable for the comparatively electron rich biphenyl-based structure but not stable for the more electron deficient fluorene derivatives because the electron-withdrawing fluorene core structure draws electron density away from the thiophene rings, leaving the thiophene S atom too electron deficient to form stable donor-acceptor contacts with the electrodes. This means the fluorene-derived compounds only permit stable molecule-electrode binding via the thiomethyl anchoring groups and hence only display single molecular conductance peaks. Also, the absence of a conductance peak corresponding to a thiophene-electrode binding mode can be attributed to the electron-withdrawing effect of the fused fluorene core structure as opposed to the carbonyl substituents, as the single conductance peak for TFLT (**6**) resembles the features observed for the substituted fluorene derivatives TFOT (**7**) and TPDOT (**8**) rather than the bistable conductance signature observed for TBPT (**5**).

The electrical properties of the 'control' TBPT molecule (**5**) have also been measured at the increased bias voltage of 200 mV, again using the same technique, sample preparation method and solvent as the fluorene-derived compounds (Figure 3.6). This measurement also displays two conductance peaks, with the high conductance peak at $10^{-3.5}$ G_0 and the low conductance peak at $10^{-4.7}$ G_0. Comparison of the conductance plots obtained from this experiment with the measurement of this molecule at 100 mV bias shows that the low conductance peak is less pronounced and gives a lower conductance value than at lower bias. This suggests that the hemilabile thiophene S-binding junction geometry is less stable at higher bias voltage and a larger proportion of the molecular junctions formed bind via the thiomethyl terminal groups. The high conductance peak from this measurement gives a conductance value of $10^{-3.5}$ G_0 and this result is in agreement with both key trends observed for this series of molecules. First, the molecule shows an increase in conductance on raising the bias voltage to 200 mV in agreement with the trend observed for all three fluorene-derived compounds, which suggests the HOMO is the dominant charge transport pathway through the core structure. Second, the conductance is comparable to that obtained for TFLT (**6**) under the same conditions but higher than the values measured for the cross-conjugated compounds TFOT (**7**) and TPDOT (**8**). This again suggests that DQI effects lower the conductance of the molecules containing one or more cross-conjugated ketone moieties relative to the analogous linearly conjugated structures.

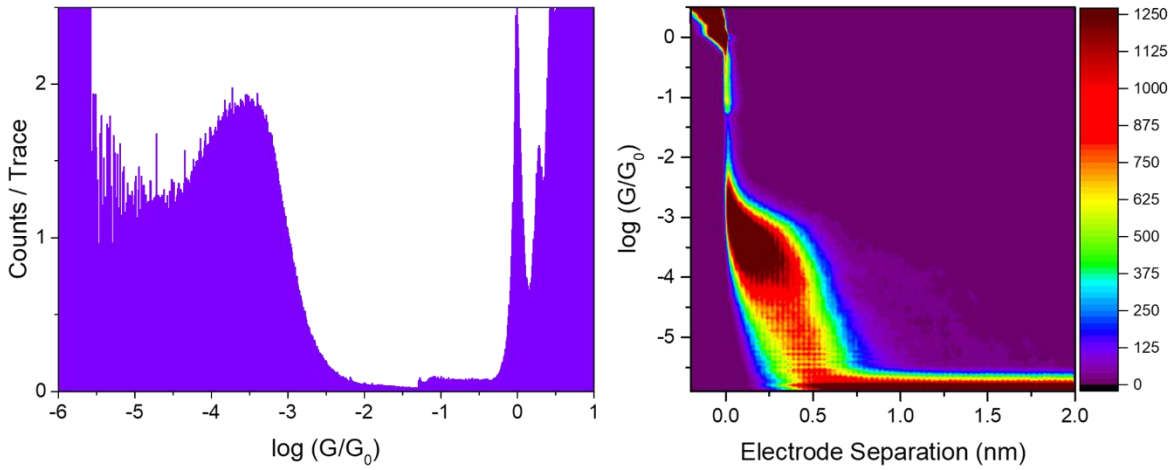

Figure 3.6. STM-BJ measurement of the molecular wire TBPT (**5**) in solution (solvent: 1,2,4-trichlorobenzene) at 200 mV bias voltage.

For the fluorene-derived compounds (**6-8**) it is notable that the decrease in molecular conductance observed on introducing one or more cross-conjugated ketone groups to the central unit at both 100 mV and 200 mV bias is consistent with the predicted occurrence of an

equivalent number of Fano resonances (one and two respectively) in the TFOT (**7**) and TPDOT (**8**) molecules. This negative correlation between the number of carbonyl groups and the conductance provides evidence that DQI phenomena influence the electrical properties of the fluorene-derived molecular wires. However, the decrease in conductance on introducing each carbonyl moiety to the core unit is relatively small, with similar decreases (about one-fifth of an order of magnitude) observed at fixed bias voltages of 100 mV and 200 mV. This may indicate that the Fano resonances resulting from the introduction of the cross-conjugated ketone moieties occur too far from the Au electrode E_F to cause a major decrease in the electronic transmission and molecular conductance. Another possible explanation is that the availability of a charge transport pathway through the fluorene core structure may limit the influence of the orthogonal carbonyl groups on the molecular conductance. This would require further theoretical investigation, specifically the calculation of electronic transmission plots for the three molecules in this study, before this could be confirmed.

It should be acknowledged that the conductance of all three molecules increases on raising the bias voltage, as this suggests that the fluorene-derived molecules predominantly conduct via the HOMO pathway. This is significant because the electron withdrawing effect of the carbonyl groups may influence the alignment of the metallic E_F and frontier orbitals. One possible explanation for the reduced conductance of TFOT (**7**) and TPDOT (**8**) compared to TFLT (**6**) could be that the carbonyl groups lower the HOMO energy of the molecules, leading to increased energy separation between the HOMO and E_F. However, the HOMO-LUMO gap for these molecules is predicted to decrease from TFLT to TPDOT (**6**-**8**). The increase in conductance on raising the bias voltage from 100 mV to 200 mV for all three molecules indicates that the HOMO-E_F energy separation is also likely to decrease with the same trend. This is particularly significant for the fluorene derivatives as the molecular conductance is typically expected to increase as the frontier orbital-E_F energy separation decreases,[48] whereas the opposite trend is observed in the experimental conductance measurements. Also, it is apparent when comparing the conductance values obtained for the TFLT (**6**) and TPDOT (**8**) molecules in both series of measurements that there is a significant difference in conductance between these two structures. TFLT (**6**) displays a higher conductance than TPDOT (**8**) by approximately half an order of magnitude at both 100 mV and 200 mV bias, which indicates that the incorporation of multiple cross-conjugated ketone moieties in the core unit leads to a significant decrease in conductance. It is unlikely that a simple electron withdrawing effect could account for such a large discrepancy between these two structures. This combined

evidence suggests that DQI effects are responsible for lowering the conductance of TFOT (**7**) and TPDOT (**8**).

Further evidence of DQI lowering the conductance of TPDOT (**8**) can be found by comparing the conductance values in this work with the results reported by Vonlanthen *et al*. in a study investigating the electrical properties of a series of biphenyldithiol molecular wires. They found that the molecule with a fluorene-based core structure displayed a lower conductance than the compound with a 9,10-dihydrophenanthrene core unit.[103] This is in direct contrast to the values obtained from this set of measurements, as the fluorene-based molecule TFLT (**6**) gives a higher conductance than the phenanthrene-based compound TPDOT (**8**). Although the molecules in the earlier work possess structural differences expected to influence the electrical properties, as they have shorter linking groups and thiol contact groups instead of thiomethyl contacts, comparison with these results suggests that the presence of cross-conjugated carbonyl groups in TPDOT (**8**) significantly reduces the molecular conductance compared to an equivalent structure with no ketone groups. This is in accordance with the predicted occurrence of DQI phenomena for the cross-conjugated molecules.

In this study, it is important to determine the lengths of the molecular junctions formed to assess whether the differences in measured molecular conductance values may be the result of variations in the break-off distance as opposed to the intrinsic characteristics of the molecular wires. For the fluorene-derived molecules in this work, it is also important to identify the most probable molecule-electrode binding sites, as the thiophene S atoms in the linker structure may also enable molecule-electrode binding in addition to the thiomethyl anchoring groups. Theoretical molecular junction length values were determined by performing calculations using MM2 parameters (Chem3D, Perkin Elmer). These calculations produced approximate molecular junction lengths of 1.75 nm for TFLT (**6**), 1.77 nm for TFOT (**7**) and 1.74 nm for TPDOT (**8**) respectively. The results of these calculations indicate that the three molecules have highly comparable molecular lengths and therefore the presence of one or more cross-conjugated moieties has relatively little influence on the molecular backbone.

The molecular break-off distance values were obtained from all experimental measurements at 100 mV and 200 mV bias voltage (Table 3.2). The measured electrode separation distances for TFLT (**6**) (1.27 nm) and TPDOT (**8**) (1.25 nm) at 100 mV bias voltage are highly similar. In order to obtain the accurate break-off distance for the molecular junction, the snap-back distance on junction cleavage (approximately 0.5 nm)[82] must be added to the measured

separation distance between the Au electrodes. This value represents the distance of the nanogap formed upon the abrupt rupture of the Au-Au contact prior to molecular junction formation. When the snap-back distance is added to the electrode separation distance values, this gives approximate molecular junction lengths of 1.77 nm for TFLT (**6**) and 1.75 nm for TPDOT (**8**). These values are in good agreement with the theoretically predicted lengths of the two molecules, providing clear proof of molecular junction formation and subsequent stretching of the molecule in the junction as the tip moves away from the substrate.

Table 3.2. Lengths of Molecular Junctions for molecules **5-8** (TBPT, TFLT, TFOT and TPDOT) from Theoretical Calculations using MM2 Parameters and Experimental Measurements.

Molecule	**L(MM2)[a]/ nm**	$\boldsymbol{\Delta s = \Delta s^* + s_{corr}}$ **[b]/ nm**	
		100 mV	**200 mV**
5/TBPT	1.75	1.32	1.10
6/TFLT	1.75	1.77	1.71
7/TFOT	1.77	1.36	1.64
8/TPDOT	1.74	1.75	1.60

[a]L(MM2) corresponds to the distance calculated using MM2 parameters after minimization of energy for the molecular structure between the binding S atoms on the thiomethyl anchoring groups at opposite ends of the molecule. [b]Values of molecular break-off distance (Δs) calculated by the addition of the electrode separation distance (Δs*) obtained from the relevant 2-D conductance-distance histogram to the snap-back distance (s_{corr}).

The strong agreement between the theoretical molecular lengths and measured break-off distances is also significant because the break-off distance values are consistent with a molecular junction configuration where the molecule binds to the electrodes via the two thiomethyl terminal groups, as opposed to binding via the thiomethyl anchoring group at one end and the thiophene ring S atom at the opposite end. This is in agreement with the predicted behaviour of these compounds as donor-acceptor binding via the thiophene S atoms is less feasible in molecules with electron deficient core structures. This means the fluorene-derived molecules are expected to bind to electrodes via the thiomethyl anchoring moieties, allowing the molecular junctions to be stretched to approximately the same distance as the maximum theoretical molecular length. Additionally, these measurements provide further evidence that the difference in molecular conductance between TFLT (**6**) and TPDOT (**8**) is likely to be

influenced by the number of carbonyl units and presence or absence of cross-conjugation in the molecular wire, as the measured break-off distance lengths for these molecules are very similar and therefore cannot account for the different charge transport behaviour displayed by the two structures.

The molecular junction length of TFOT (**7**) at 100 mV bias voltage, however, is significantly shorter than expected, with a measured electrode separation distance of 0.86 nm at 100 mV bias voltage corresponding to a molecular break-off distance of 1.36 nm on addition of the snap-back distance, approximately 0.4 nm shorter than the predicted molecular length. Having said this, comparison of the conductance value for this molecule with the other 100 mV bias measurements (Figure 3.3) indicates that the conductance of TFOT (**7**) is not significantly lower than the other two molecules at this bias voltage and is consistent with the predicted trend in molecular conductance. This strongly indicates that the molecular junction conductance obtained in this measurement is not influenced by the shorter than expected break-off distance. Another explanation for this unexpected result could be that the fully stretched molecular junction configuration may not be the most probable junction geometry for this molecule, although it is unlikely that the preferred molecular junction configuration differs significantly from the structurally similar TFLT (**6**) or TPDOT (**8**) molecules. The most likely explanation for this discrepancy is that the data collected in this experiment represented a larger number of molecular junctions which underwent cleavage prior to attaining the maximum stretching distance, with fewer traces representing junctions at longer electrode separation distances being recorded than the equivalent measurements of the other two compounds. This would account for TFOT (**7**) giving a significantly shorter break-off distance than TFLT (**6**) or TPDOT (**8**) whereas the conductance measurement gives a value intermediate between the other two molecules, in agreement with the predicted result.

When the bias voltage is increased to 200 mV, the break-off distances obtained after adding the snap-back length to the measured electrode separation distances for TFLT (**6**) (1.71 nm), TFOT (**7**) (1.64 nm) and TPDOT (**8**) (1.60 nm) are all in good agreement with theory. For all three molecules, the measured values are approximately 0.05 – 0.15 nm shorter than the theoretically predicted molecular length. As for the 100 mV bias voltage measurements, the similar molecular junction lengths for all three compounds suggest that the difference between the measured conductance values can be attributed to the intrinsic properties of metal-molecule-metal junctions rather than variations in the molecular junction configuration. These results imply that at 200 mV bias the molecular junctions comprising the respective fluorene

derivatives undergo significant stretching as the tip-substrate separation increases but are cleaved before the maximum stretching distance is attained, suggesting that the junction stability decreases as the bias voltage is raised. It is unlikely that the lower measured break-off distances for the fluorene-derived molecules result from molecule-electrode binding via the thiophene S atoms as the observation of single molecular conductance peaks in the conductance plots for these compounds indicates that molecule-electrode binding is likely to be predominantly via the thiomethyl anchoring moieties. The lengths of the molecules studied and therefore the resulting molecular junctions formed, as indicated by the measured break-off distance, may provide another explanation for the relatively small drop in conductance on addition of one cross-conjugated ketone moiety, in other words the difference between TFLT (**6**) and TFOT (**7**), as well as that between TFOT (**7**) and TPDOT (**8**). This is because the efficiency of electronic transmission is lower in longer molecular wires, which may minimise the influence of cross-conjugation on the overall electrical properties of the molecule as the carbonyl groups are located relatively far from the molecule-electrode contacts.

The same theoretical approaches were also used to predict the molecular length of the 'control' molecular wire TBPT (**5**), which was calculated to be 1.75 nm, very similar to the fluorene-derived compounds. However, the experimental measurement at 100 mV bias voltage gives an electrode separation distance of 0.82 nm, corresponding to a break-off distance of 1.32 nm for this compound including the snap-back distance. This value is approximately 0.45 nm shorter than the theoretically predicted length, similar to the measured break-off distance of TFOT (**7**) but in contrast to the experimental break-off distances for TFLT (**6**) and TPDOT (**8**) molecules which display excellent agreement with the theoretical lengths at 100 mV bias. However, the conductance cloud in the 2-D conductance plot is sufficiently long to indicate stable molecular junction formation, which suggests the molecular junctions formed for TBPT (**5**) are less stable than the fluorene derivatives and are more likely to be cleaved prior to the molecule attaining the maximum possible stretching distance. The experimental measurement of TBPT (**5**) at increased bias voltage (200 mV) displays a break-off distance of 1.10 nm after addition of the snap-back length. This is significantly shorter than the break-off distance recorded for the fluorene-derived compounds at the same bias, in agreement with the measurement at 100 mV bias. The break-off distance is also shorter than that measured for this compound at lower bias (by approximately 0.2 nm), which matches the trend observed for the fluorene derivatives. This result therefore indicates that junction cleavage occurs at a shorter stretching distance at higher

bias voltage for all the extended molecular wires in this series, suggesting that molecular junction stability is lower at increased bias.

The shorter experimental break-off distances obtained for TBPT (**5**) relative to the fluorene-derived molecules (**6**-**8**) at 100 mV and 200 mV bias are significant as they indicate differences in the molecule-electrode binding geometries. These measured break-off distances suggest that the comparatively electron rich biphenyl-based compound forms stable molecular junctions with molecule-electrode binding via the thiophene S atom at one end of the molecule in addition to the geometry with binding via the thiomethyl anchoring moieties at both ends. Molecular junctions formed with the thiophene S-binding geometry are expected to display shorter break-off distances as the maximum junction stretching length is shorter than the theoretical end-to-end molecular length. This is in agreement with the data for TBPT (**5**), as the experimental break-off distances for this molecule are shorter than the theoretically predicted molecular length. This also supports the observation of multiple conductance peaks in the 1-D conductance plots for TBPT (**5**), corresponding to different molecular junction configurations, in contrast to the single peaks observed for the more electron deficient fluorene derivatives, particularly TFOT (**7**) and TPDOT (**8**) which possess strong electron withdrawing groups in the core structures. In these molecules the thiophene S atoms are too weakly electron donating to form stable donor-acceptor contacts with the electrodes and hence molecular junctions only form with stable molecule-electrode binding via the thiomethyl terminal groups.

In order to provide additional evidence that the conductance features observed in the 1-D and 2-D conductance plots for the TFLT (**6**) and TFOT (**7**) molecules correspond to metal-molecule-metal junctions, an additional series of STM-BJ measurements was performed using a lower sample concentration solution of 0.1 mM. Reducing the concentration of the sample solution decreases the number of molecules available for molecular junction formation, so it follows that the probability of stochastic molecular junction formation events at 0.1 mM concentration is likely to be lower than at 1 mM concentration. However, as the measured conductance value represents charge transport through an individual molecular junction, it is expected that lowering the sample solution concentration will not lead to a significant increase or decrease in the molecular conductance of the fluorene-derived molecules.

The experiments in this series were again performed at fixed bias voltage values of 100 mV and 200 mV bias. The measurement of 0.1 mM TFLT (**6**) at 100 mV bias voltage displays a conductance value of $10^{-3.7}$ G_0 and the measurement of 0.1 mM TFOT (**7**) also gives a

conductance value of $10^{-3.7}$ G_0 at 100 mV bias voltage (Figure 3.7). The conductance plots for both molecules show similar conductance features to the measurements performed using 1 mM concentration sample solutions of the respective compounds, as both molecules give a single sharp conductance peak and the peaks represent similar molecular conductance values. The strong agreement between the two sets of results indicate that the peaks observed at higher concentration also correspond to molecular junctions, which enhances the reliability of the conductance data from the higher concentration measurements.

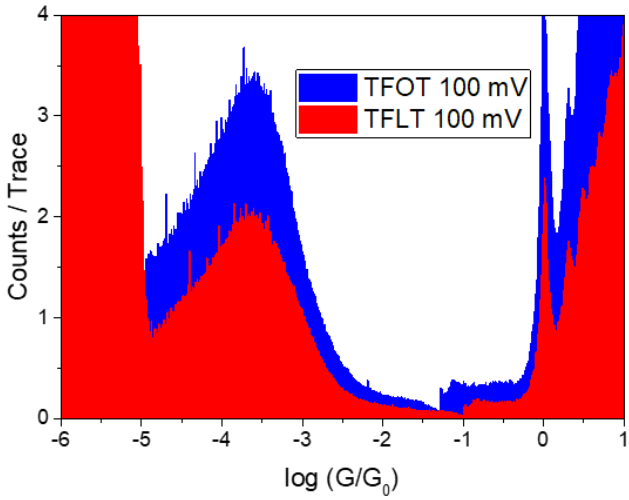

Figure 3.7. Comparison of the STM-BJ conductance measurements of molecular wires TFLT (**6**) and TFOT (**7**) at 100 mV bias voltage using a 0.1 mM concentration sample solution.

When the bias voltage is increased to 200 mV, the measurement of 0.1 mM TFLT (**6**) displays a conductance value of $10^{-3.7}$ G_0, very similar to the value measured at 100 mV bias. The measurement of 0.1 mM TFOT (**7**) displays a conductance value of $10^{-3.6}$ G_0 at 200 mV bias voltage, slightly higher than the value of $10^{-3.7}$ G_0 observed at 200 mV bias (Figure 3.8). The results obtained from the TFOT (**7**) experiments are consistent with the trend observed on raising the bias from 100 mV to 200 mV for all three molecules with a 1 mM concentration sample solution, as the conductance increases with increasing bias. The molecular conductance value of TFLT (**6**), however, does not increase when the bias voltage is raised to 200 mV, although both conductance values are similar to the measured conductance recorded for this molecule at the same fixed bias voltage values. This suggests that the charge transport behaviour is not significantly modified on changing the sample concentration. The conductance plots obtained for both molecules again show similar conductance features to those observed using a 1 mM concentration sample solution for the respective compounds, again displaying a single sharp molecular conductance peak.

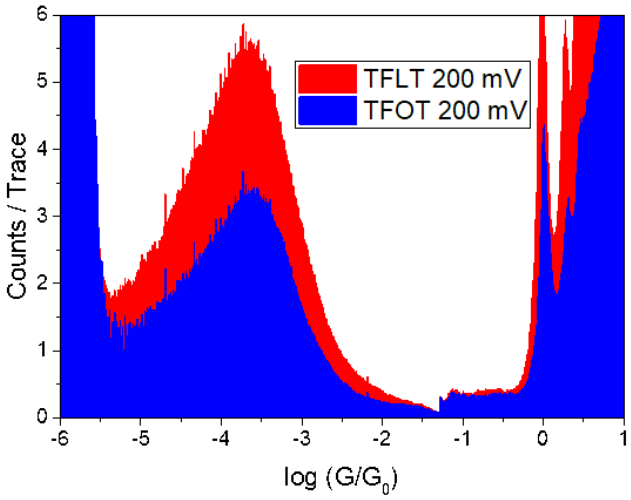

Figure 3.8. Comparison of the STM-BJ conductance measurements of molecular wires TFLT (**6**) and TFOT (**7**) at 200 mV bias voltage using a 0.1 mM concentration sample solution.

All conductance values obtained from the measurement of the TFLT (**6**) and TFOT (**7**) molecules using 0.1 mM concentration sample solutions are summarised (Table 3.3). Comparison of this set of results with the data obtained for these compounds using 1 mM concentration sample solutions makes it apparent that changing the sample concentration has very little effect on the electrical properties of these molecules. Both fluorene-derived molecules display similar molecular conductance at 0.1 mM concentration at a given fixed bias voltage to the values obtained from the measurements at higher sample concentration, suggesting the molecular junctions formed display similar charge transport behaviour regardless of the sample concentration.

Table 3.3. Conductance values for molecules **6-7** (TFLT and TFOT) obtained from STM-BJ measurements at 100 mV and 200 mV bias voltage using a 0.1 mM concentration sample solution.

Molecule	**Conductance (G) / G_0**	
	100 mV	**200 mV**
6/TFLT	$10^{-3.7}$	$10^{-3.7}$
7/TFOT	$10^{-3.7}$	$10^{-3.6}$

The molecular break-off distance values were obtained from all experimental measurements at 100 mV and 200 mV bias voltage (Table 3.4). This allows the stability of the molecular junctions formed using a 0.1 mM concentration solution of the relevant target molecule to be

assessed in comparison with the theoretically predicted molecular junction length values. For the TFLT molecule (**6**), electrode separation distances of 0.62 nm at 100 mV bias and 1.51 nm at 200 mV bias were obtained. For the TFOT molecule (**7**), electrode separation distances of 0.69 nm at 100 mV bias and 1.23 nm at 200 mV bias were obtained. As for the other experiments in this chapter, in order to obtain the accurate break-off distance for the molecular junction, the snap-back distance on junction cleavage (approximately 0.5 nm)[82] must be added to the measured separation distance between the Au electrodes. This value represents the distance of the nanogap formed upon the abrupt rupture of the Au-Au contact. When the snap-back distance is added to the electrode separation distance values, this gives approximate molecular junction lengths of 1.12 nm for TFLT (**6**) and 1.19 nm for TFOT (**7**) at 100 mV bias voltage. For the measurements performed at 200 mV bias voltage, measured molecular junction lengths of 1.73 nm for TFOT (**7**) and 2.01 nm for TFLT (**6**) are obtained after addition of the snap-back distance.

Table 3.4. Lengths of Molecular Junctions for molecules **6**-**7** (TFLT and TFOT) from Theoretical Calculations using MM2 Parameters and Experimental Measurements.

Molecule	**L(MM2)[a]/ nm**	$\boldsymbol{\Delta s = \Delta s^* + s_{corr}}$ **[b]/ nm**	
		100 mV	**200 mV**
6/TFLT	1.75	1.12	2.01
7/TFOT	1.77	1.19	1.73

[a]L(MM2) corresponds to the distance calculated using MM2 parameters after minimization of energy for the molecular structure between the binding S atoms on the thiomethyl anchoring groups at opposite ends of the molecule. [b]Values of molecular break-off distance (Δs) calculated by the addition of the electrode separation distance (Δs*) obtained from the relevant 2-D conductance-distance histogram to the snap-back distance (s_{corr}).

The experimental break-off distance values recorded can also be directly compared with the measurements performed at higher sample concentration. The trend in break-off distance length for the 0.1 mM concentration experiments is the opposite to the trend observed for the 1 mM measurements, as the break-off distance values measured at 200 mV bias are higher than those recorded at 100 mV. For both TFLT (**6**) and TFOT (**7**), the measured break-off distance at 100 mV bias is in the region of 0.6 nm shorter than the theoretically predicted length. By contrast, the molecular break-off distance for TFLT (**6**) at 200 mV bias is approximately 0.25 nm longer than the theoretical length, and the measured break-off distance for TFOT (**7**) is in

good agreement with the theoretically predicted value. The most significant implication of these results is that at 100 mV bias voltage, the molecular junctions formed using a 1 mM concentration sample solution appear to be more stable than junctions formed using a 0.1 mM solution, whereas the reverse is true in the measurements at 200 mV bias. It is not clear why the measured break-off distances are shorter in the experiments using a 0.1 mM concentration solution at 100 mV bias than in measurements using the same sample concentration at 200 mV bias. This could be attributed to the combination of low sample concentration with low applied bias reducing the stability of molecular junctions in the highly stretched junction geometry, causing the junctions to rupture at distances significantly shorter than the maximum stretching length. However, further experiments under the same conditions would be required to prove or disprove this theory, as it differs significantly from the behaviour observed in the 1 mM concentration measurements at both 100 mV and 200 mV bias.

The formation of stable molecular junctions for both TFLT (**6**) and TFOT (**7**) at 100 mV and 200 mV bias voltage further supports the conclusion that the conductance features observed in the experiments performed using 1 mM concentration sample solutions represent molecular junctions comprising the target molecules. Also, although the break-off distance values measured for these molecules at 100 mV bias using a 0.1 mM concentration sample solution are significantly shorter than the theoretically predicted lengths, it is probable that the molecular wires bind to the electrodes via the thiomethyl anchoring groups at each end of the molecular junction. This is because the 1-D conductance plots for both molecules show sharp single conductance peaks, consistent with the formation of molecular junctions in a single stable configuration with molecule-electrode binding via the thiomethyl moieties. This is in contrast to the two conductance peaks observed for TBPT (**5**) at 1 mM concentration, where a distinct low conductance peak is observed at a conductance value just under one order of magnitude lower than the high conductance peak. The absence of a second peak in the conductance plots suggests that TFLT (**6**) and TFOT (**7**) do not bind to the electrodes via the thiophene S atoms at either 0.1 mM or 1 mM sample concentration. These experiments enhance the reliability of the results in this study and provide further evidence that the observed changes in molecular conductance between the different compounds in this series can be attributed to the influence of altering the core unit structure on charge transport behaviour.

3.4 Conclusions

In this project, the influence of cross-conjugation on the electrical properties of a series of fluorene-derived molecular wires has been investigated at 100 mV and 200 mV bias voltage. The experimental results show that molecular conductance decreases on the addition of one or more carbonyl moieties orthogonal to the primary charge transport pathway. The data shows a consistent trend at both bias voltage values, as the linearly conjugated fluorene-based molecule displays the highest conductance value, whereas the fluorenone-based molecule (incorporating one carbonyl group) has a lower conductance and the phenanthrene-9,10-dione-based molecule (incorporating two carbonyl groups) has the lowest conductance of the three compounds. The significant difference in conductance between the fluorene- and phenanthrene-9,10-dione-based molecules suggests destructive interference effects influence the properties of the cross-conjugated molecules, supporting the predicted occurrence of Fano resonances. For all three molecules, the conductance increases on raising the bias from 100 mV to 200 mV, indicating that charge transport predominantly occurs via the HOMO-dominated pathway. The molecular break-off distance values from the majority of experiments are in good agreement with theoretically predicted molecular lengths, indicating that the changes in conductance are likely to result from the intrinsic molecular characteristics rather than differences in molecular junction configuration. Comparison with the electrical properties of the 'control' biphenyl-based molecule shows that the conductance features observed for the fluorene derivatives are consistent with formation of molecular junctions comprising extended molecular wires. The biphenyl derivative has a higher conductance than the two molecules with cross-conjugated carbonyl moieties, supporting the prediction that destructive interference lowers the conductance of the cross-conjugated molecules. However, break-off distance measurements indicate that this molecule exhibits different molecule-electrode binding behaviour to the fluorene-derived structures, displaying a greater variety of junction geometries. Additionally, the electrical properties of the fluorene- and fluorenone-based molecules were measured using a lower concentration sample solution (0.1 mM) at 100 mV and 200 mV bias voltage. The conductance values were similar to the values measured using higher concentration solutions, indicating that sample concentration has little influence on the conductance properties. This provides further evidence that the conductance features correspond to the formation of molecular junctions, enhancing the reliability of the higher concentration measurements. These results show that chemical substitution of cross-conjugated ketone moieties plays an important role in controlling conductance and QI behaviour in molecular junctions. The experiments

performed in this chapter have provided insight into structure-property relationships influencing charge transport through molecules with fluorene-derived structures and the effect of side groups orthogonal to the primary charge transport pathway on molecular conductance.

Chapter 4: Investigation of Structure-Property Relationships in Molecular Wires with Bidentate Anchoring Moieties: Triazole-Terminated Molecules

4.1 Introduction to Triazole-Terminated Molecular Wires

Anchoring groups play a crucial role in mediating charge transport through molecular junctions as they allow electrical contact to be established between the molecule of interest and the electrode materials. As the anchoring moieties directly control the characteristics of the molecule-electrode interface, they determine the strength of the molecule-electrode electronic coupling and therefore exert a strong influence on the overall conductance of the molecular junction. This means that optimization of the molecule-electrode contacts provides an effective method for tuning the electrical properties of the junction. As a consequence, understanding the structure-property relationships that control the effectiveness of anchoring the molecule to the electrodes is important for tuning the electrical properties of the molecular junction with a view to potential applications.

There are two main classes of anchoring groups which can be used to establish contact between molecular wires and metallic electrodes in metal-molecule-metal junctions. The first class includes covalent bonding groups such as thiols (–SH)[37] whereas the second class consists of donor-acceptor binding groups, which involve electron transfer from π-donors, such as fullerenes,[43] or lone pair donors, a category which includes σ-donor groups such as amines, to the metal surface.[20] The interactions between the two classes of binding groups and metallic electrodes differ substantially, as covalent binding anchoring moieties bind strongly to the electrodes, whereas the molecule-electrode contact for donor-acceptor binding groups is via dative interactions and is therefore significantly weaker. The binding strength has further implications for the electrical properties as the weaker donor-acceptor binding groups preferentially bind to specific sites on the electrode surface. This means the resulting molecular junctions display better defined conductance signatures and a narrower range of conductance values than covalent anchoring groups, which bind in a wider range of configurations.[20]

In this work, the electrical properties of two molecular wires with 1,2,4-triazolyl terminal groups, DMTB (**9**) and DETB (**10**), have been investigated. These two structures share a simple identical benzene core in addition to the same 1,2,4-triazolyl anchoring moieties (Scheme 4.1). They differ only in the alkyl chains substituted on the terminal rings in the 3- and 5- positions, as DMTB (**9**) features methyl groups (-CH_3) whereas DETB (**10**) features ethyl groups (-C_2H_5). This allows the influence of the alkyl side chains on the molecular conductance to be assessed in a direct comparison, as the molecules should otherwise possess highly similar electronic structures and have very similar molecular lengths. The primary function of the alkyl chains is to improve the stability of the molecules in metal-molecule-metal junctions, which should

increase the probability of obtaining stable current-distance traces from the electrical measurements in this study. It is not expected that the lengths of the two alkyl chains will lead to any significant difference between the electrical properties of the two molecules, as the electron donating capabilities of the two groups are similar and ethyl groups do not present significantly higher steric bulk compared to methyl groups.

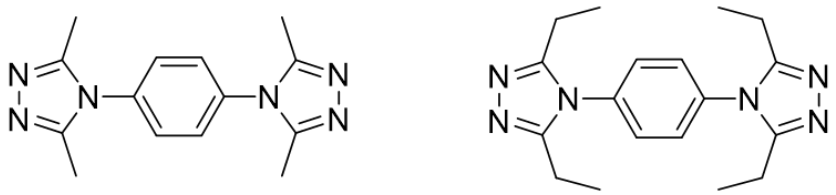

9 **10**

Scheme 4.1. Molecular structures of compounds **9-10**, DMTB and DETB.

The most significant features of the triazolyl-terminated molecular wires with regard to this study are the multiple heteroatoms (nitrogen) present on each terminal group. The majority of metal-molecule-metal junctions comprise molecules with a single anchoring site at each terminus. The five-membered aromatic ring structure of 1,2,4-triazole, however, incorporates three N atoms, including a pair of pyridine-like N atoms in the 1- and 2- positions. In the context of molecular electronics, the triazolyl moiety can be classified as a multidentate contact group because the pyridine-like N atoms on each terminal group provide multiple anchoring points for molecule-electrode binding. The ability of the 1,2,4-triazolyl anchoring group to bind via multiple points of contact is analogous to the chelate effect and is predicted to lead to enhanced metal-molecule binding compared to functional groups with only one anchoring point such as amines or pyridines. This is potentially very promising, as the molecule-electrode contacts formed for triazolyl anchoring moieties could enable binding interactions which combine the high binding strength of covalent binding groups such as thiols with the high binding specificity for under-coordinated surface sites shown by donor-acceptor binding groups.[20,37] This would overcome the main limitations of thiol-terminated molecules, which typically form molecular junctions with several different geometries and therefore display a broad range of conductance values, and amine-terminated molecules, which bind via weak molecule-electrode contacts resulting in lower junction stability and lower molecular conductance values.

Other research groups have previously investigated the influence of anchoring groups enabling molecule-electrode binding via multiple anchoring sites on each moiety on the electrical properties of molecular wires. One early example involved the measurement of the

conductance of a series of alkanes by Chen *et al*., which included an alkane molecular wire with carboxylic acid anchoring moieties permitting multidentate binding via the terminal O atoms.[37] However, they found that this molecule displays a lower molecular conductance and lower binding strength than analogous alkanes with thiol or amine terminal groups. These results indicate that the carboxylic acid anchoring moiety does not lead to enhanced charge transport properties compared to monodentate binding groups. This is attributed to weak molecule-electrode binding via the terminal O atoms and weak electronic coupling between the molecule and electrodes, which suggests that the poor charge transport properties result from the specific characteristics of the carboxylic acid anchoring group.

More recent studies investigating the electrical properties of molecules with multidentate anchoring groups have displayed more promising results, indicating that molecules with multiple anchoring sites have significant potential for optimising electrical properties in molecular junctions. For example, a study by Herrer *et al*. has found that the pyrazolyl-terminated molecule 1,4-bis(1H-pyrazol-4-ylethynyl)benzene provides a bidentate binding platform which enables strong double anchoring of the molecule to Au electrodes at both termini.[104] The high measured conductance values observed for this molecule in both high and low conductance molecular junction configurations also indicate that the pyrazole anchoring moieties facilitate strong molecule-electrode coupling. The triazolyl-terminated molecules have the potential to provide similar bidentate molecule-electrode binding and if they provide similar molecule-electrode coupling strength could offer significant advantages in mechanical stability and electronic transmission compared to molecules binding via a single donor-acceptor site. This is supported by another study which reported that an oligo(phenyleneethynylene) (OPE) molecular wire with bidentate 2-aminepyridine anchoring groups displays a single molecule conductance value approximately one order of magnitude higher than analogous molecules with either pyridine or amine anchoring groups.[105] This provides further evidence that multidentate anchoring moieties enable the formation of strong, robust molecule-electrode contacts which permit efficient charge transport through the molecular junction.

It should also be emphasised that other advantages of using triazolyl-based anchoring groups can be attributed to the similarities between the 1,2,4-triazole moiety and more conventional monodentate nitrogen-based binding groups. Research by Venkataraman *et al*. found that amine-terminated molecular wires give narrow conductance distributions compared to equivalent thiol-terminated molecules as a result of the weaker dative molecule-electrode

binding for the amine moieties.[20] Likewise, a study by Arroyo *et al*. indicated that amine binding groups form better defined molecular junctions than thiol groups as thiol-terminated molecules are more likely to form multiple molecular junctions, which can significantly deform the metallic electrodes.[46] This behaviour has been attributed to the more uniform binding geometry of the amine anchoring group, which preferentially binds to under-coordinated sites on the electrode surface, whereas thiols can bind to a wider range of sites on the metallic electrode surface and therefore display greater variation in anchoring group-electrode contact geometry, resulting in broader conductance features. If similar binding behaviour is observed for triazolyl anchoring moieties, this suggests these functional groups would be ideal for achieving robust, stable and highly selective molecule-electrode binding. This would be highly useful for molecular electronics applications as the molecular junctions could potentially combine high conductance with a narrow distribution of conductance values, offering a desirable combination of properties for functional devices.

The electrical properties of conjugated molecular wires with terminal moieties incorporating multiple heteroatoms have been investigated by Li *et al*., who performed STM-BJ measurements on a series of molecules with oxazole anchoring moieties.[106] Their work showed that the oxazolyl-terminated molecules displayed measurable conductance values (significantly above $10^{-6.0}$ G_0), indicating that the terminal moieties permit efficient metal-molecule binding, leading to the formation of stable molecular junctions. This study is particularly interesting from the perspective of this project as several of the molecules investigated have structures consisting of a benzene core attached to terminal five-membered rings in the 1- and 4- positions (*para*-linked) featuring multiple heteroatoms, in common with the triazolyl-terminated molecular wires featured in this work.

The N atoms linking the triazolyl rings to the central benzene ring are another important structural feature of the two molecules, as the electronic transmission pathway through the molecular wire must pass through both 4-position N atoms. This means no through-bond conductance pathway avoiding the linking heteroatoms is available, maximising the influence of these two N atoms on the electrical properties of the molecules. The presence of the 4-position N atom in the 1,2,4-triazole group means this moiety is similar to the five-membered ring structure of imidazole. This is significant because Fu *et al*. have previously investigated the electrical properties of imidazole-terminated molecules. They reported the formation of stable molecular junctions for compounds with imidazole anchoring groups, albeit featuring alkyl linkers rather than conjugated core units. The measured single molecule conductance

values for junctions incorporating these compounds fell in the range of $10^{-4.0}$ to $10^{-6.0}$ G_0, indicative of efficient metal-molecule binding via this anchoring group.[107] This moiety differs from 1,2,4-triazole as the ring only possesses one pyridine-like N atom, but this result suggests the 1- and 2-position N atoms in the triazolyl anchoring moieties should have the capability to bind to metallic electrodes to form stable molecular junctions. The experimental investigation of the electrical properties of these structures is significant as it expands the range of anchoring moieties used for forming metal-molecule-metal junctions and allows the influence of 1,2,4-triazolyl terminal groups on charge transport behaviour in molecular wires to be evaluated.

4.2 STM-BJ Measurement of Triazole-Terminated Molecular Wires

The electrical properties of the two triazole-terminated molecular wires have been measured in solution using the STM-BJ technique. The 1,2,4-triazole-terminated molecules **9** and **10** (Scheme 4.1) were synthesised by our collaborator Dr Amal Al-Azmi at Kuwait University. For each measurement, a 10^{-3} M solution of each molecular wire was prepared by dissolving the relevant compound in 1,2,4-trichlorobenzene and the measurements were performed at a fixed bias voltage (100 mV – 500 mV). The electrical properties of the molecules have been measured at different fixed bias voltage values to study the influence of raising the bias on the molecular conductance and junction stability. Thousands of current-distance (I-s) curves were collected from each STM-BJ experiment and all traces obtained were analysed, with no data selection methods used to construct the conductance histograms.

4.3 Experimental Results for Triazole-Terminated Molecular Wires

The experimental results from the measurement of the electrical properties of the triazolyl-terminated molecular wires are presented in the form of 1-dimensional (1-D) conductance plots and 2-dimensional (2-D) conductance-distance histograms. Measurement of the low-bias single molecule conductance values (100 mV) of these compounds using the STM-BJ technique gives conductance values of $10^{-4.5}$ G_0 for DMTB (**9**) and $10^{-4.4}$ G_0 for DETB (**10**) respectively (Figure 4.1). The well-defined molecular conductance peaks and discernible conductance values (significantly higher than the noise level below $10^{-6.0}$ G_0) indicate that the 1,2,4-triazolyl anchoring moieties provide strong molecule-electrode binding, allowing the formation of stable molecular junctions with measurable conductance values. The 1-D plots for both compounds display relatively short peaks with comparatively narrow conductance

distributions, consistent with the expected observation for molecular junctions comprising molecular wires with short end-to-end lengths and donor-acceptor anchoring groups. The 2-D conductance plots for the two molecules show that the conductance decreases as the electrode separation distance increases and this behaviour is consistent with the formation and stretching of molecular junctions. These results suggest that triazolyl anchoring groups have considerable potential in the development of single molecule-based devices, as the clearly resolved conductance peaks provide strong evidence of charge transport through the molecular wires.

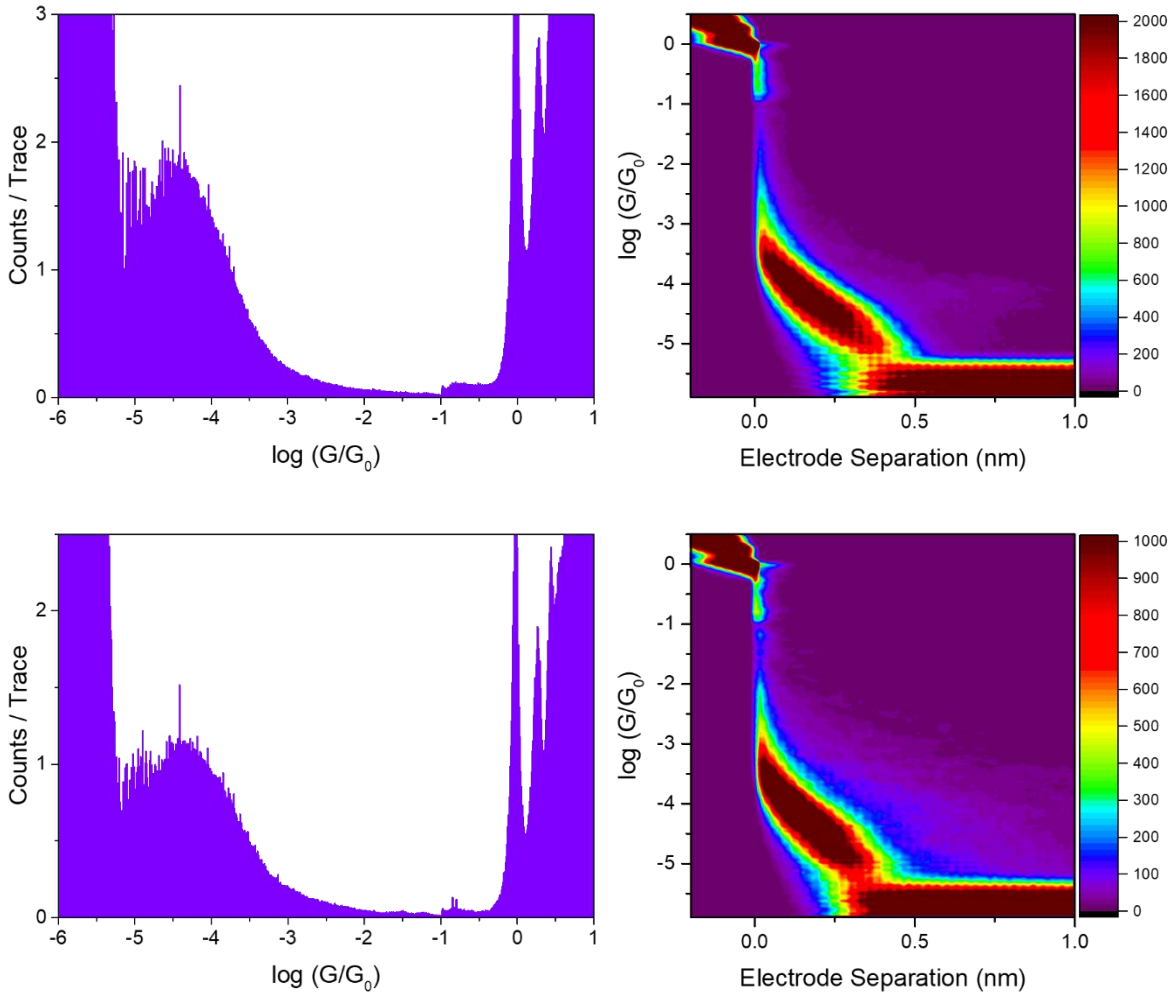

Figure 4.1. Top: STM-BJ measurement of the molecular wire DMTB (**9**) in solution (solvent: 1,2,4-trichlorobenzene) at 100 mV bias voltage. Bottom: STM-BJ measurement of the molecular wire DETB (**10**) in solution (solvent: 1,2,4-trichlorobenzene) at 100 mV bias voltage.

Direct comparison of the 1-D conductance plots of the DMTB (**9**) and DETB (**10**) molecules at 100 mV bias voltage (Figure 4.2) indicates that the two molecules display highly similar conductance features in addition to very similar conductance values. This suggests that a small

increase in the length of the alkyl chain has little influence on the electrical properties, implying that this does not significantly change the electronic structure in agreement with the expected observation. More significantly, these plots provide further clear evidence that the 1,2,4-triazolyl terminal groups enable reproducible formation of stable metal-molecule-metal junctions, as a characteristic peak profile is observed in the measurement of both molecules. This suggests that the molecular junctions formed display comparable charge transport behaviour and implies that the molecule-electrode binding strength at the anchoring sites is also similar.

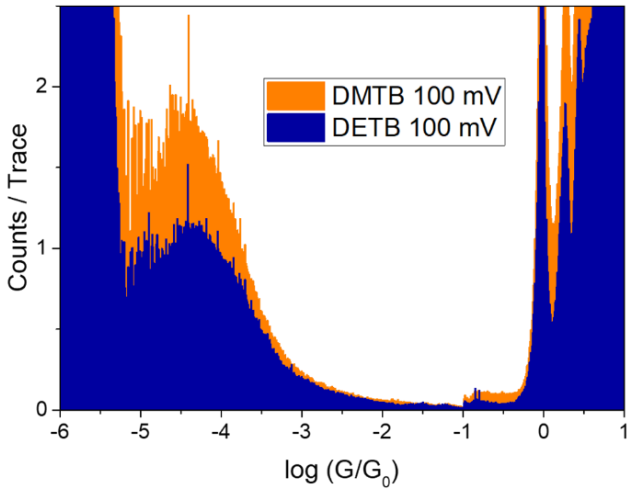

Figure 4.2. Comparison of the STM-BJ conductance measurements of DMTB (**9**) and DETB (**10**) molecular wires at 100 mV bias voltage.

The molecular conductance values of the main conductance peaks for the triazolyl-terminated compounds have been measured in all experiments. When the STM-BJ experiments for DMTB (**9**) and DETB (**10**) were performed at increased bias voltage (200 mV) under the same conditions, the molecular conductance values obtained were comparable to the 100 mV bias measurements, with both molecules giving a conductance value of $10^{-4.4}$ G_0. The measured conductance values were again found to be similar when the bias voltage was further raised to 300 mV bias, with conductance values of $10^{-4.5}$ G_0 for DMTB (**9**) and $10^{-4.7}$ G_0 for DETB (**10**) being obtained. Comparison of the 1-D conductance plots for the two molecules at fixed bias voltage values from 100 mV to 300 mV shows that the behaviour of the two molecules as the bias is incrementally raised is very similar, with no significant increase or decrease in conductance or alterations in the conductance features observed (Figure 4.3). This is particularly apparent for the peaks observed for DMTB (**9**) in the experiments at 200 mV and 300 mV bias, which display very similar conductance values and peak profiles in the 1-D plots.

The minimal change in molecular conductance with increased bias voltage indicates that increasing the flow of current through the molecular junction does not significantly enhance transmission through the junction. This is important as the consistently low conductance values imply that electronic transmission may be suppressed by poor molecule-electrode coupling efficiency, which could be attributed to either the molecular backbone or the anchoring groups.

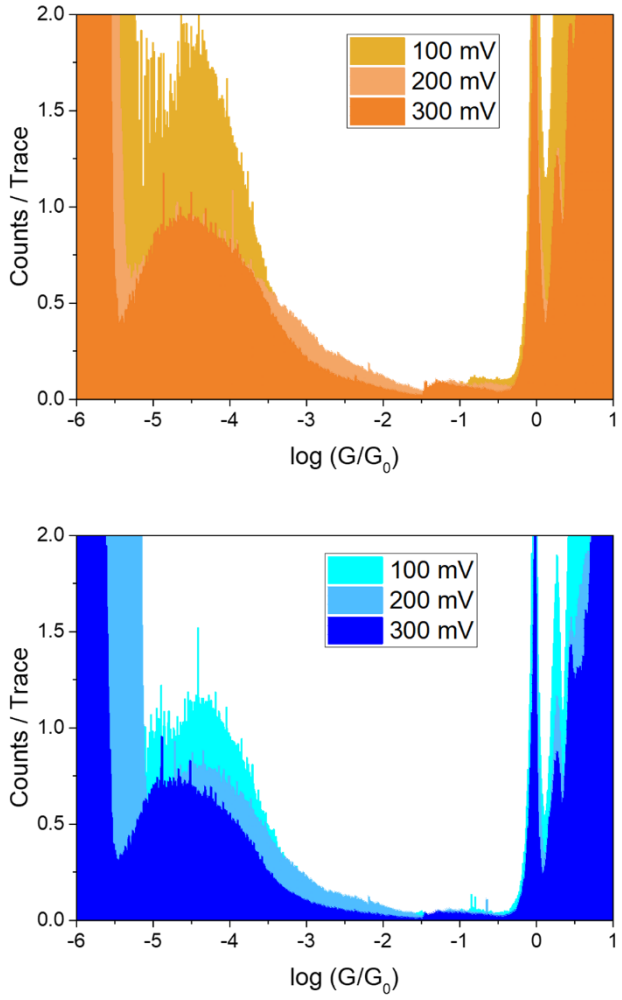

Figure 4.3. Top: Comparison of the STM-BJ measurements of the molecular wire DMTB (**9**) at 100 mV to 300 mV bias voltage. Bottom: Comparison of the STM-BJ measurements of the molecular wire DETB (**10**) at 100 mV to 300 mV bias voltage.

Both molecules again showed similar conductance behaviour when the bias voltage was further raised to 400 mV, with values of $10^{-4.4}$ G_0 for DMTB (**9**) and $10^{-4.6}$ G_0 for DETB (**10**), although the conductance peaks are less clearly resolved than at lower bias. This suggests that increasing the bias to 400 mV lowers the molecular junction stability but does not alter the charge transport properties. However, a significant change is observed in the conductance plots of the two molecules when the bias is increased to 500 mV, as two conductance peaks are observed in the

1-D plots for both DMTB (**9**) and DETB (**10**) (Figure 4.4). For both molecules, the measurement at 500 mV bias shows a high conductance peak with a similar conductance to the peaks observed at lower fixed bias voltage ($10^{-4.6}$ G_0), in addition to a lower conductance peak at $10^{-4.9}$ G_0 (DMTB) (**9**) and $10^{-5.0}$ G_0 (DETB) (**10**). This second peak is not observed in any of the lower bias experiments but can be clearly distinguished in the conductance plots for both triazolyl-terminated molecules at 500 mV bias voltage. It is not clear whether the low conductance features observed in these plots correspond to a molecular junction configuration which only occurs when the applied bias is raised to 500 mV or whether the peaks for the equivalent junctions are obscured by the noise level in the lower bias measurements.

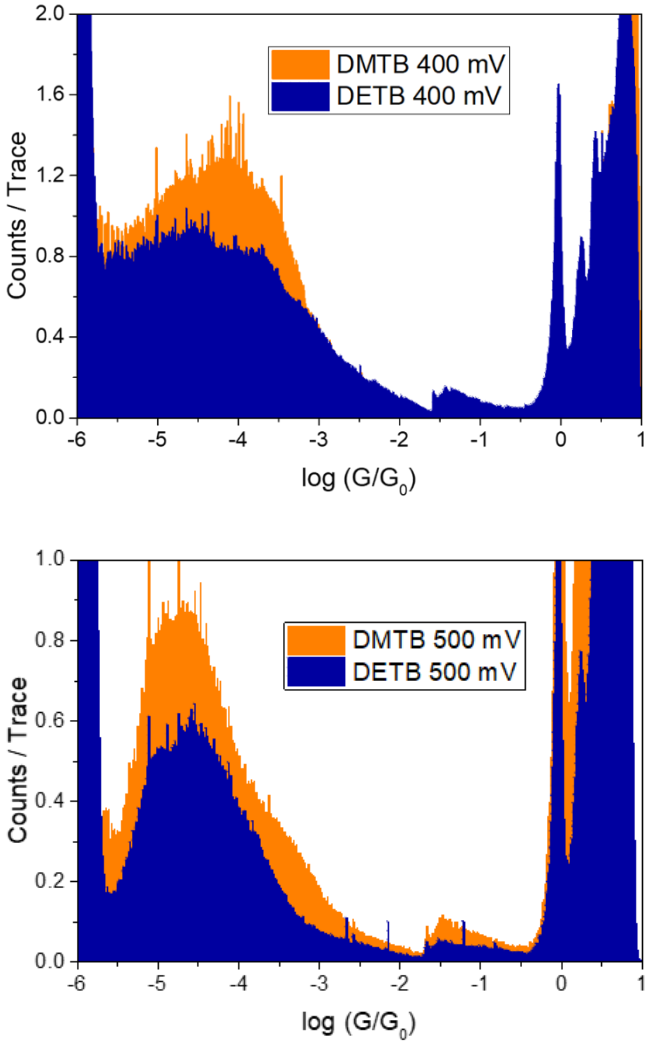

Figure 4.4. Top: Comparison of the STM-BJ conductance measurements of DMTB (**9**) and DETB (**10**) molecular wires at 400 mV bias voltage. Bottom: Comparison of the STM-BJ conductance measurements of DMTB (**9**) and DETB **(10)** molecular wires at 500 mV bias voltage.

It should be noted that the bistable conductance signatures observed for both triazole-terminated molecules in the 500 mV bias measurements resemble the distinct high and low conductance features reported for pyridine-terminated molecular wires.[39] This is useful for gaining information about the characteristics of the metal-molecule-metal junctions as it suggests the two conductance peaks are likely to correspond to different molecular junction configurations. It has previously been shown that the molecular conductance in pyridine-terminated molecular junctions increases as the Au-N bond tilt angle increases. This is significant because as the electrode separation distance increases, the molecular junction is stretched and this is accompanied by a decrease in the Au-N bond tilt angle. The conductance therefore decreases with increasing electrode separation distance as the molecular wire is stretched in the junction.[12] As the 1,2,4-triazolyl anchoring moieties include two pyridine-like N atoms, a similar relationship between molecular junction stretching length and conductance is predicted for the triazolyl-terminated molecules. From this, it can be deduced that the high conductance feature is likely to represent molecular junctions with a shorter electrode separation distance and larger tilt angle between tip and substrate, whereas the low conductance feature is expected to correspond to a molecular junction geometry with a larger electrode separation distance with the molecule in a stretched configuration. This is supported by comparing the conductance features observed for DMTB (**9**) and DETB (**10**) at 500 mV bias voltage with the conductance signatures for the dipyridylamine molecules studied elsewhere in this work (Chapter 2), which were found to display two distinct peaks in the conductance plots, corresponding to high and low conductance junction geometries.

Comparison of the measured molecular conductance values for DMTB (**9**) and DETB (**10**) shows that the two 1,2,4-triazolyl-terminated molecules consistently display very similar conductance values at bias voltages ranging from 100 mV to 500 mV (Table 4.1). This strongly indicates that changing the length of the alkyl side chain does not significantly influence charge transport through the molecular junctions. This is in agreement with the expected behaviour for these compounds as ethyl and methyl groups are electronically very similar and switching between these two alkyl chains is not expected to significantly affect the position or alignment of the molecular orbitals. This is consistent with earlier work studying alkyl-substituted fluorene derivatives, which also showed that changing the length of the alkyl chain had little effect on the electrical properties of the molecules.[96] This implies that the molecule-electrode coupling strength is likely to be comparable for the two structures. This is significant because, although the conductance data provides clear evidence of stable molecular junction formation

for both triazole-terminated molecular wires, the measured conductance values are comparatively low, as all experiments give molecular conductance values below $10^{-4.0}$ G_0, typically in the range between approximately $10^{-4.5}$ G_0 and $10^{-5.0}$ G_0. The consistency of the measured conductance values for these two molecules becomes particularly apparent if the low conductance peaks displaying conductance values in the region of $10^{-5.0}$ G_0 from the 500 mV bias measurements, which are likely to represent a different molecular junction configuration, are excluded. Closer analysis of the data reveals that the conductance values for all other peaks observed for these molecules, including all peaks reported from 100 mV to 400 mV bias voltage, are separated by less than half an order of magnitude, with conductance values ranging from $10^{-4.4}$ G_0 to $10^{-4.7}$ G_0.

Table 4.1. Conductance values for molecules **9** and **10** (DMTB and DETB) obtained from STM-BJ measurements at fixed bias voltage from 100 mV to 500 mV.

Molecule	**Conductance (G) / G_0**				
	100 mV	**200 mV**	**300 mV**	**400 mV**	**500 mV**
9/DMTB	$10^{-4.5}$	$10^{-4.4}$	$10^{-4.5}$	$10^{-4.4}$	$10^{-4.6}$ (HC)[a] $10^{-4.9}$ (LC)
10/DETB	$10^{-4.4}$	$10^{-4.4}$	$10^{-4.7}$	$10^{-4.6}$	$10^{-4.6}$ (HC) $10^{-5.0}$ (LC)

[a]HC and LC denote experimentally measured high and low conductance values corresponding to distinct molecular conductance peaks in the conductance plots.

One possible explanation for the consistently low measured conductance values is weak molecule-electrode binding between the triazolyl anchoring moieties and the Au electrodes. However, the similar conductance values obtained for DMTB (**9**) and DETB (**10**) at different fixed bias voltages indicate that the charge transport characteristics do not change significantly with increased bias. This is significant as electronic transmission behaviour is controlled by the overall characteristics of the molecular junction and cannot be explained by the binding strength alone, as this is not expected to significantly influence the properties of the molecular bridge. It should also be emphasised that the 1,2,4-triazolyl terminal groups share several similarities with pyridyl anchoring groups, the properties of which have been studied in detail by other groups.[12,39] These studies indicate that molecule-electrode binding for pyridine-terminated molecules is relatively strong compared to other donor-acceptor anchoring groups such as amines. Significantly, combined conductance and force measurements by Frei *et al.*

demonstrated that the binding strength and molecular conductance are not directly related. They showed that the bond rupture force for the Au-N bond in 4,4′-bipyridine molecular junctions is higher than for the Au-N bond in 1,4-benzenediamine junctions, indicating that the binding strength of the pyridyl anchoring groups is higher, but the conductance value of the amine-terminated molecule is over one order of magnitude higher.[83] Additionally, Herrer *et al*. reported that molecular wires incorporating pyrazolyl terminal groups, which have similar structures to the triazolyl moieties, exhibit strong molecule-electrode binding and display high conductance values compared to the molecular junction length.[104] These results suggest that the 1,2,4-triazolyl anchoring moieties, which are based on five-membered heterocyclic ring structures with two pyridine-like N atoms on each terminal group, are likely to display efficient molecule-electrode binding. This means the low measured conductance values for the triazole-terminated molecules are unlikely to be caused by weak binding at the anchoring sites.

Another explanation for the relatively low conductance of the triazole-terminated molecules is poor electronic coupling through the molecular core structure resulting from poor orbital overlap between the metal and molecule, which would inhibit electronic transmission through the molecular junction. It is known that transmission through molecules with pyridyl anchoring moieties predominantly occurs through the LUMO, which for pyridyl-terminated compounds is expected to be significantly closer in energy to the Fermi energy (E_F) for Au electrodes than the HOMO.[39] Likewise, Li *et al*. reported that the LUMO is the dominant charge transport pathway for oxazolyl-terminated molecules.[106] This implies that the LUMO is highly likely to represent the main charge transport pathway for the triazole-terminated compounds in this series of experiments. This suggests that the consistently low ($< 10^{-4.0}$ G_0) conductance values displayed by the triazolyl-terminated molecules are likely to result from unfavourable conductance properties of the LUMO, leading to poor electronic coupling through the molecular wire, rather than from weak molecule-electrode coupling at the anchoring sites. This would also explain the lack of variation in the measured conductance as the bias voltage is increased from 100 mV to 500 mV. This differs from the expected behaviour for molecules where the LUMO is the dominant charge transport pathway, as conductance is predicted to decrease on increasing the bias voltage for these molecules.[35] However, in the triazolyl-terminated molecules, weak electronic coupling prevents efficient transmission through the molecular junction and hence no significant change in conductance is observed on raising the bias. This observation is supported by experiments performed on imidazole-terminated molecules by Fu *et al*., who found that these molecules displayed relatively low conductance

values and also reported that changing the applied bias voltage had very little influence on the molecular conductance. This result is significant as imidazole anchoring moieties also bind to the metal electrodes via pyridine-like N atoms, in agreement with the favoured binding mode for the triazolyl-terminated compounds.[107]

It is also significant that the conductance behaviour displayed by the triazole-terminated molecules is more similar to imidazole-terminated molecules than pyrazole-terminated compounds, as Herrer *et al*. reported that molecules with pyrazolyl anchoring groups display high conductance values relative to their molecular length.[104] The 1,2,4-triazole moiety differs from both the imidazolyl and pyrazolyl groups as it possesses three heteroatoms on each ring. However, molecules with triazolyl anchoring groups closely resemble imidazole-terminated compounds in one key structural aspect because the anchoring groups are linked to the molecular bridge structure via N atoms,[107] whereas in pyrazole-terminated compounds the anchoring moieties are linked to the molecular bridge structure via C atoms.[104] The better agreement in charge transport behaviour between triazole-terminated molecules and imidazole-terminated molecules suggests that the 4-position N atoms in the 1,2,4-triazole moieties inhibit electronic transmission through the molecular wire. This is consistent with the observation of low measured conductance values which do not significantly change on raising the bias and explains why the conductance values for DMTB (**9**) and DETB (**10**) are lower than the values measured for longer pyrazole-terminated compounds. This provides further evidence that weak electronic coupling is responsible for the conductance behaviour reported for these molecules.

In order to determine whether 1,2,4-triazole has the potential to provide a viable anchoring group in molecular electronics, it is important to establish the lengths of the molecular junctions, which provide an indication of the stability of the junctions formed. If the measured molecular break-off distances are in good agreement with the theoretically predicted molecular junction lengths, this suggests that the molecules form stable molecular junctions which can undergo stretching to approximately the maximum distance between the metallic electrodes. The theoretically predicted lengths of the DMTB (**9**) and DETB (**10**) molecules are both predicted to be 0.96 nm according to calculations performed using MM2 parameters (Chem3D, Perkin Elmer). These calculations show that the two compounds have very similar lengths, which indicates that the length of the alkyl side chains on the triazolyl anchoring groups is expected to exert very little influence on the molecular backbone structure.

The experimental break-off distance values for these molecules were obtained from all measurements from 100 mV to 500 mV bias voltage (Table 4.2). The measured electrode separation distances at 100 mV bias are highly similar, giving distances of 0.46 nm for DMTB (**9**) and 0.45 nm for DETB (**10**). In order to obtain the accurate molecular break-off distance, the snap-back distance on junction cleavage (approximately 0.5 nm)[82] must be added to the measured separation distance between the Au electrodes, giving approximate molecular junction lengths of 0.96 nm for DMTB (**9**) and 0.95 nm for DETB (**10**). These experimentally obtained values are in very good agreement with the theoretically predicted molecular lengths calculated for both triazolyl-terminated molecules. This indicates that for both molecules, junction cleavage is likely to occur when the molecule is almost completely fully stretched in the junction, providing strong evidence of stable molecular junction formation. These results support the theory that the low measured conductance values are caused by weak electronic coupling through the molecular wire, as they suggest that the anchoring groups form mechanically strong molecule-electrode contacts with high binding strength. If the molecule-electrode binding at the anchoring sites was weak, the measured break-off distance values would be expected to be shorter than the predicted molecular lengths, in contrast to the strong agreement between theory and experiment observed. It can also be inferred from this data that the molecular junction configurations for the two molecules are highly similar at low bias, as predicted for two compounds with practically identical core structures and in agreement with the strong resemblance between the conductance peak profiles in the 1-D plots.

Upon increasing the bias voltage to 200 mV and 300 mV, the measured electrode separation distances for DMTB (**9**) and DETB (**10**) are again similar, although in these experiments the distance values are slightly shorter than the theoretical molecular lengths calculated for the two structures. However, as the measured separation distances are in the region of 0.05 – 0.15 nm shorter than the theoretical lengths, this suggests that these differences can simply be attributed to junction cleavage occurring prior to the junction attaining the maximum stretching distance. At 200 mV bias, electrode separation distances of 0.34 nm for DMTB (**9**) and 0.29 nm for DETB (**10**) were recorded, corresponding to molecular break-off distances of 0.84 nm for DMTB (**9**) and 0.79 nm for DETB (**10**), respectively. When the bias was increased to 300 mV, electrode separation distances of 0.40 nm for DMTB (**9**) and 0.36 nm for DETB (**10**) were measured, which give molecular break-off distances of 0.90 nm for DMTB (**9**) and 0.86 nm for DETB (**10**) after addition of the snap-back length. The same trend is also observed at the higher fixed bias voltage of 500 mV, with electrode separation distances of 0.46 nm for DMTB (**9**)

and 0.38 nm for DETB (**10**) respectively, corresponding to molecular break-off distances of 0.96 nm for DMTB (**9**) and 0.88 nm for DETB (**10**). All of these values are in reasonably good agreement with the theoretically calculated molecular lengths, providing further evidence that the multidentate triazolyl anchoring moieties enable strong molecule-electrode binding and thus permit the reproducible formation of stable molecular junctions.

Table 4.2. Lengths of Molecular Junctions for molecules **9** and **10** (DMTB and DETB) from Theoretical Calculations using MM2 Parameters and Experimental Measurements.

Molecule	**L(MM2)[a]/ nm**	$\boldsymbol{\Delta s = \Delta s^* + s_{corr}}$ **[b]/ nm**				
		100 mV	**200 mV**	**300 mV**	**400 mV**	**500 mV**
9/DMTB	0.96	0.96	0.84	0.90	1.21	0.96
10/DETB	0.96	0.95	0.79	0.86	1.01	0.88

[a]L(MM2) corresponds to the distance calculated using MM2 parameters after minimization of energy for the molecular structure between the binding N atoms on the anchoring groups at opposite ends of the molecule. [b]Values of molecular break-off distance (Δs) calculated by the addition of the electrode separation distance (Δs*) obtained from the relevant 2-D conductance-distance histogram to the snap-back distance (s_{corr}).

The only significant deviation from the overall pattern of the results is observed in the measurement of DMTB (**9**) at 400 mV bias, which gives an electrode separation distance of 0.71 nm and a molecular break-off distance of 1.21 nm, approximately 0.25 nm longer than the theoretical molecular length. This discrepancy can be attributed to a high noise level in this specific measurement at relatively high bias voltage, as the number of I-s traces collected was relatively low, making it more difficult to accurately measure this distance. The measurement of DETB (**10**) at the same bias voltage, by contrast, displays an electrode separation distance of 0.51 nm and a break-off distance of 1.01 nm, which is only slightly longer than the theoretically calculated molecular length (0.96 nm) and in reasonably good agreement with the other experimental values. Also, the similar molecular break-off distance values obtained from all other measurements of DMTB (**9**) at 100 mV to 500 mV bias strongly indicate that the unexpectedly long distance value recorded for this molecule at 400 mV is an anomalous result.

The molecular break-off distance values obtained from the measurement of these compounds can also be used to gain further insight into the characteristics of the 1,2,4-triazolyl anchoring moieties. Comparisons can be drawn with work by Arroyo *et al.*, which reported the measurement of the maximum stretching distances of thiol-terminated and amine-terminated

alkane molecules using the STM-BJ technique.[46] They found that the measured stretching distance values for the diaminoalkanes were similar to the theoretical molecular lengths, implying that these molecules typically form single molecule junctions. By contrast, the stretching distances recorded for the dithiolalkanes were longer than the predicted lengths, suggesting that thiol-terminated molecules frequently form multiple molecular junctions. The strong agreement between the theoretically predicted molecular lengths and experimentally obtained stretching distances suggests that 1,2,4-triazole-terminated molecules predominantly form single molecule junctions and therefore the measured conductance values are likely to correspond to the conductance of individual molecular junctions. Additionally, this result provides evidence that the triazolyl anchoring groups bind via donor-acceptor (dative) interactions, as their junction stretching behaviour is more similar to the molecules with dative binding amine moieties than the behaviour of covalent binding thiol-terminated compounds. This also implies that the triazolyl anchoring moieties do not significantly deform the Au electrodes during molecular junction stretching, consistent with the observation of well-defined conductance features and narrow distributions of conductance values for these molecules.

These results indicate that the molecular wires with triazolyl anchoring moieties form stable molecular junctions at a range of fixed bias voltage values, with junction cleavage occurring at similar length to the predicted maximum stretching distance of the molecules in almost all measurements. The consistent agreement between theoretical and experimental break-off lengths at different bias voltage values provides strong evidence that the measured conductance values correspond to the formation of molecular junctions incorporating the triazole-terminated molecules. Also, the close similarity between the molecular break-off lengths in measurements at different bias voltage values indicates that the mechanical stability of the molecular junctions formed is high and does not change significantly as the bias voltage is increased. Additionally, the high level of agreement between the theoretical molecular lengths and experimental break-off distances provides further evidence that substituting the methyl groups in DMTB (**9**) for the ethyl groups in DETB (**10**) has very little effect on the electrical properties. This is because the molecular conductance values for the two molecules are similar, and as the molecular junctions are cleaved at comparable separation distances, this indicates that the efficiency of electronic transmission through the molecular junctions should also be approximately the same. This is in agreement with the predicted behaviour for the triazole-terminated molecules, as the electronic structures for the two compounds are expected to be very similar.

4.4 Conclusions

In this project, the ability of the multidentate 1,2,4-triazole moiety to function as an anchoring group for linking molecular junctions to Au electrodes has been investigated using the STM-BJ technique. The two primary aims of this series of experiments have been to determine the conductance of 1,2,4-triazolyl-terminated molecular wires and assess the stability of molecular junctions formed using these novel bidentate anchoring moieties. The experimental measurements of the electrical properties of the triazole-terminated molecules, DMTB and DETB, have been performed at a range of fixed bias voltage values. The measured conductance values obtained for these molecules are relatively low (approximately $10^{-4.4}$ G_0 to $10^{-4.7}$ G_0), indicative of low charge transport efficiency, although the consistent molecular conductance signatures provide clear evidence of stable molecular junction formation. Both molecules display minimal variation in conductance on raising the bias voltage from 100 mV to 500 mV, which shows that the applied bias has little effect on the charge transport efficiency. The conductance values for the two molecules at a given bias voltage are also very similar, indicating that changing the alkyl side group length on the 1,2,4-triazole rings between methyl and ethyl chains has little influence on the electrical properties. Comparison with other studies suggests that the low molecular conductance values are likely to be caused by poor orbital overlap between the metal and molecule, resulting in weak electronic coupling, rather than weak molecule-electrode binding at the anchoring sites. Further evidence of stable junction formation is provided by the molecular break-off distance data, with very good agreement between theoretically predicted and experimentally measured molecular lengths for the majority of experiments. The strong agreement between theoretical and experimental length values also suggests that the triazole-terminated molecules predominantly form single molecule junctions between the electrodes. The experiments performed in this study have provided insight into structure-property relationships influencing charge transport through molecular wires incorporating triazolyl anchoring moieties. More generally, they have also demonstrated the potential viability of multidentate anchoring groups as metal-molecule contacts for molecular junctions.

Chapter 5: Experimental Methods

5.1 General Synthetic Approaches

All molecules prepared in this project were synthesised using standard preparative chemistry techniques. All reactions in this study were performed under N_2 in oven-dried glassware using dry solvents to exclude moisture and oxygen. All chemicals were purchased from Sigma-Aldrich and used without further modification or purification except where stated otherwise. All solvents were purchased from Fisher and used without modification or purification unless stated otherwise.

The molecules synthesised in this work were analysed shortly after synthesis via Nuclear Magnetic Resonance (NMR) and mass spectrometry. ^{1}H and ^{13}C NMR spectra were obtained using a Bruker Avance 400 Ultrashield spectrometer using dimethyl sulfoxide (DMSO) or chloroform ($CDCl_3$) as the solvent, with chemical shifts reported in parts per million (ppm) downfield from trimethylsilane (TMS). High Resolution Mass Spectra (HRMS) were recorded by the Liverpool University Analytical Services using an Agilent Quadrupole Time-of-Flight Mass Spectrometer (QTOF-MS) 7200 spectrometer. The purity of the compounds was assessed by CHN elemental analysis. The molecules were stored in a refrigerator to prevent degradation of the samples.

Thin layer chromatography was performed using Merck Silica Gel F-254 plates and flash chromatography was performed using Sigma Aldrich technical grade silica (230-400 mesh, pore size 60 Å).

The quantity of sample required to investigate the conductance of the molecular wires featured in this work is small (less than 20 mg of sample is required for a typical experiment). As a consequence, optimisation of the reaction conditions to obtain higher yields was considered less important than obtaining the required sample in sufficiently high purity for conductance measurement. For this reason, the reactions were not repeated after an adequate quantity of sample for characterisation and measurement had been obtained.

5.2 Synthesis of Pyridine-Terminated Molecular Wires

The pyridine-terminated molecules 3,3′-dipyridylamine (**2**) and 3,4′-dipyridylamine (**3**) were prepared by single Buchwald-Hartwig C-N cross coupling using $Pd_2(dba)_3.CHCl_3$ as the palladium source and the bulky phosphine ligand 2-Dicyclohexyl-phosphino-2′,4′,6′-triisopropylbiphenyl (XPhos) in toluene (Scheme 5.1).

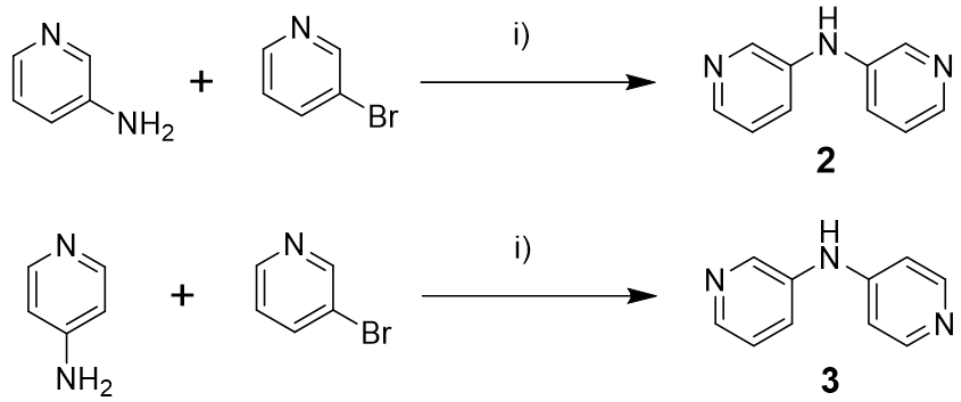

Scheme 5.1. Synthetic pathway to dipyridylamine molecules **2** and **3** prepared in this study. (i) $Pd_2(dba)_3.CHCl_3$, XPhos, KO^{t}Bu (20 h, 90 °C, Toluene).

The pyridine-terminated 'control' molecule 4,4′-dipyridylethyne (**4**) was prepared by a double Ullmann type cross-coupling using $PdCl_2(PPh_3)_2$ as the palladium source and CuI as the copper source, together with the bulky ligand 1,8-diazabicyclo[5.4.0]undec-7-ene (DBU) and H_2O in toluene (Scheme 5.2).

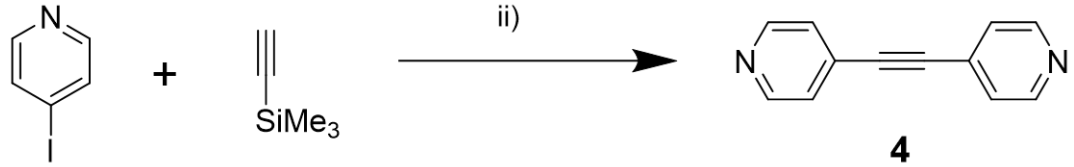

Scheme 5.2. Synthetic pathway to dipyridylethyne molecule **4** prepared in this study. (ii) CuI, $Pd_2(dba)_3.CHCl_3$, DBU, H_2O (19 h, room temperature, Toluene)

All reactions were performed under N_2 in oven-dried glassware using dry solvents. All reagents were purchased from Sigma-Aldrich (Merck) and used without further modification or purification with the following exceptions:

- 4-aminopyridine was purchased from Fluorochem and used without further modification or purification.

- Dibenzylideneacetone was prepared via condensation of benzaldehyde and acetone, and was recrystallized from hot ethyl acetate prior to use.
- $Pd_2(dba)_3 \cdot CHCl_3$ was prepared by adding $PdCl_2$ (1 equiv) to a stirred suspension of dibenzylideneacetone (dba, 3.3 equiv) and sodium acetate (8 equiv) in MeOH at 50 °C. After stirring for 4 h at 40 °C, the resulting suspension was filtered and the residue washed with water and acetone. This gave a crude yellow solid which was dissolved in hot $CHCl_3$ and filtered while hot. Diethyl ether was slowly added to the solution, which was left to stand at room temperature, allowing $Pd_2(dba)_3 \cdot CHCl_3$ to precipitate as dark purple needles.

5.2.1 Preparation of 3,3′-Dipyridylamine

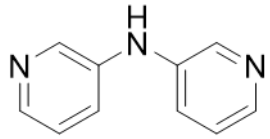

Dry toluene (10 ml) was degassed with nitrogen for 30 minutes prior to the addition of 3-aminopyridine (165 mg, 1.64 mmol, 1.1 equiv), 3-bromopyridine (0.15 ml, 1.58 mmol, 1 equiv), $Pd_2(dba)_3.CHCl_3$ (34 mg, 0.032 mmol, 2 mol%), XPhos (30 mg, 0.063 mmol, 4 mol%) and KO^tBu (252 mg, 2.22 mmol, 1.4 equiv). The resulting reaction mixture was heated at 90 °C under reflux with continuous stirring for 21 hours, cooled to 25 °C, filtered through a silica plug and washed with MeOH/EtOAc (1:1) (5 × 50 ml). The solvent was evaporated *in vacuo* and the crude product was purified by column chromatography (SiO_2; EtOAc/MeOH 9:1, R_F = 0.24) to give the target compound as a yellow solid (0.084 g, 31 %). ^1H NMR (400 MHz, DMSO-d6) δ: 8.55 (s, 1H), 8.37 (d, J = 2.4 Hz, 2H), 8.09 (d, J = 4.5 Hz, 2H), 7.51 (dq, J = 8.3, 2.4 Hz, 2H), 7.27 (dd, J = 8.3, 4.5 Hz, 2H). ^{13}C NMR (100 MHz, DMSO-d6) δ: 141.8, 139.9, 139.7, 124.4, 123.2. *m/z* (HRMS, CI^+, CH_4) 172.0873 $[M + H]^+$. $C_{10}H_9N_3$ calc. 172.2061.

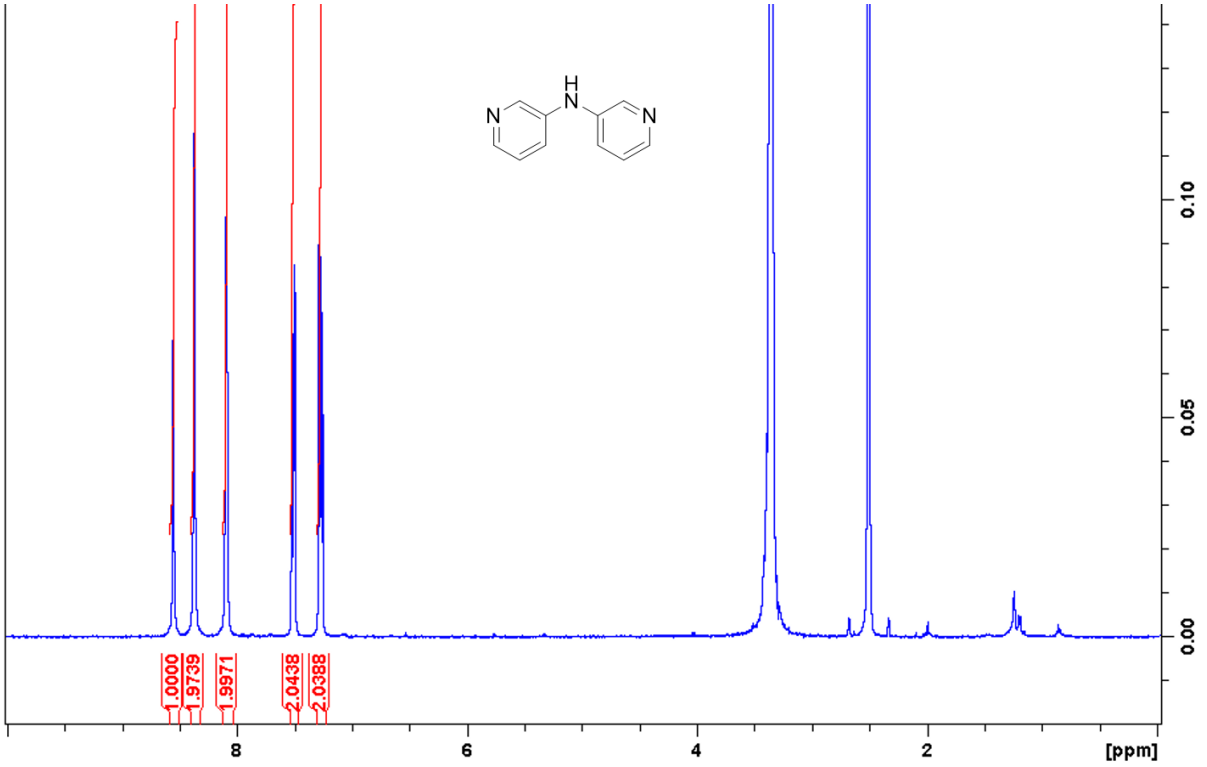

Figure 5.1. ^{1}H NMR spectrum for the molecule 3,3′-dipyridylamine (**2**) in DMSO.

Evidence of the successful preparation of the target molecule 3,3′-dipyridylamine (**2**) can be found in the ^{1}H NMR spectrum obtained shortly after synthesis (Figure 5.1). The sharp singlet peaks observed at 3.33 ppm and 2.50 ppm can be ignored as these peaks correspond to H_2O and the dimethyl sulfoxide (DMSO) solvent, leaving five peaks at comparatively high chemical shift values. This is consistent with the molecular structure, as the NMR spectrum for this compound is expected to display four distinct chemical environments for the pyridine ring H atoms in addition to the environment for the H atom attached to the linking amine N atom. In the ^{1}H NMR spectrum, the peak corresponding to the amine H atom is easy to identify as this environment is expected to give an integral of one and is not expected to be coupled to any neighbouring H atoms. The peak at a chemical shift of 8.55 ppm can thus be attributed to the amine H atom (Scheme 5.3). The remaining four peaks correspond to the pyridine ring H atoms. Assignment of the four pyridine ring peaks is more challenging as all four peaks are in the aromatic region and require investigation of the peak splitting, chemical shifts and coupling constants for identification. Each peak has an integral of two, which is in agreement with the prediction for this structure as this shows that each 3-pyridyl ring has four ^{1}H environments but the environments for the two rings are chemically indistinguishable.

For pyridine-based structures it is very important to note that H atoms do not display coupling to other H atoms directly across N atoms, which assists peak assignment as ^{1}H environments adjacent to the pyridyl N are expected to display simpler peak structures. The doublet peak at 8.37 ppm is assigned to the H atom in the *ortho*-position relative to the pyridyl N atom and amine N atom, as this peak has the highest chemical shift (attributed to its proximity to the electron withdrawing pyridine N atom) and the splitting results from long range coupling. The doublet peak at 8.09 ppm is assigned to the H atom *ortho*- to the pyridyl N atom and *para*- to the amine N atom, as this peak has the second highest chemical shift and the splitting results from coupling to the adjacent ring H atom. The peak at 7.51 ppm, which displays a more complex splitting pattern of a doublet of quartets, is assigned to the H atom *para*- to the pyridyl N atom and *ortho*- to the amine N atom. This is because this peak represents a ^{1}H environment with one adjacent H atom but where long range coupling with non-adjacent H atoms causes further peak splitting. The peak at 7.27 ppm displaying a splitting pattern of a doublet of doublets is assigned to the H atom *meta*- to the pyridyl N atom and amine N atom. This ^{1}H environment has two adjacent H atoms in different environments with further splitting again caused by long range coupling. The two peaks at lower chemical shift both have a coupling constant with J = 8.3 Hz, indicating that these two environments are coupled to each other. Also, the other coupling constant for the peak at 7.27 ppm has a value of 4.5 Hz, which is the same as the coupling constant for the peak at 8.09 ppm, providing more evidence that this peak corresponds to the H atom *meta*- to the pyridyl N atom and amine N atom.

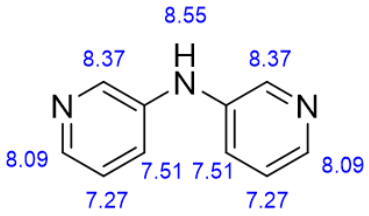

Scheme 5.3. Assignment of ^{1}H NMR spectrum peaks for the pyridine-terminated molecular wire 3,3′-dipyridylamine (**2**).

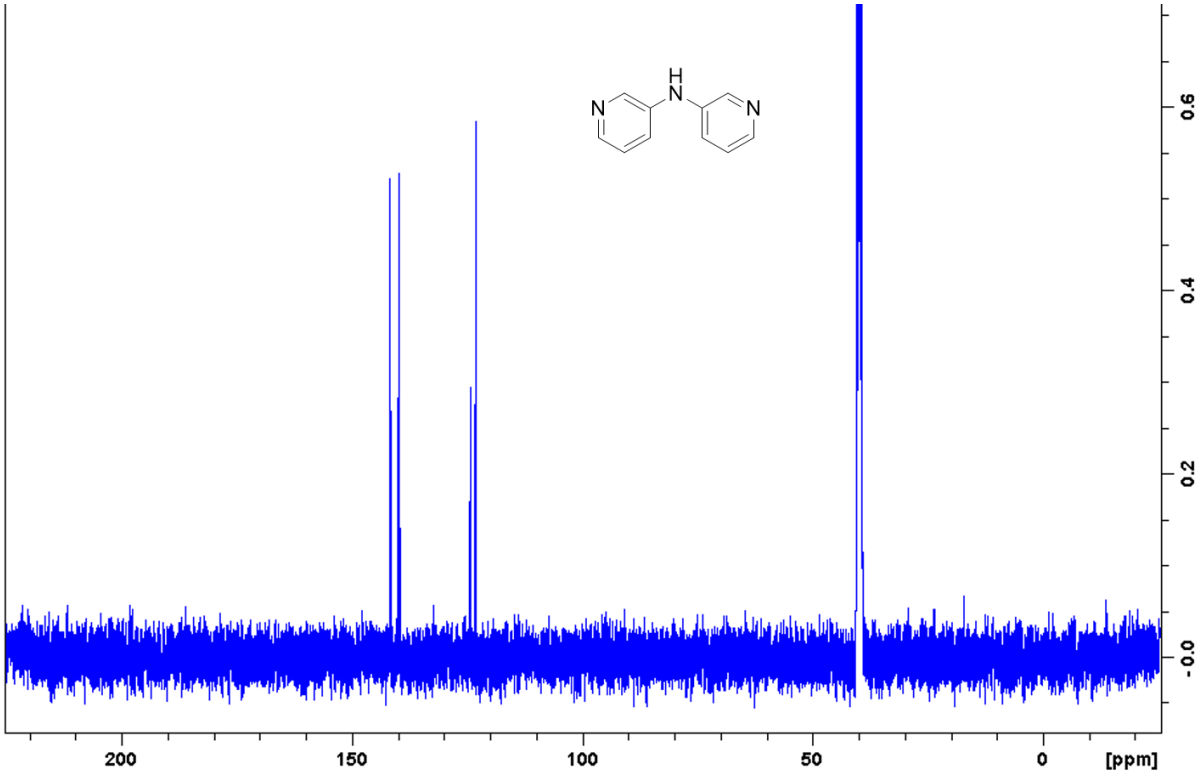

Figure 5.2. ^{13}C NMR spectrum for the molecule 3,3′-dipyridylamine (**2**) in DMSO.

Further evidence that the target molecule 3,3′-dipyridylamine (**2**) was successfully synthesised has been provided by the ^{13}C NMR spectrum, which was also obtained shortly after synthesis (Figure 5.2). The tall peak at 40.0 ppm can be ignored as this corresponds to the signal from the solvent (DMSO), leaving five singlet peaks at relatively high chemical shift values. All five peaks in the aromatic region represent ^{13}C atoms in the 3-pyridine rings, which is consistent with the chemical structure as this compound is expected to display five distinct ^{13}C environments, one for each C atom in each pyridyl ring but the two rings are expected to be chemically indistinguishable. All five environments give singlet peaks as the low abundance of the ^{13}C isotope prevents splitting of the signal. As for the ^{1}H NMR spectrum, C atoms located near the electronegative pyridyl N atoms are expected to display higher chemical shift values. The peak with the highest chemical shift value of 141.8 ppm is therefore assigned to the C atom adjacent to the pyridyl N atom and opposite to the amine N atom as this site is deshielded by the electron withdrawing pyridine N atom (Scheme 5.4). There are two peaks with very similar chemical shift values of 139.9 ppm and 139.7 ppm which are also highly deshielded. The peak at 139.9 ppm is assigned to the C atom adjacent to both the pyridyl and amine N atoms, whereas the peak at 139.7 ppm is assigned to the C atom directly attached to the amine N atom. This leaves the two more shielded C atoms, which give peaks at lower chemical shift values. The

peak at 124.4 ppm is assigned to the C atom which is not directly adjacent to either the pyridyl N atom or amine N atom and the peak at 123.2 ppm is assigned to the C atom adjacent to the amine N atom opposite to the pyridyl N atom.

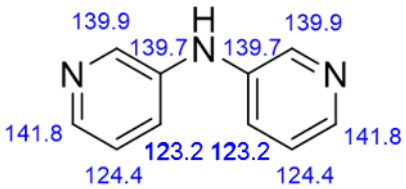

Scheme 5.4. Assignment of ^{13}C NMR spectrum peaks for the pyridine-terminated molecular wire 3,3′-dipyridylamine (**2**).

5.2.2 Preparation of 3,4′-Dipyridylamine

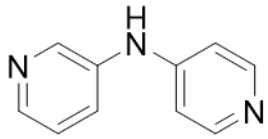

Dry toluene (10 ml) was degassed with nitrogen for 30 minutes prior to the addition of 4-aminopyridine (166 mg, 1.74 mmol, 1.1 equiv), 3-bromopyridine (0.15 ml, 1.58 mmol, 1 equiv), $Pd_2(dba)_3.CHCl_3$ (34 mg, 0.032 mmol, 2 mol%), XPhos (30 mg, 0.063 mmol, 4 mol%) and KO^{t}Bu (250 mg, 2.22 mmol, 1.4 equiv). The resulting reaction mixture was heated at 90 °C under reflux with continuous stirring for 21 hours, cooled to 25 °C, filtered through a silica plug and washed with MeOH/EtOAc (1:1) (6 × 50 ml). The solvent was evaporated *in vacuo* and the crude product was then purified by column chromatography (SiO_2; EtOAc/MeOH 9:1, R_F = 0.23) to give the target compound as a pale yellow solid (0.266 g, 98 %). ^1H NMR (400 MHz, DMSO-d6) δ: 9.00 (s, 1H), 8.46 (d, J = 2.0 Hz, 1H), 8.23 (d, J = 4.7 Hz, 3H), 7.65 (d, J = 8.2 Hz, 1H), 7.36 (dd, J = 8.2, 4.7 Hz, 1H), 6.94 (d, J = 4.7 Hz, 2H). ^{13}C NMR (100 MHz, DMSO-d6) δ: 150.7, 150.1, 143.7, 142.3, 137.7, 126.9, 124.5, 109.9. *m/z* (HRMS, CI$^+$, CH_4) 172.0875 $[M + H]^+$. $C_{10}H_9N_3$ calc. 172.2061.

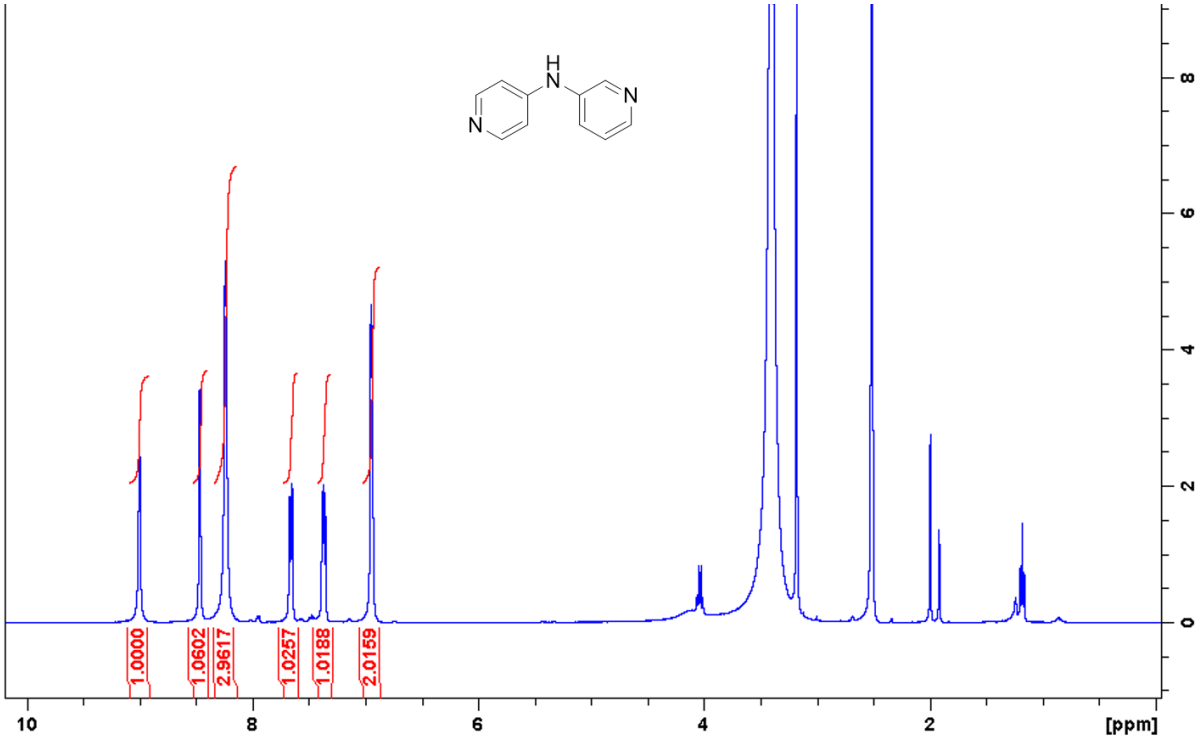

Figure 5.3. ^{1}H NMR spectrum for the molecule 3,4′-dipyridylamine (**3**) in DMSO.

Evidence of the successful preparation of the target molecule 3,4′-dipyridylamine (**3**) can be found in the ^{1}H NMR spectrum obtained shortly after synthesis (Figure 5.3). The sharp singlet peaks at 3.33 ppm and 2.50 ppm can be ignored as these peaks correspond to H_2O and the dimethyl sulfoxide (DMSO) solvent, leaving six peaks at comparatively high chemical shift values. The number of peaks is surprising, as the molecule possesses one 3-pyridyl ring, which is expected to display four distinct ^{1}H environments, and one 4-pyridyl ring, which is expected to display two ^{1}H environments, in addition to the amine H atom to give a predicted total of seven peaks. As with compound **2** (3,3′-dipyridylamine), the peak corresponding to the amine H atom is easy to identify as it has an integral of one and is not coupled to any neighbouring H atoms. This means the peak at a chemical shift of 9.00 ppm can be attributed to the amine H atom (Scheme 5.5).

Assignment of the pyridyl ring H atoms is assisted by the differences between the ^{1}H environments in the 3-pyridyl and 4-pyridyl rings. The 4-pyridyl ring is expected to contain two pairs of H atoms in each chemical environment, whereas each H atom in the 3-pyridyl ring is expected to display a unique chemical shift. It can therefore be deduced that the peaks with integrals greater than one (at 8.23 ppm and 6.94 ppm) correspond to H atoms in the 4-pyridyl ring. The electron withdrawing pyridyl N atom is expected to deshield the adjacent H atoms, so it is predicted that the peak with the higher chemical shift (8.23 ppm) corresponds to the H

atoms *ortho*- to the pyridyl N atom. The peak at lower chemical shift (6.94 ppm) can therefore be assigned to the more shielded H atoms *meta*- to the pyridyl N atom. Further evidence that the peaks at 8.23 ppm and 6.94 ppm correspond to the 4-pyridyl H atoms is apparent from the splitting pattern, as both peaks are split into doublets and have equal coupling constants (J = 4.7 Hz for both compounds).

Close inspection of the ^{1}H NMR spectrum shows that the peak at 8.23 ppm has an integral of approximately three. This assists peak assignment for the 3-pyridyl rings as this indicates that one of the H atoms in the 3-pyridyl ring has the same chemical shift as the 4-pyridyl H atoms *ortho*- to the pyridyl N atoms, making them chemically indistinguishable and explaining why only six peaks (rather than the predicted seven) are observed in the NMR spectrum. The doublet peak at 8.46 ppm is assigned to the H atom in the *ortho*-position relative to the pyridyl N atom and amine N atom, as this peak has the highest chemical shift (attributed to its proximity to the electron withdrawing pyridine N atom) and the splitting results from long range coupling. This peak has a unique coupling constant (J = 2.0 Hz) indicating that it is not directly coupled to the other 3-pyridyl ring H atoms. The doublet peak at 8.23 ppm is assigned to the H atom *ortho*- to the pyridyl N atom and *para*- to the amine N atom, as this peak has the second highest chemical shift and the splitting results from coupling to the adjacent ring H atom. The two peaks at lower chemical shift can be identified as both have a coupling constant with J = 8.2 Hz, indicating that these two environments are coupled to each other. This is very similar to the coupling constants obtained for the equivalent 3-pyridyl H atom environments in compound **2** (3,3′-dipyridylamine). From this evidence the doublet peak at 7.65 ppm can be assigned to the H atom *para*- to the pyridyl N atom and *ortho*- to the amine N atom and the peak at 7.36 ppm displaying a splitting pattern of a doublet of doublets is assigned to the H atom *meta*- to both the pyridyl N atom and amine N atom. The more complex splitting for this peak is attributed to direct coupling to two chemically distinct nearest neighbour ^{1}H environments.

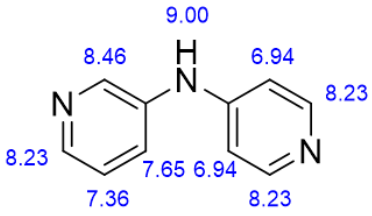

Scheme 5.5. Assignment of ^{1}H NMR spectrum peaks for the pyridine-terminated molecular wire 3,4′-dipyridylamine (**3**).

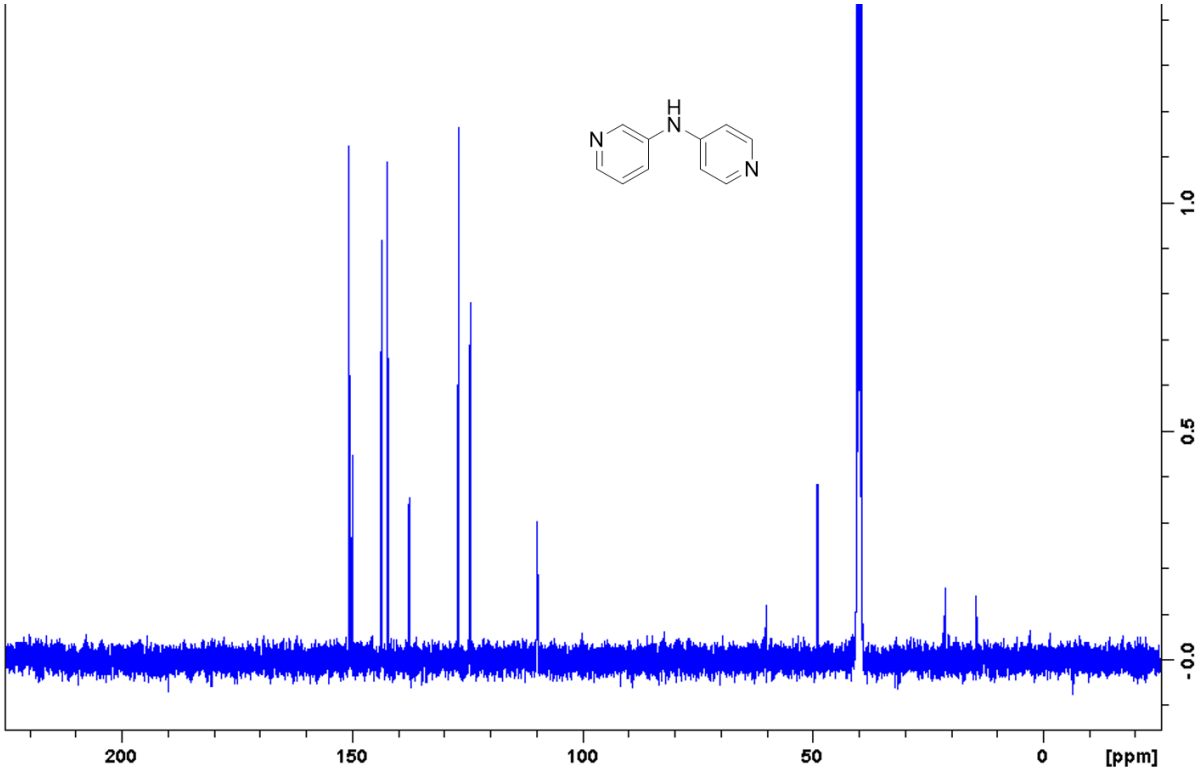

Figure 5.4. ^{13}C NMR spectrum for the molecule 3,4′-dipyridylamine (**3**) in DMSO

Further evidence that the target molecule 3,4′-dipyridylamine (**3**) was successfully synthesised has been provided by the ^{13}C NMR spectrum, which was also obtained shortly after synthesis (Figure 5.4). The tall peak at 40.0 ppm can be ignored as this corresponds to the signal from the solvent (DMSO), leaving eight singlet peaks at relatively high chemical shift values. Having previously assigned the peaks in the ^{13}C NMR spectrum for the symmetric molecule 3,3′-dipyridylamine (**2**), it can be established that there are five ^{13}C environments in the 3-pyridine ring, implying that the remaining three peaks correspond to ^{13}C environments in the 4-pyridine ring. This is consistent with the molecular structure as the 3-pyridyl ring is expected to display five distinct ^{13}C environments, whereas the 4-pyridyl ring is expected to display only three ^{13}C environments, including two matching pairs of C atoms in the same environment.

The five peaks corresponding to the C atoms in the 3-pyridyl ring are expected to be observed at similar chemical shift values to the analogous peaks in the ^{13}C NMR spectrum for 3,3′-dipyridylamine (**2**). The spectrum displays two peaks at chemical shifts higher than any of the peaks for the 3,3′-isomer (**2**) (at 150.7 and 150.1 ppm) and one peak at a significantly lower chemical shift (109.9 ppm), which can be assigned to ^{13}C environments in the 4-pyridyl ring. From this, it can be deduced that the peak at a chemical shift of 150.7 ppm corresponds to the pair of C atoms adjacent to the pyridine N atom in the 4-pyridyl ring, which are deshielded by

the electron withdrawing pyridine N atom (Scheme 5.6). The shielded peak at 109.9 ppm (the lowest chemical shift of any peak in this structure) is assigned to the pair of C atoms adjacent to the amine N atom in the same ring. This leaves the peak at 150.1 ppm, which is assigned to the C atom directly attached to the amine N atom opposite to the pyridine N atom in the 4-pyridyl ring.

The remaining five peaks in the ^{13}C NMR spectrum correspond to C atoms in the 3-pyridyl rings. The three higher chemical shift peaks represent ^{13}C environments deshielded by the electronegative 3-pyridyl N atom. The highest chemical shift peak at 143.7 ppm corresponds to the C atom adjacent to the pyridyl N atom and opposite the amine N atom, and the peak at 142.3 ppm is assigned to the C atom adjacent to both the pyridyl N atom and amine N atom. The peak at a slightly lower chemical shift of 137.7 ppm corresponds to the C atom directly attached to the amine N atom. The two more shielded peaks represent ^{13}C environments less exposed to the electron withdrawing effect of the pyridine N atom. The peak at 126.9 ppm corresponds to the C atom which is not directly adjacent to either the pyridyl N atom or amine N atom, while the peak at 124.5 ppm corresponds to the C atom adjacent to the N atom and opposite the pyridyl N atom.

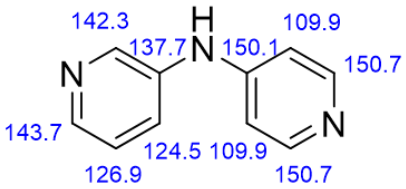

Scheme 5.6. Assignment of ^{13}C NMR spectrum peaks for the pyridine-terminated molecular wire 3,4′-dipyridylamine (**3**).

5.2.3 Preparation of 4,4′-Dipyridylethyne

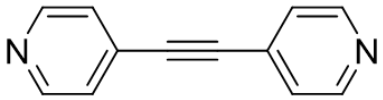

Dry toluene (15 ml) was degassed with nitrogen prior to the addition of 4-iodopyridine (328 mg, 1.6 mmol, 1 equiv), $PdCl_2(PPh_3)_2$ (67 mg, 0.096 mmol, 6 mol%) and CuI (31 mg, 0.16 mmol, 10 mol%). This was followed by the addition of dry degassed 1,8-diazabicyclo-[5.4.0]undec-7-ene (DBU) (1.46 g, 9.6 mmol, 6 equiv) and trimethylsilylacetylene (79 mg, 0.8 mmol, 0.5 equiv) immediately followed by the addition of deionised H_2O (12 mg, 0.64 mmol,

0.4 equiv). The resulting reaction mixture underwent continuous stirring at room temperature for 19 hours. The reaction mixture was then extracted with diethyl ether (50 ml) and H_2O (50 ml) and the organic layer was washed with H_2O (3 × 50 ml) and brine (50 ml). The extracts were dried with $MgSO_4$ and the drying agent was removed by gravity filtration. The solvent was evaporated *in vacuo* to give the crude product, a white solid with traces of Ph_3PO, which was dissolved in CH_2Cl_2 (50 ml) and extracted with 1 M HCl (50 ml). The aqueous layer was washed with CH_2Cl_2 (2 × 50 ml) and then 2 M NaOH was added until the solution pH turned basic (pH 8). The aqueous layer was extracted with CH_2Cl_2 (3 × 50 ml) and the organic extracts were dried with $MgSO_4$, with the drying agent removed by gravity filtration. The solvent was evaporated *in vacuo* to give the target compound as a white solid (0.126 mg, 43 %). ^{1}H NMR (400 MHz, $CDCl_3$) δ: 8.66 (dd, J = 4.5, 1.7 Hz, 4H), 7.41 (dd, J = 4.5, 1.7 Hz, 4H). ^{13}C NMR (100 MHz, $CDCl_3$) δ: 150.0, 130.2, 125.6, 90.9.

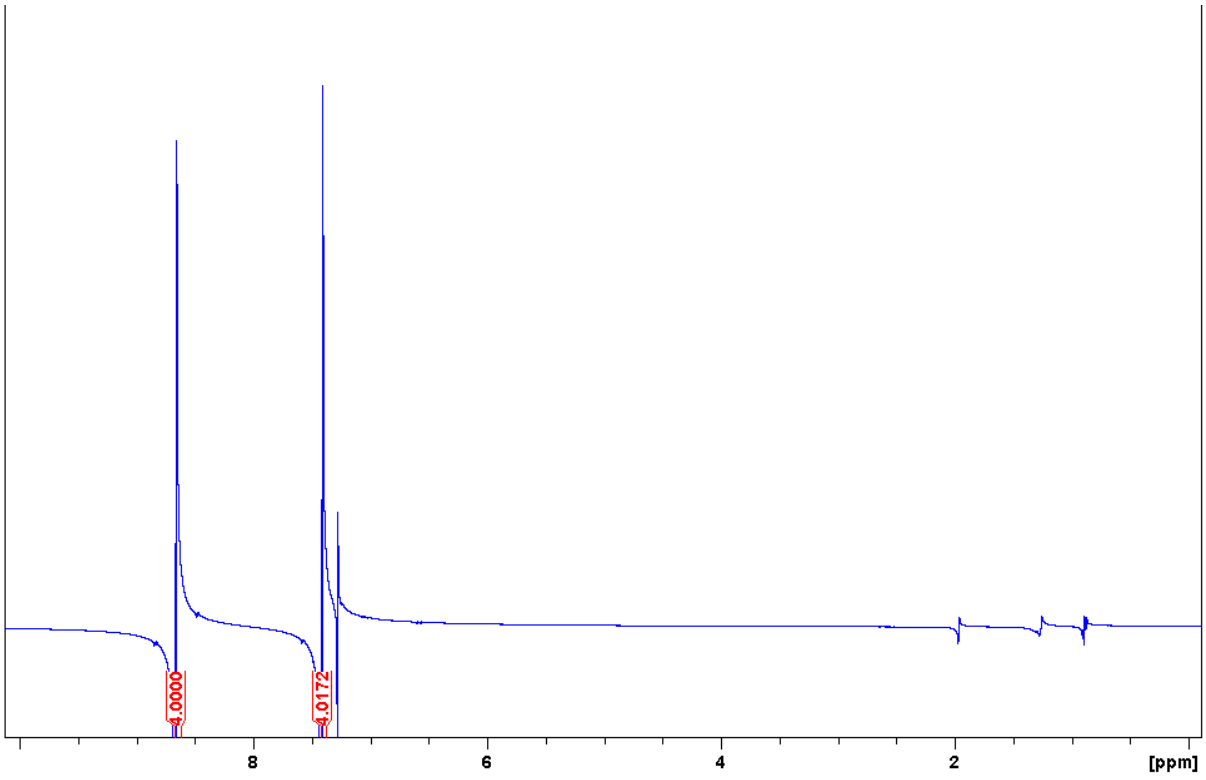

Figure 5.5. ^{1}H NMR spectrum for the molecule 4,4′-dipyridylethyne (**4**) in $CDCl_3$.

Evidence of the successful preparation of the target molecule 4,4′-dipyridylethyne (**4**) can be found in the ^{1}H NMR spectrum obtained shortly after synthesis (Figure 5.5). The singlet peaks observed at 7.28 ppm and 1.96 ppm can be ignored as these peaks correspond to deuterated chloroform ($CDCl_3$) solvent and water respectively. The spectrum shows two other peaks at relatively high chemical shift values of 8.66 ppm and 7.41 ppm, which is consistent with the

molecular structure as this molecule is expected to display two ^{1}H environments. The two peaks have very similar integrals, indicating that each peak represents the same number of H atoms, with each peak corresponding to H atoms in one of the two distinct chemical environments of the 4-pyridyl rings. This is also consistent with the observation of two peaks for the 4-pyridine ring in the asymmetric 3,4′-dipyridylamine molecule. Only two peaks are observed because the symmetrical structure means the pyridine ring H atoms in the equivalent positions of the two 4-pyridyl rings are chemically indistinguishable. The H atoms adjacent to the electronegative pyridine N atom are more deshielded than the H atoms adjacent to the ethynyl linker group, so the peak at 8.66 ppm is assigned to the H atoms *ortho*- to the pyridine N whereas the peak at 7.41 ppm is assigned to the H atoms *meta*- to the pyridine N atom (Scheme 5.7). Both peaks display splitting into a doublet of doublets as each peak is split by coupling to one nearest neighbour H atom with further splitting resulting from long range coupling. The two coupling constants for these peaks have the same values (4.5 Hz and 1.7 Hz), which indicates that the H atoms in the two different environments are coupled to each other, providing further evidence that the peaks correspond to neighbouring ^{1}H environments.

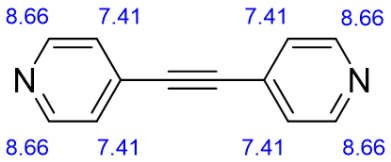

Scheme 5.7. Assignment of ^{1}H NMR spectrum peaks for the pyridine-terminated molecular wire 4,4′-dipyridylethyne (**4**).

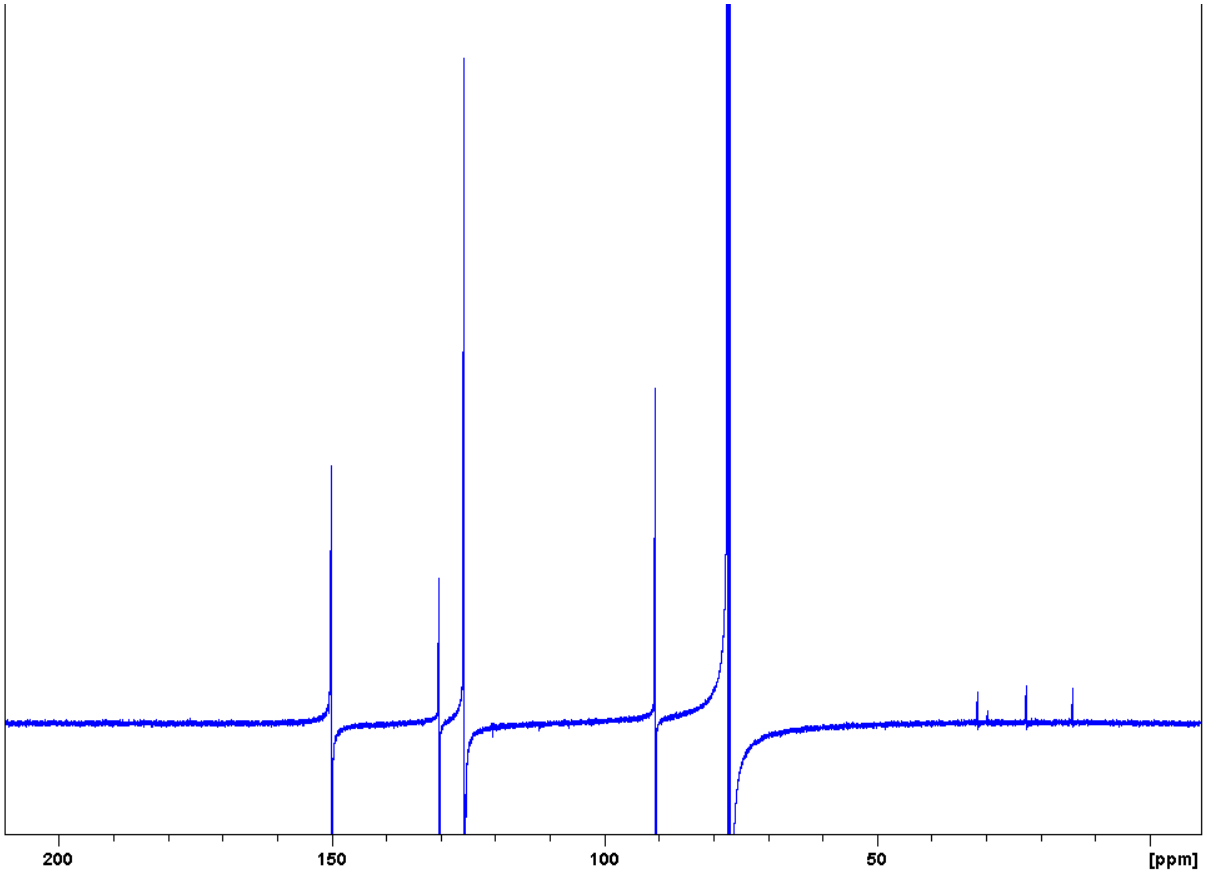

Figure 5.6. ^{13}C NMR spectrum for the molecule 4,4′-dipyridylethyne (**4**) in $CDCl_3$.

Further evidence that the target molecule 4,4′-dipyridylethyne (**4**) was successfully synthesised has been provided by the ^{13}C NMR spectrum, which was also obtained shortly after synthesis (Figure 5.6). The tall peak at 77.1 ppm can be ignored as this corresponds to the signal from the solvent ($CDCl_3$), leaving four singlet peaks, with three peaks at relatively high chemical shift values and a fourth peak at a significantly lower chemical shift, closer to the solvent peak. The structure is symmetric so each peak corresponds to multiple C atoms in the same ^{13}C environment and the total of four peaks is in agreement with the predicted total of four ^{13}C environments in this molecule. The three peaks at higher chemical shifts are in the aromatic region and can be assigned to the C atoms in the 4-pyridine rings and these peaks can be individually assigned based on the chemical shift values. The peak at 150.0 ppm can be assigned to the two pairs of C atoms adjacent to the pyridyl N atoms on each ring as the C atoms closest to the electronegative pyridyl N atom are strongly deshielded, giving the highest chemical shift values (Scheme 5.8). The peak at 130.2 ppm can be assigned to the two C atoms directly attached to the ethynyl linker, at the opposite end of the rings to the pyridyl N atoms, and the peak at 125.6 ppm can be assigned to the two pairs of C atoms adjacent to the ethynyl linker on each ring, as these ^{13}C environments are less exposed to the electron withdrawing

effect of the pyridyl N atom. The C atoms adjacent to the ethynyl linker are expected to be less exposed to the electron withdrawing effect of the pyridine N atoms, so the peak at the lower of the two comparable chemical shift values is assigned to this environment with the peak at the higher chemical shift value assigned to the C atoms directly attached to the ethynyl linker. The remaining peak at the lower chemical shift value of 90.9 ppm can therefore be assigned to the two C atoms forming the ethynyl linker group, which are significantly more shielded than any of the three ^{13}C environments in the pyridine rings and have a chemical shift value significantly lower than expected for aromatic ring C atoms.

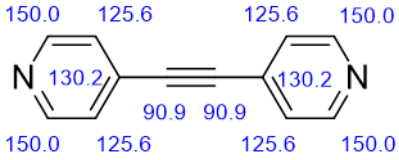

Scheme 5.8. Assignment of ^{13}C NMR spectrum peaks for the pyridine-terminated molecular wire 4,4′-dipyridylethyne (**4**).

5.3 STM Measurements and Sample Preparation

All single molecule conductance measurements in this study were based on the repeated formation and breakage of molecular junctions, performed using the STM break junction (STM-BJ) technique.[10] The electrical measurements were performed at room temperature under ambient conditions using a modified STM (Agilent 5500 SPM, Agilent Technologies Inc., USA) equipped with a home-built 4-channel current amplifier and a National Instruments NI 9215 USB data acquisition board. These measurements were recorded using an Agilent (Keysight) STM running Picoscan 5.3.3 software. All single molecule conductance measurements were performed at fixed bias voltage (to prevent electrochemical modification of the target molecules during the experiment) and a set-point current of 30 nA was used for all experiments. The monitoring of the current at fixed bias voltage allows the conductance (G) to be calculated, as G = I/V. The measured conductance value is given relative to the conductance quantum G_0 (77.48 µS), which represents the conductance value for a Au-Au single atomic point contact.

In all STM-BJ measurements, the STM tip was fabricated from a freshly cut gold wire (99.99%+ Au wire, 0.25 mm diameter, Goodfellow Cambridge Ltd.). The substrates were prepared from gold-on-glass slides (Arrandee, Germany) and rinsed with water, ethanol and

acetone. The substrate was then flame-annealed by heating the substrate with a butane torch, reducing the roughness of the gold surface to give large area flat Au(111) terraces. This step is necessary as it is difficult to obtain clean current-distance traces with low levels of noise when using rough substrates. The annealing process involved heating the substrate three times with the butane torch held at an angle of 45° to the surface for ~20 s until a slight orange glow was observed, with the sample then removed from the flame to avoid overheating. The atomically flat Au(111) surfaces prepared using this method are suitable for use as substrates in the STM-BJ measurements after being left to cool to room temperature.

All of the STM-BJ measurements in this work were performed in solution. This approach was used in order to facilitate the formation of metal-molecule-metal junctions by presenting the sample molecules in solution and to minimise contamination from the surrounding environment. The molecular wires to be measured were dissolved in a suitable solvent to form a dilute solution and the tip and substrate were then immersed in the resulting solution. The sample concentrations used were comparatively low (1 mM unless stated otherwise) to ensure low sample coverage of the Au substrate, favouring the formation of single molecule junctions. High sample solubility in the solvent was important to ensure that the molecules fully dissolved in the solvent at the required concentration in order to prevent contamination of the Au substrate with solid compounds, which could inhibit molecular junction formation. Low solvent volatility was also desired to prevent changes in the solution concentration resulting from evaporation of the solvent. Depending on the molecules being studied, the two main solvents or solvent systems used were a mixed solution of mesitylene with THF (4:1) (for the pyridine-terminated molecular wires) and 1,2,4-trichlorobenzene (for the fluorene-derived and triazole-terminated molecules). The same solvent system was used for all measurements in each series of molecules to minimise the influence of the solvent and thus permit direct comparison between the measured electrical properties of the related molecular wires in each series of experiments.

In each STM-BJ experiment, the STM tip was approached towards the substrate surface until the tip collided with the substrate to form a Au-Au metallic contact. The tip was then withdrawn until rupture of the Au-Au contact, allowing molecules to adsorb between the tip and substrate to form metal-molecule-metal junctions. The conductance was measured as a function of the tip-substrate displacement and the tip was withdrawn further, stretching the molecule towards its fully extended state until the molecular junction was ruptured. Each cycle of junction formation and rupture resulted in a trace of conductance vs electrode separation distance and

this process was repeated thousands of times in every measurement to enable the collection of a large number of conductance-distance traces. The traces from the experiments were used to construct 1-dimensional (1-D) and 2-dimensional (2-D) conductance histograms.

The 1-D conductance histograms allow the most probable molecular junction conductance values to be obtained by recording the conductance value at the highest point of the molecular conductance peak. For molecules displaying multiple conductance features, the conductance value is determined using the same approach for all peaks, with the measured values allowing the high and low conductance peaks to be distinguished. The 2-D conductance histograms, which show the evolution of the molecular junction as the electrodes are pulled apart, were generated by aligning the conductance traces used in the 1-D plots with the electrode separation distance. In these histograms, the maximum electrode separation represents the distance at which additional stretching of the molecular junction results in cleavage of the molecule-electrode contacts and this value is determined by finding the maximum electrode separation distance for the molecular conductance plateau. In order to accurately align each conductance-distance trace to a common scale, the first data point where the molecular conductance (G) is lower than 0.1 G_0 is defined as zero electrode separation distance ($\Delta s = 0$). This allows the maximum electrode separation distance to be recorded relative to the distance at which the Au-Au metallic point contact is cleaved.[41]

For all measurements in this work, except where stated otherwise, the molecular break-off distance is obtained by adding the Au-Au 'snap-back' distance (0.5 nm) to the measured electrode separation distance recorded in the 2-D conductance-distance histogram. This value acts as a correction for the discrepancy in electrode displacement resulting from the reorganisation of the Au electrode contacts after rupture of the initial metallic point contact, which leaves a nanogap of approximately 0.5 nm prior to the adsorption of the molecular wire to the electrodes via the anchoring sites to form the molecular junction.[82] This allows the most probable displacement of the electrode contacts prior to molecular junction cleavage to be determined, which corresponds to the length of the molecular junction at the maximum stretching distance. These experimental values are compared relative to theoretically predicted molecular lengths calculated using MM2 parameters (Chem 3D, Perkin Elmer), providing information about the evolution of the molecular junction and the molecular junction stability.

In order to demonstrate how the 1-D conductance histograms and 2-D conductance-distance histograms are used to investigate the electrical properties of the molecules in this study, data

obtained from the measurement of molecule **6** (TFLT) at 100 mV bias voltage is used to illustrate how the conductance and break-off distance are determined (Figure 5.7). In the 1-D conductance histogram, the molecular conductance is determined by reading the conductance value off the x-axis (log (G/G_0)) at the highest point of the conductance peak, showing that **6** (TFLT) has a single molecular conductance value of $10^{-3.8}$ G_0. In the 2-D conductance-distance histogram, the molecular break-off distance is determined by first reading the electrode separation distance at the end of the molecular conductance plateau furthest from a separation distance of zero on the x-axis (i.e. on the right hand side of the plot). There is a large drop in conductance at this point resulting from cleavage of the Au-Au point contact prior to molecular junction formation. Using the arbitrary colour scale representing the number of traces with a given conductance value in the 2-D histogram, this distance is defined by finding the separation distance at the edge of the green region. This represents a sharp drop in molecular conductance on cleavage of the molecular junction. Reading the conductance values from the y-axis (log (G/G_0)) shows that conductance decreases with increasing electrode separation distance, as the length of the tunnelling pathway increases. The accurate molecular break-off distance is determined by adding the Au-Au 'snap-back' distance (0.5 nm) to this electrode separation value (unless stated otherwise), representing the maximum distance the molecular junction can be stretched prior to undergoing cleavage at the molecule-electrode contacts. For TFLT (**6**) at 100 mV bias, a measured electrode separation distance of 1.27 nm therefore corresponds to a molecular break-off distance of 1.77 nm after addition of the 'snap-back' distance.

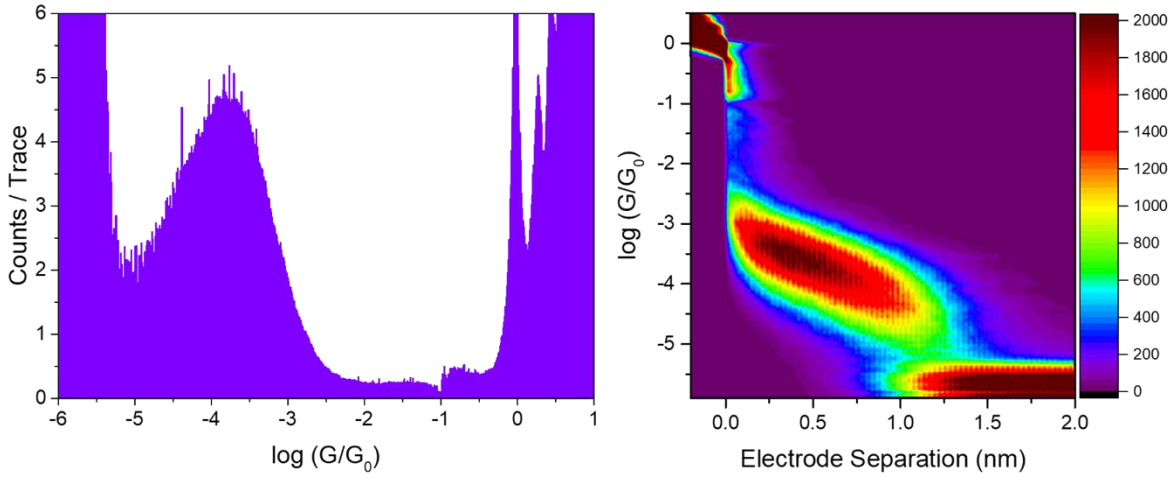

Figure 5.7. 1-D conductance histogram (*left*) and 2-D conductance-distance histogram (*right*) obtained from the STM-BJ measurement of the molecular wire TFLT (**6**) in solution (1,2,4-trichlorobenzene) at 100 mV bias voltage, used to illustrate how the two plots allow the molecular conductance and molecular break-off distance to be determined respectively.

For all experiments performed in this study, the contact-based STM-BJ technique has been employed as opposed to non-contact based approaches such as the I(s) technique. This is because the STM-BJ method allows a far larger number of traces (typically 3000 or more traces) to be obtained from a single experimental measurement compared to the I(s) approach (typically around 500 traces) and therefore does not require any data selection to obtain adequate conductance-distance traces. In addition to improving the reliability of the results, this also minimises the influence of variations in the atomic-scale structure of the molecular junctions formed and eliminates the possibility of bias in trace selection on the part of the user, both of which reduce the likelihood of systematic errors in the conductance values. Also, in the specific case of the fluorene-derived molecular wires, the long theoretically predicted molecular lengths (~1.75 nm for all structures) make the STM-BJ approach more suitable as it is easier to form stable metal-molecule-metal junctions for longer molecules with the contact-based method. Additionally, the increased noise level observed for STM-BJ measurements compared to I(s) experiments is less of an issue for longer molecular wires, which tend to give cleaner conductance traces due to the larger separation between tip and substrate when the target molecule is adsorbed to the two surfaces.

The conductance data from all STM measurements is reported in the Appendix.

Chapter 6: Conclusions and Future Work

6.1 Conclusions

The primary aims of this project were to investigate structure-property relationships in metal-molecule-metal junctions comprising different series of molecular wires and to determine how quantum interference effects and anchoring moieties influence the conductance behaviour of the molecules studied. The electrical properties of the compounds in this work have been investigated using the STM-BJ technique, which has provided insight into the relationships between the chemical structures and observed conductance features.

The first series of experiments focused on the electrical properties of pyridyl-terminated molecular wires with the aim of investigating the influence of the pyridyl N anchoring site positions on the conductance of three isomers of dipyridylamine. The pyridine-terminated molecules have been prepared using cross-coupling synthetic methodology and characterised prior to measurement. The experimental conductance data shows that all three molecules display two conductance peaks, representing distinct high and low conductance molecular junction geometries. The measurements of the two symmetric dipyridylamine isomers (3,3′- and 4,4′-) exhibit similar conductance properties, in contrast to theoretical transmission calculations predicting a very high conductance for the 3,3′- isomer. It is postulated that the proximity of the LUMO to the metallic E_F minimises the influence of constructive interference effects on the electrical properties. The asymmetric 3,4′- isomer gives significantly lower conductance values and this is attributed to weak molecule-electrode coupling. Comparison of the conductance features for the dipyridylamine compounds with the 'control' dipyridylethyne molecule and strong agreement between theoretical and measured molecular lengths confirm that the conductance signatures are consistent with pyridine-terminated molecular junctions.

The second study focused on the electrical properties of fluorene-derived molecular wires with the primary aim of investigating the influence of cross-conjugation on the molecular conductance of fluorene derivatives. The experimental conductance data shows that the conductance decreases on addition of cross-conjugated carbonyl moieties to the core structure. The measurements show an inverse relationship between the number of ketone moieties and the conductance, as the linearly conjugated fluorene molecule and 'control' biphenyl molecule display higher conductance values than the molecules featuring cross-conjugated carbonyl groups. The conductance of these compounds is also consistently found to increase on raising the bias voltage, indicating that the predominant charge transport pathway is via the HOMO orbital. By contrast, no significant changes in behaviour are observed on lowering the sample

concentration. The trends reported for this series of measurements support the prediction that destructive interference effects lead to lower conductance in cross-conjugated structures, providing a potentially useful method for tuning conductance in conjugated molecular wires.

The third series of measurements studied the electrical properties of two triazolyl-terminated molecular wires. The main aim of these experiments was to determine the conductance and stability of molecular junctions featuring novel bidentate anchoring moieties incorporating multiple binding sites. The experimental conductance data indicates that simple benzene-based molecular wires with 1,2,4-triazolyl terminal groups form stable molecular junctions which give distinctive conductance signatures and measurable conductance values. However, the molecular conductance values are consistently low and the molecules display minimal variation in conductance at a range of bias voltage values. The low conductance is attributed to weak molecule-electrode coupling, as the maximum stretching distances are in good agreement with theoretical molecular lengths, which is indicative of high molecule-electrode binding strength and high junction stability. These experiments show that triazole anchoring groups can be used to connect molecular wires to metallic electrodes and form stable molecular junctions, broadening the range of anchoring moieties used in molecular electronics.

In conclusion, this work focused on the measurement of the electrical properties of three distinct series of molecular wires using the STM-BJ technique and investigating the role of quantum interference effects and anchoring moieties in influencing molecular conductance. The investigation of the conductance properties of these compounds has expanded knowledge and enhanced understanding of relationships between molecular structure and charge transport behaviour. This work has provided insight into the role of CQI and DQI effects in controlling molecular conductance and has reported formation of stable molecular junctions with novel 1,2,4-triazole anchoring moieties. It is hoped this work will advance the field of molecular electronics and assist the design of molecular wires with suitable properties for electronic device applications. One possibility for future work expanding on this study would involve measuring the electrical properties of 1,2,4-triazole terminated molecules with different core structures to improve understanding of how this anchoring moiety influences charge transport behaviour. Another direction for further experimental work would focus on investigating the properties of these molecules using techniques beyond conductance measurements, including exploration of current-voltage relationships and thermoelectric properties, which would provide more information about their suitability for different applications.

Appendices: Data from STM-BJ Experiments

A.1 Single Molecule Conductance Data from STM-BJ Measurements

Single molecule conductance data collected using the STM-BJ technique in this work are presented as 1-dimensional (1-D) conductance plots and 2-dimensional (2-D) conductance-distance histograms.

In the 1-D conductance plots, the x-axis represents the conductance (in units of nS) and the y-axis represents arbitrary counts of the number of traces. The 1-D plots show the distribution of conductance values recorded during the measurements, with the position of the main peak indicating the conductance of the molecular junction. The conductance is binned on a logarithmic scale and the number of traces is binned on a linear scale. For the construction of the 1-D plots, current-distance (I-s) curves which display a smooth exponential decay in the absence of a molecular junction or which exhibit excessive noise are automatically rejected. For the I-s traces representing a molecular step, no data selection methods are used, with the plots based on all I-s traces obtained from the relevant STM-BJ experiment. In all 1-D plots, the presence of a sharp peak at 1 G_0 corresponds to the conductance of a single atomic Au-Au contact, which is reproducibly formed during each experiment. The molecular conductance peaks occur at significantly lower conductance values, in the range of $10^{-3.0}$ to $10^{-5.0}$ G_0 depending on the molecular wire.

In the 2-D conductance-distance histograms, the measured conductance is given as a function of the stretching distance of the molecular junction. In all the 2-D plots, the x-axis represents the electrode separation (in nm) and the y-axis gives the conductance (in nS) with a colour scale indicating the density of data points, ranging from purple (low density) to dark red (high density). The conductance is binned on a logarithmic scale, whereas the electrode separation distance is binned on a linear scale. The origin of the electrode separation distance is defined so that this distance is zero at the point where the conductance is equal to the conductance quantum, G_0, permitting normalisation of the conductance traces. The 2-D plots give information about the molecular break-off distance, which represents the length of the molecular junction, and are correlated with the 1-D conductance plots, as the high density regions correspond to the molecular peak. The determination of the break-off distance is important for two reasons, as it allows the signal from the molecule to be identified and the length of the molecular junction to be defined, with this length representing the relative distance between formation and cleavage of the single molecule junction.

It should be noted that the length of the plateau in the 2-D conductance-distance plot is not equal to the length of the molecular junction, because the Au electrodes relax and reorganise following the formation of a nanogap on rupture of the Au-Au atomic contact. This discrepancy is known as the 'snap-back' distance and is dependent on the metallic electrode materials used in the experiment. For metal-molecule-metal junctions with two Au electrodes, the typical snap-back distance (0.5 nm) on rupture of the metallic contact is accounted for by adding this value to the plateau length to give the molecular break-off distance. As for the 1-D conductance plots, traces containing excessive noise or representing exponential decay in the absence of a molecule are automatically rejected and no data selection methods are used.

The STM-BJ experiments performed on the molecules featured in this work are presented in this section. For all measurements, the bias voltage, solvent and sample concentration are reported, in addition to the number of I-s traces used to construct the conductance histograms.

A.2 4,4′-Dipyridylamine

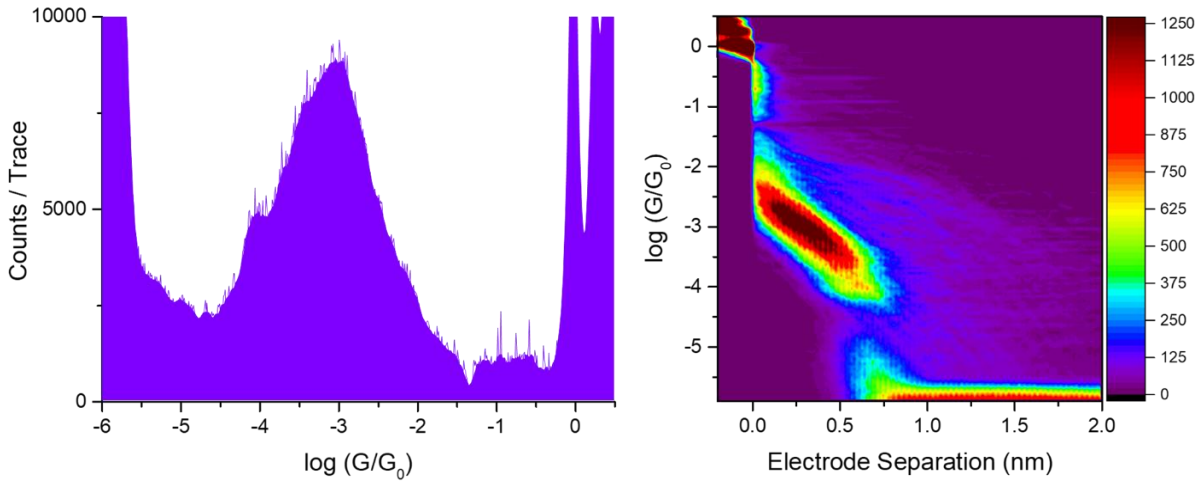

Figure A1. 1-D and 2-D conductance plots from STM-BJ measurement of 4,4′-dipyridylamine. Bias voltage: 200 mV, solvent: mesitylene/THF (4:1), concentration: 1 mM.

A.3 3,3′-Dipyridylamine

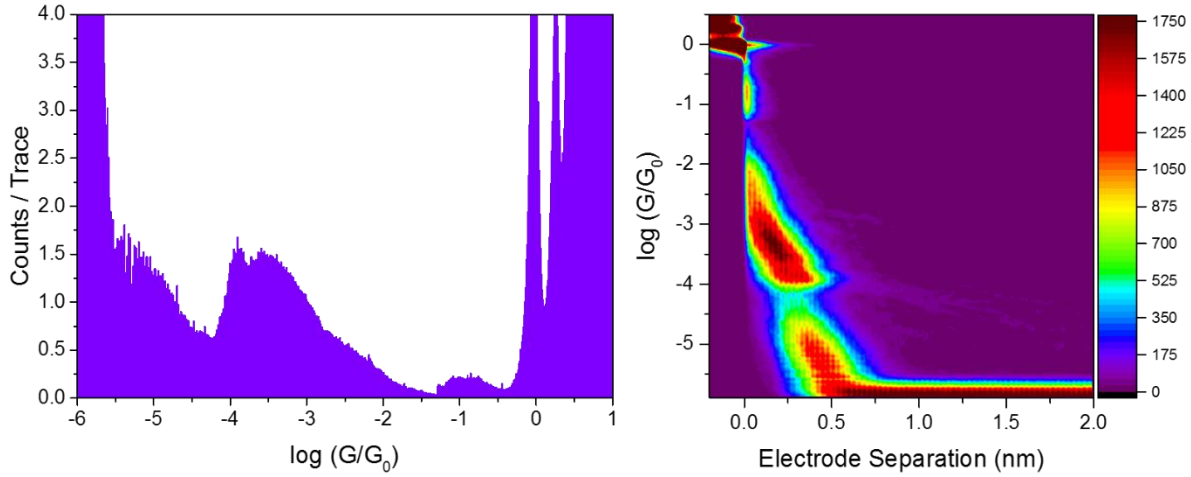

Figure A2. 1-D and 2-D conductance plots from STM-BJ measurement of 3,3′-dipyridylamine. 7751 traces. Bias voltage: 200 mV, solvent: mesitylene/THF (4:1), concentration: 1 mM.

A.4 3,4′-Dipyridylamine

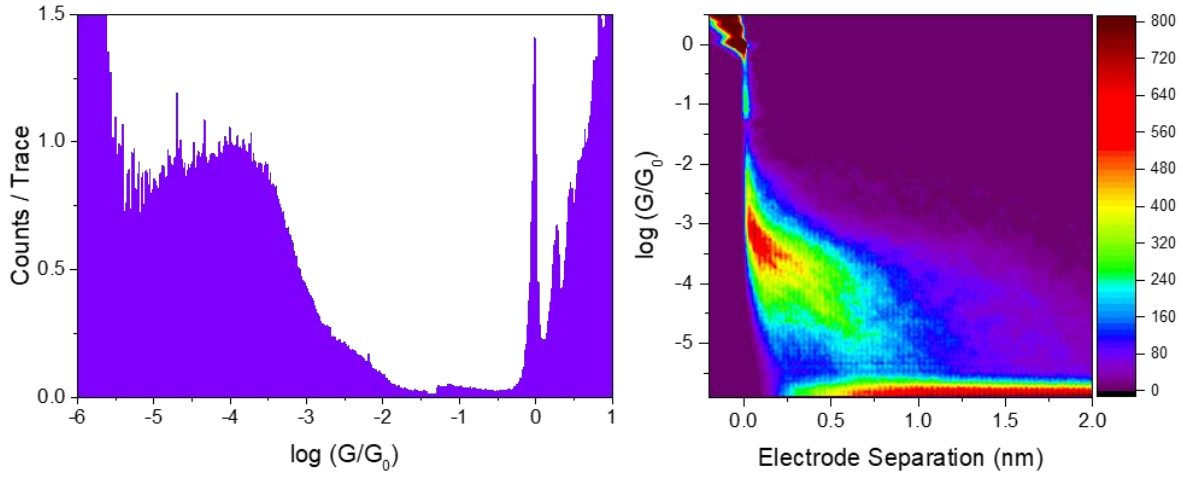

Figure A3. 1-D and 2-D conductance plots from STM-BJ measurement of 3,4′-dipyridylamine. 2864 traces. Bias voltage: 200 mV, solvent: mesitylene/THF (4:1), concentration: 1 mM.

A.5 4,4′-Dipyridylethyne

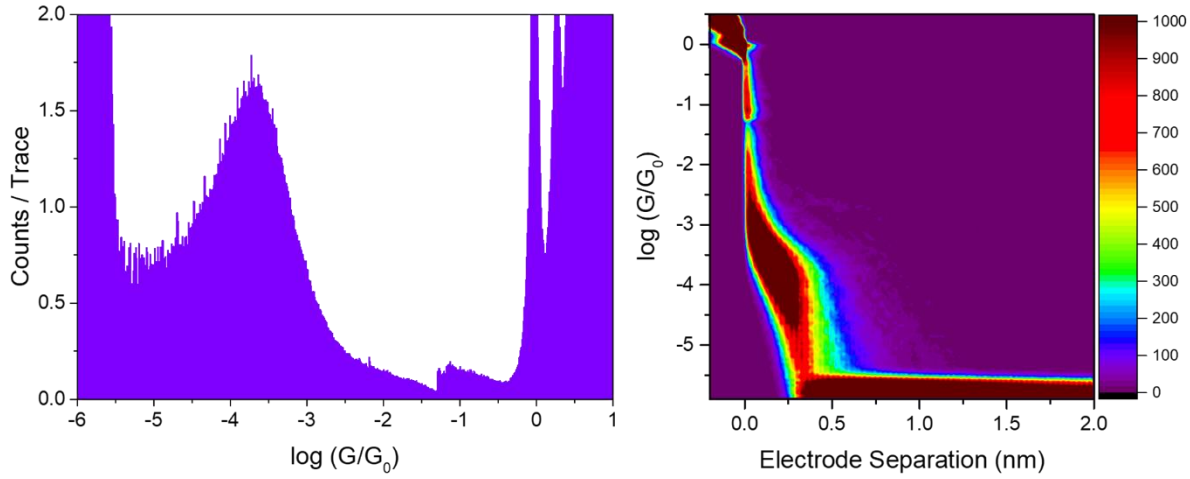

Figure A4. 1-D and 2-D conductance plots from STM-BJ measurement of 4,4′-dipyridylethyne. 7707 traces. Bias voltage: 200 mV, solvent: mesitylene/THF (4:1), concentration: 1 mM.

A.6 TBPT

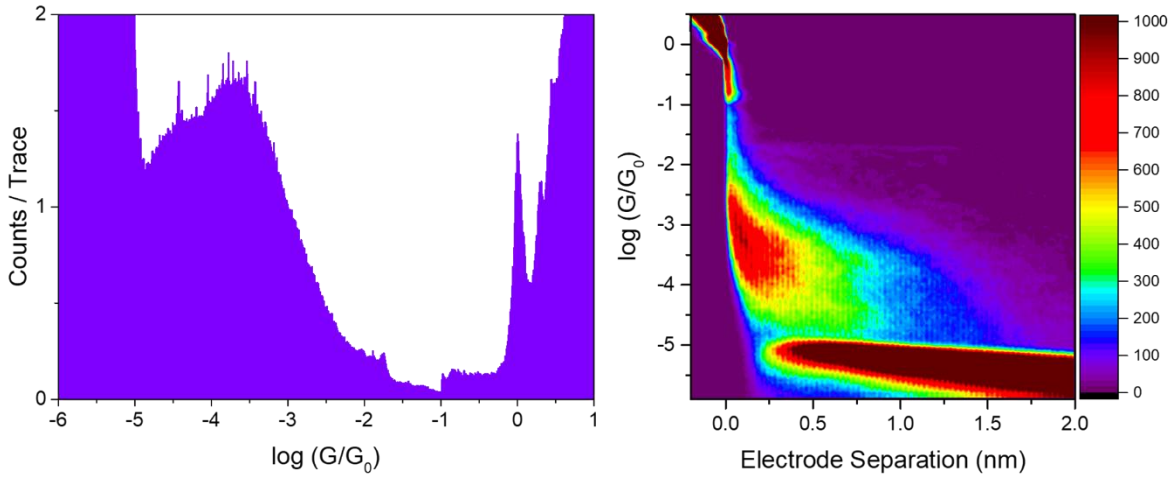

Figure A5. 1-D and 2-D conductance plots from STM-BJ measurement of TBPT. 4834 traces. Bias voltage: 100 mV, solvent: 1,2,4-trichlorobenzene, concentration: 1 mM.

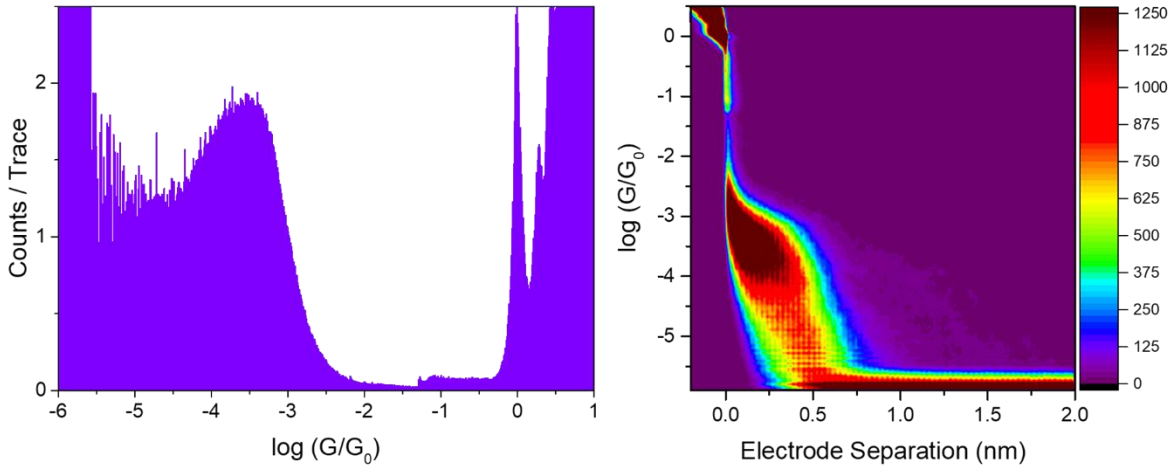

Figure A6. 1-D and 2-D conductance plots from STM-BJ measurement of TBPT. 6351 traces. Bias voltage: 200 mV, solvent: 1,2,4-trichlorobenzene, concentration: 1 mM.

A.7 TFLT

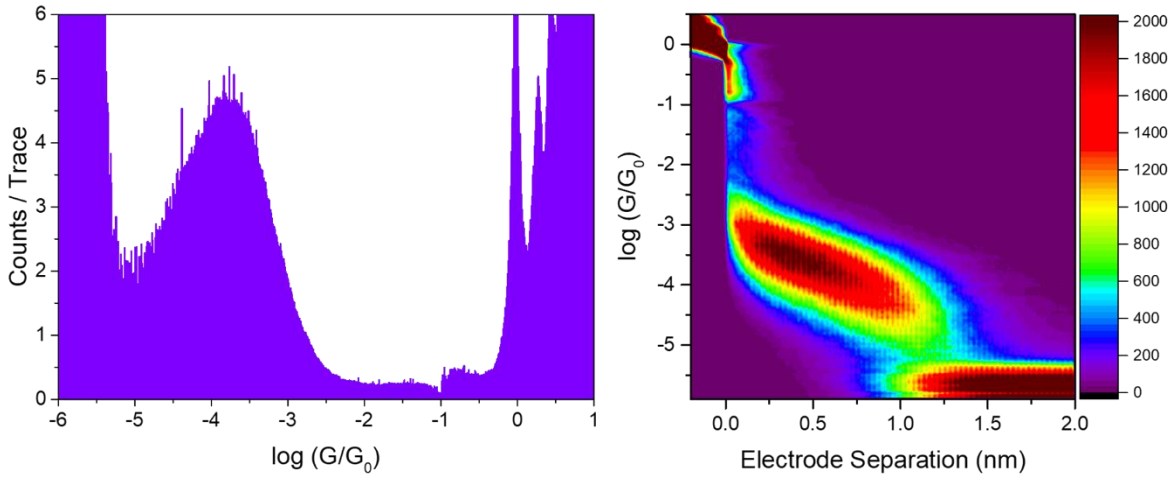

Figure A7. 1-D and 2-D conductance plots from STM-BJ measurement of TFLT. 7508 traces. Bias voltage: 100 mV, solvent: 1,2,4-trichlorobenzene, concentration: 1 mM.

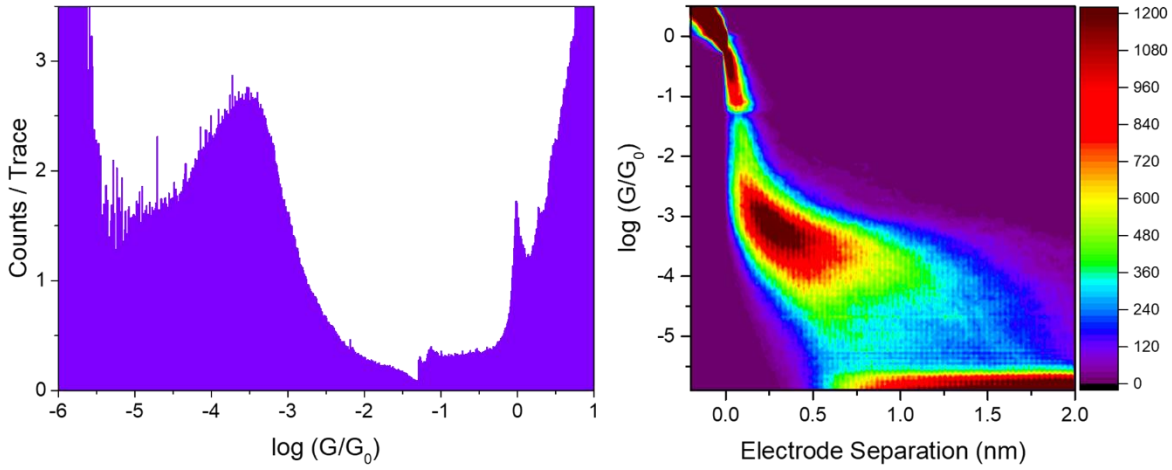

Figure A8. 1-D and 2-D conductance plots from STM-BJ measurement of TFLT. 5476 traces. Bias voltage: 200 mV, solvent: 1,2,4-trichlorobenzene, concentration: 1 mM.

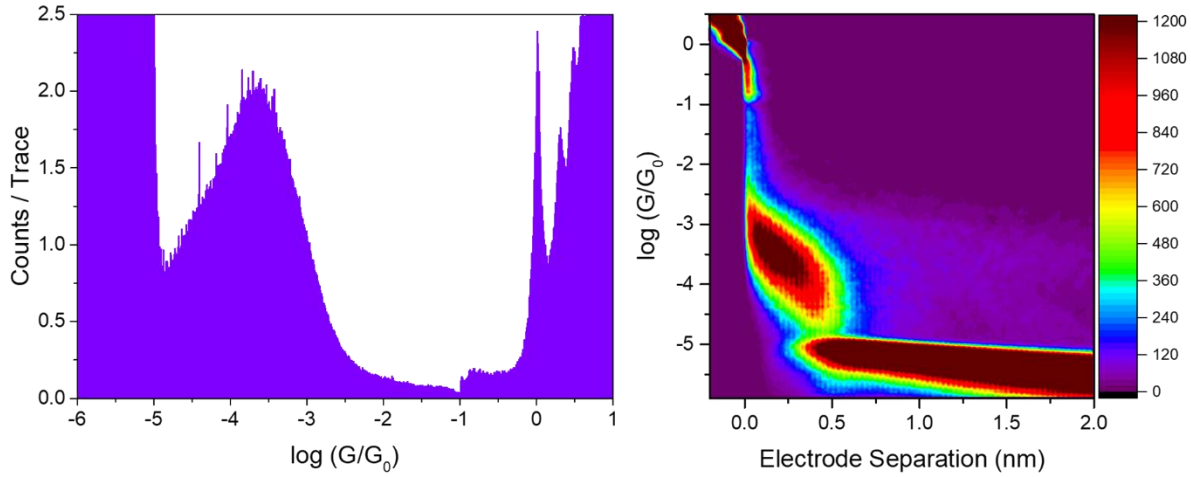

Figure A9. 1-D and 2-D conductance plots from STM-BJ measurement of TFLT. 5807 traces. Bias voltage: 100 mV, solvent: 1,2,4-trichlorobenzene, concentration: 0.1 mM.

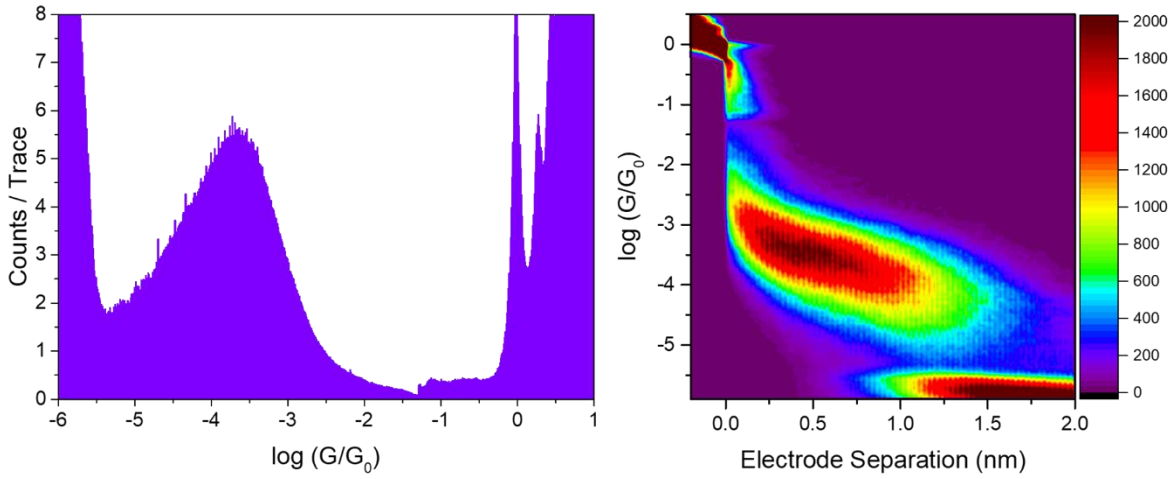

Figure A10. 1-D and 2-D conductance plots from STM-BJ measurement of TFLT. 7778 traces. Bias voltage: 200 mV, solvent: 1,2,4-trichlorobenzene, concentration: 0.1 mM.

A.8 TFOT

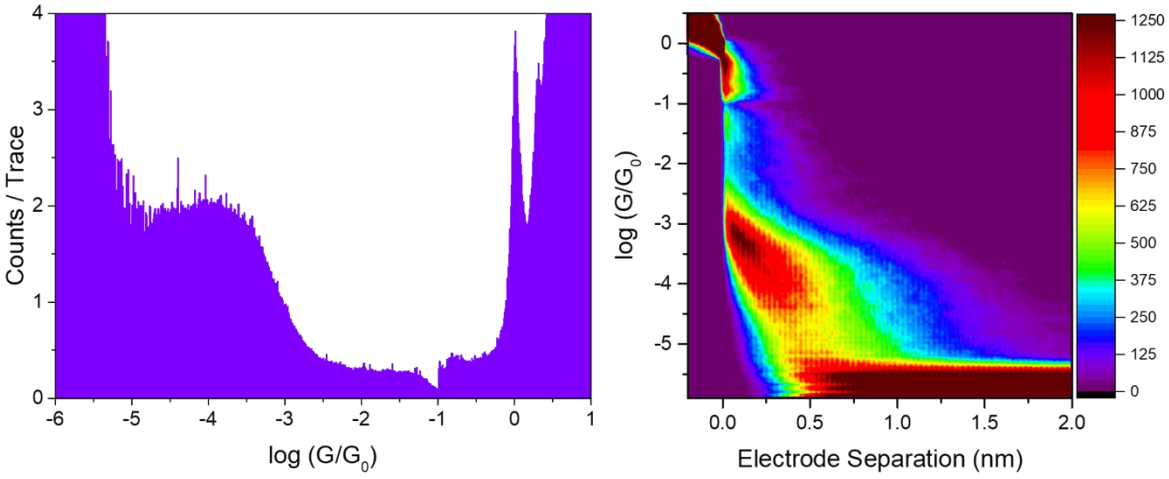

Figure A11. 1-D and 2-D conductance plots from STM-BJ measurement of TFOT. 7214 traces. Bias voltage: 100 mV, solvent: 1,2,4-trichlorobenzene, concentration: 1 mM.

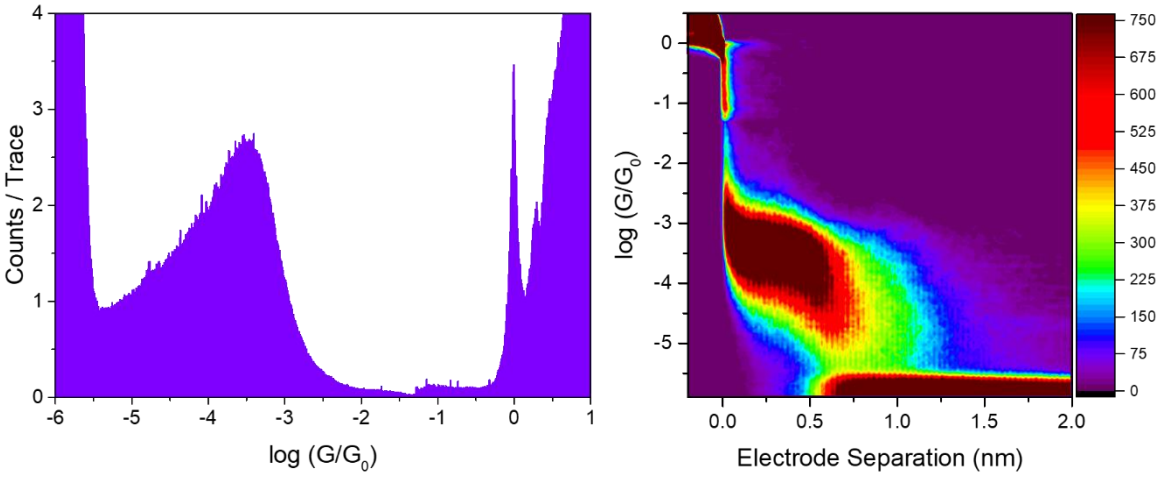

Figure A12. 1-D and 2-D conductance plots from STM-BJ measurement of TFOT. 5616 traces. Bias voltage: 200 mV, solvent: 1,2,4-trichlorobenzene, concentration: 1 mM.

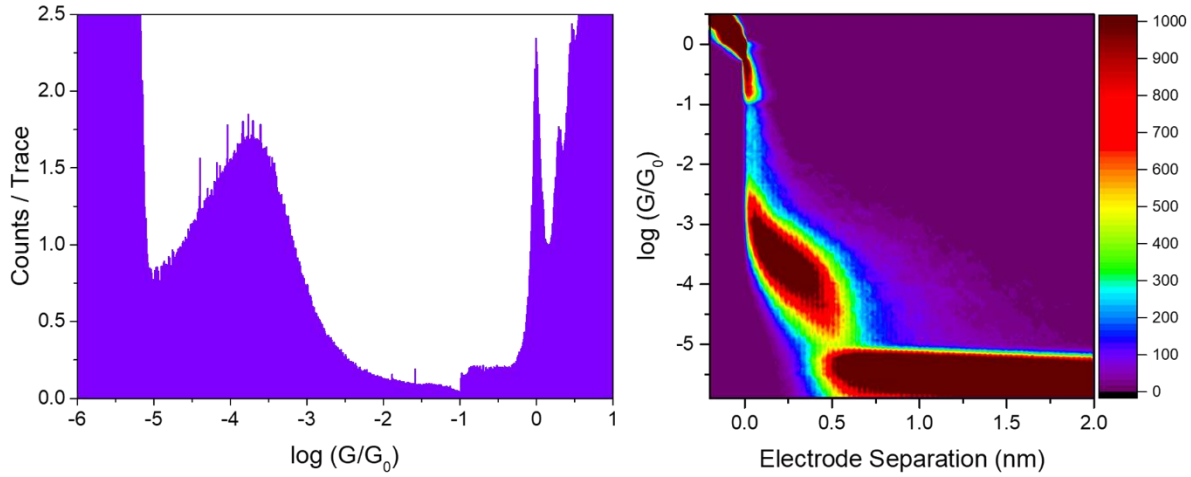

Figure A13. 1-D and 2-D conductance plots from STM-BJ measurement of TFOT. 5394 traces. Bias voltage: 100 mV, solvent: 1,2,4-trichlorobenzene, concentration: 0.1 mM.

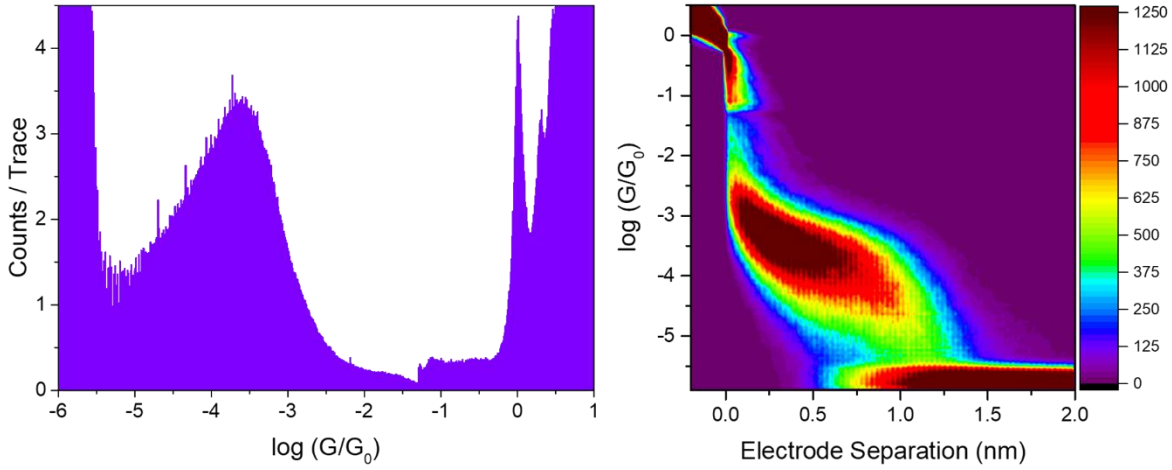

Figure A14. 1-D and 2-D conductance plots from STM-BJ measurement of TFOT. 6734 traces. Bias voltage: 200 mV, solvent: 1,2,4-trichlorobenzene, concentration: 0.1 mM.

A.9 TPDOT

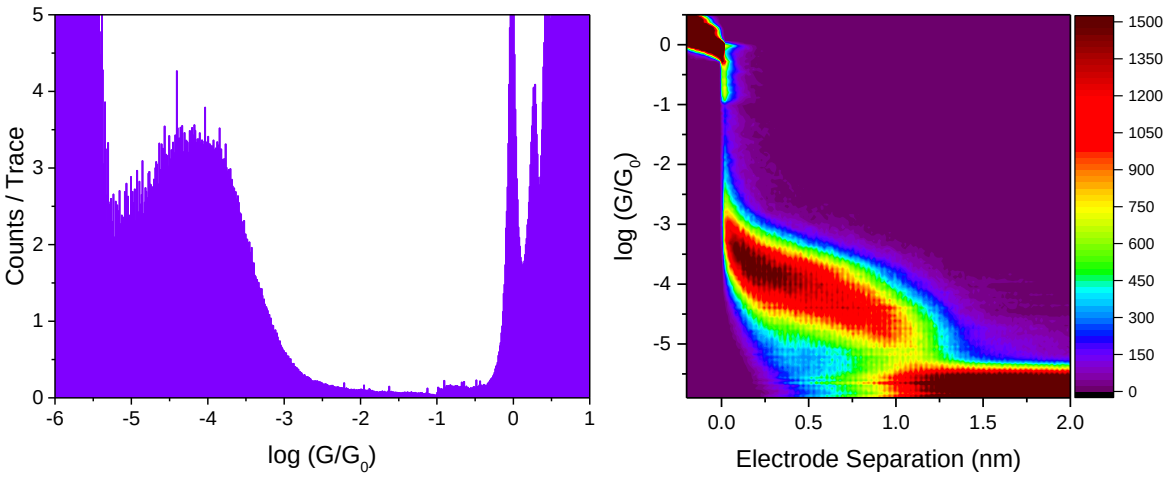

Figure A15. 1-D and 2-D conductance plots from STM-BJ measurement of TPDOT. 6390 traces. Bias voltage: 100 mV, solvent: 1,2,4-trichlorobenzene, concentration: 1 mM.

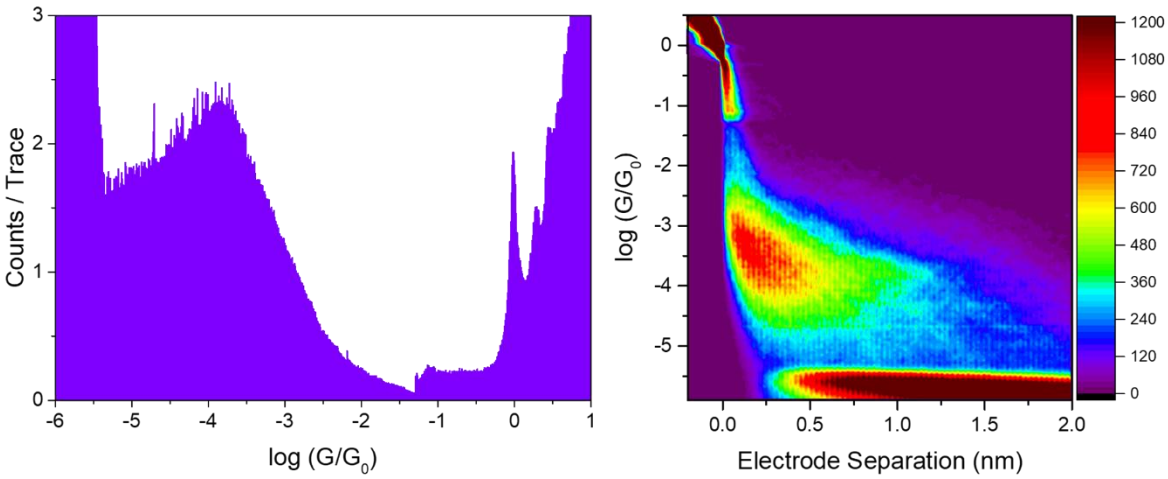

Figure A16. 1-D and 2-D conductance plots from STM-BJ measurement of TPDOT. 5356 traces. Bias voltage: 200 mV, solvent: 1,2,4-trichlorobenzene, concentration: 1 mM.

A.10 DMTB

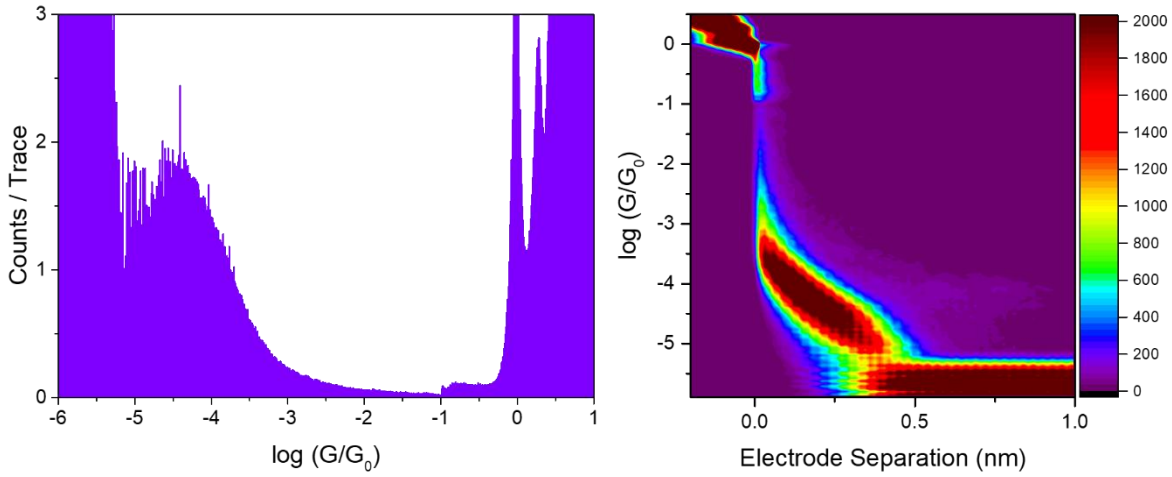

Figure A17. 1-D and 2-D conductance plots from STM-BJ measurement of DMTB. 7925 traces. Bias voltage: 100 mV, solvent: 1,2,4-trichlorobenzene, concentration: 1 mM.

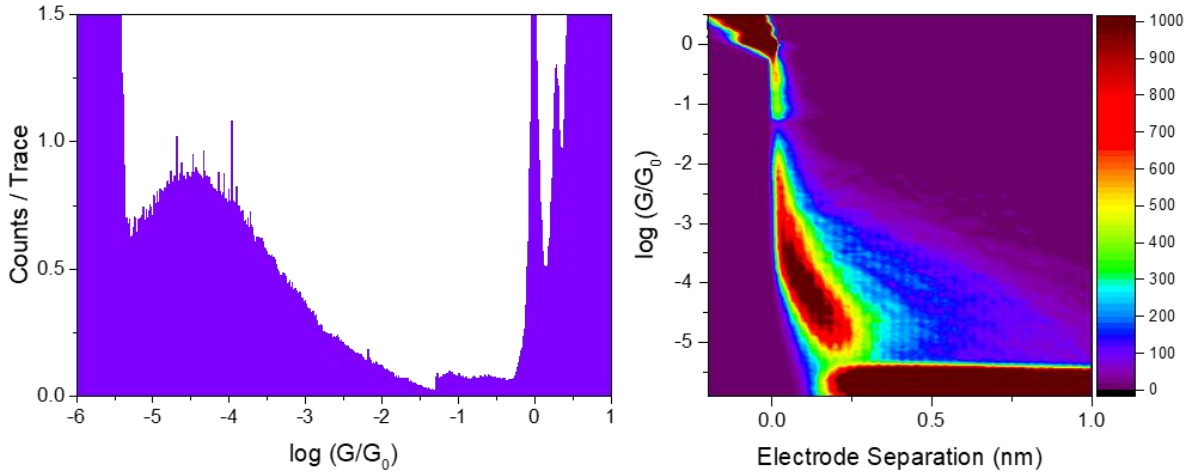

Figure A18. 1-D and 2-D conductance plots from STM-BJ measurement of DMTB. 5991 traces. Bias voltage: 200 mV, solvent: 1,2,4-trichlorobenzene, concentration: 1 mM.

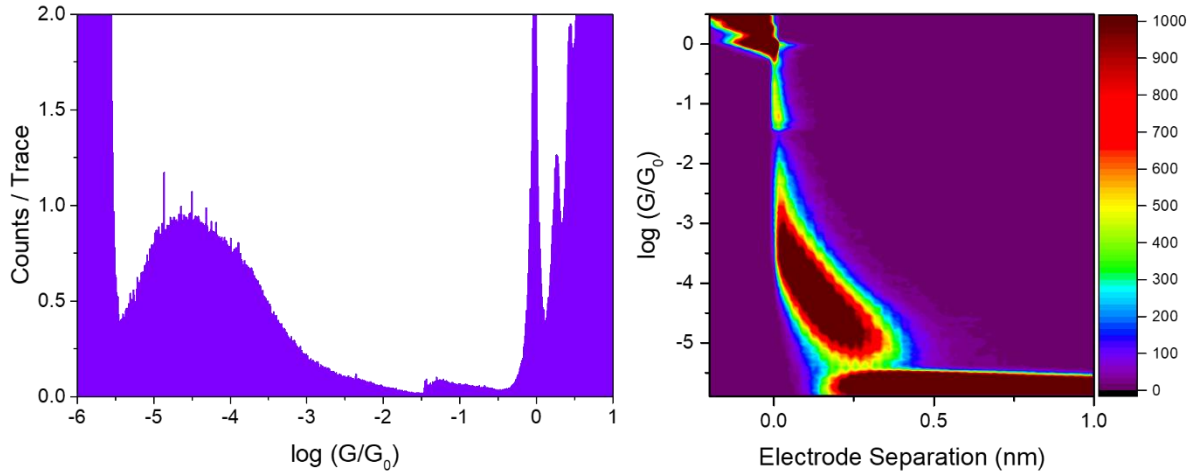

Figure A19. 1-D and 2-D conductance plots from STM-BJ measurement of DMTB. 6878 traces. Bias voltage: 300 mV, solvent: 1,2,4-trichlorobenzene, concentration: 1 mM.

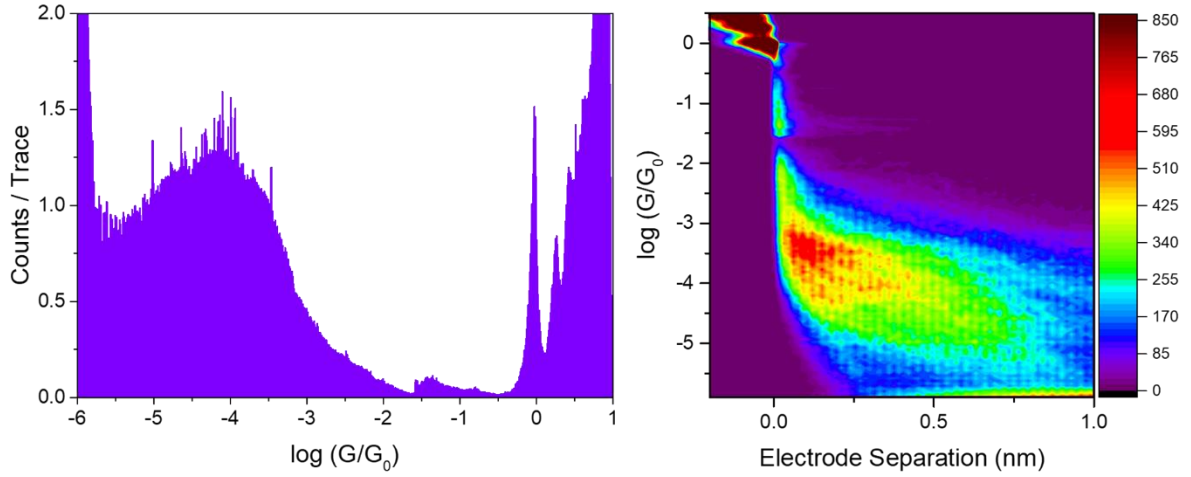

Figure A20. 1-D and 2-D conductance plots from STM-BJ measurement of DMTB. 3270 traces. Bias voltage: 400 mV, solvent: 1,2,4-trichlorobenzene, concentration: 1 mM.

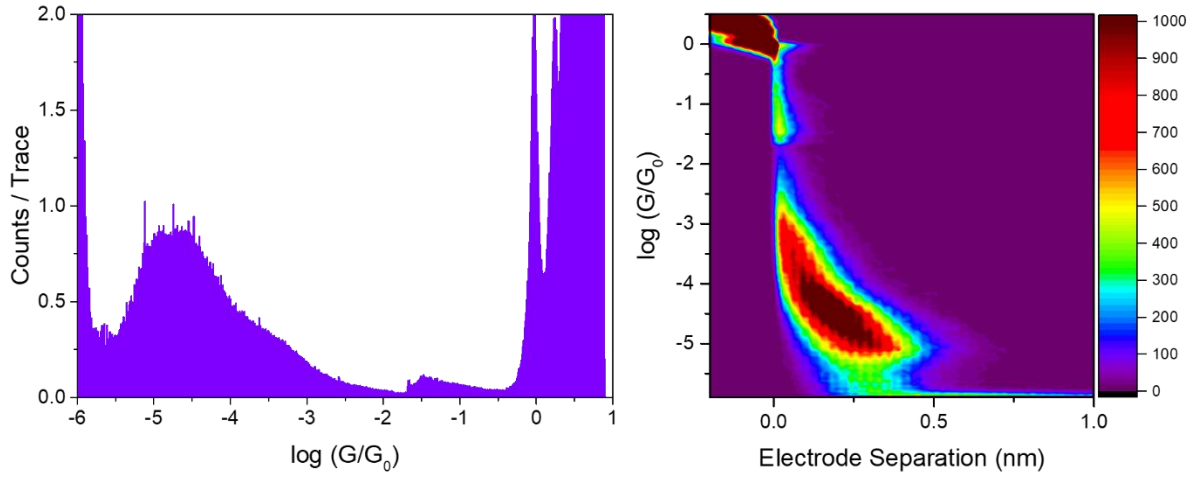

Figure A21. 1-D and 2-D conductance plots from STM-BJ measurement of DMTB. 5072 traces. Bias voltage: 500 mV, solvent: 1,2,4-trichlorobenzene, concentration: 1 mM.

A.11 DETB

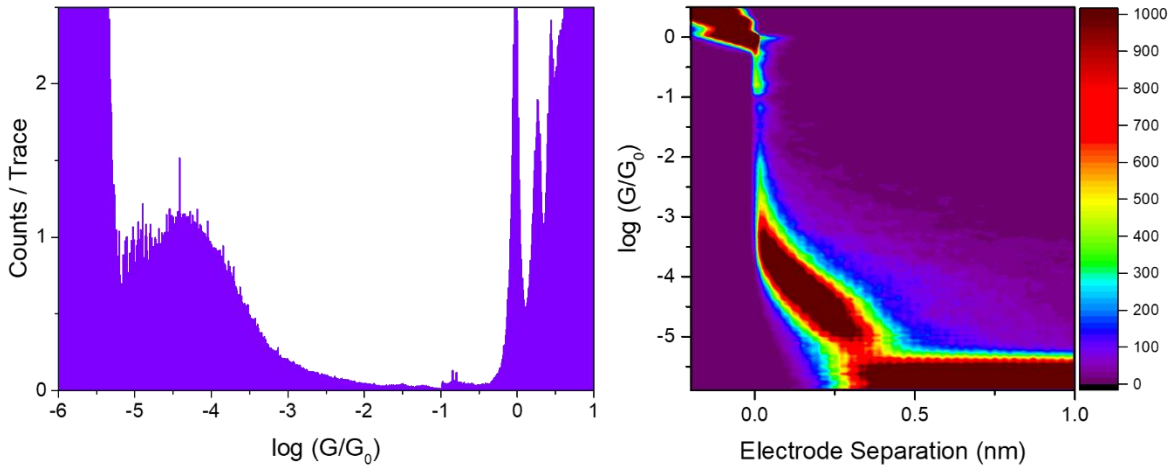

Figure A22. 1-D and 2-D conductance plots from STM-BJ measurement of DETB. 5194 traces. Bias voltage: 100 mV, solvent: 1,2,4-trichlorobenzene, concentration: 1 mM.

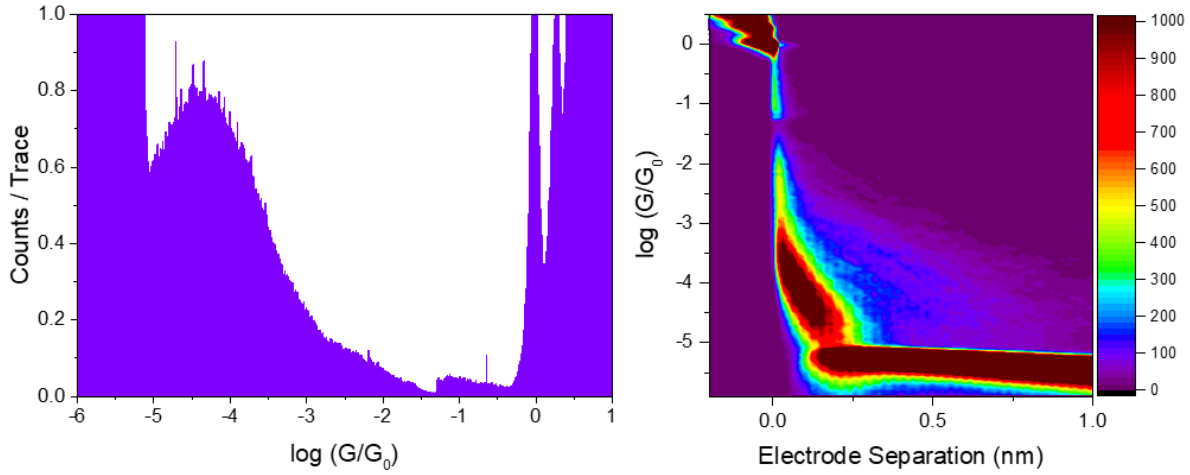

Figure A23. 1-D and 2-D conductance plots from STM-BJ measurement of DETB. 5666 traces. Bias voltage: 200 mV, solvent: 1,2,4-trichlorobenzene, concentration: 1 mM.

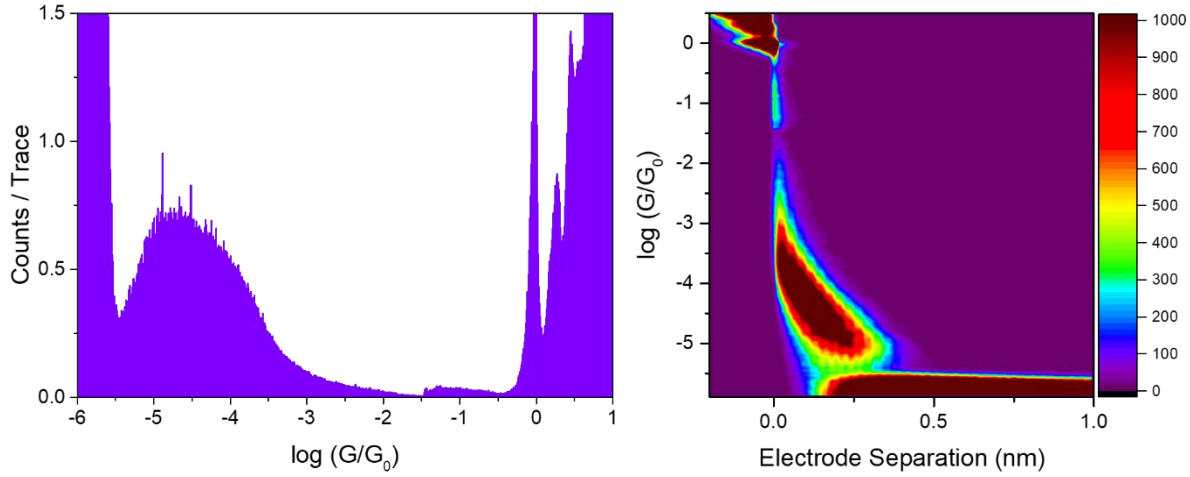

Figure A24. 1-D and 2-D conductance plots from STM-BJ measurement of DETB. 5707 traces. Bias voltage: 300 mV, solvent: 1,2,4-trichlorobenzene, concentration: 1 mM.

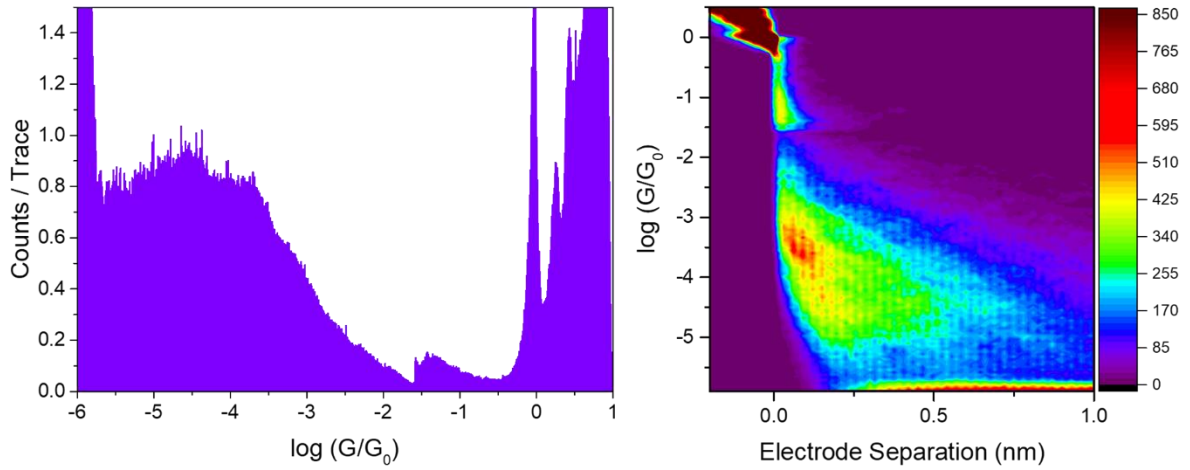

Figure A25. 1-D and 2-D conductance plots from STM-BJ measurement of DETB. 3660 traces. Bias voltage: 400 mV, solvent: 1,2,4-trichlorobenzene, concentration: 1 mM.

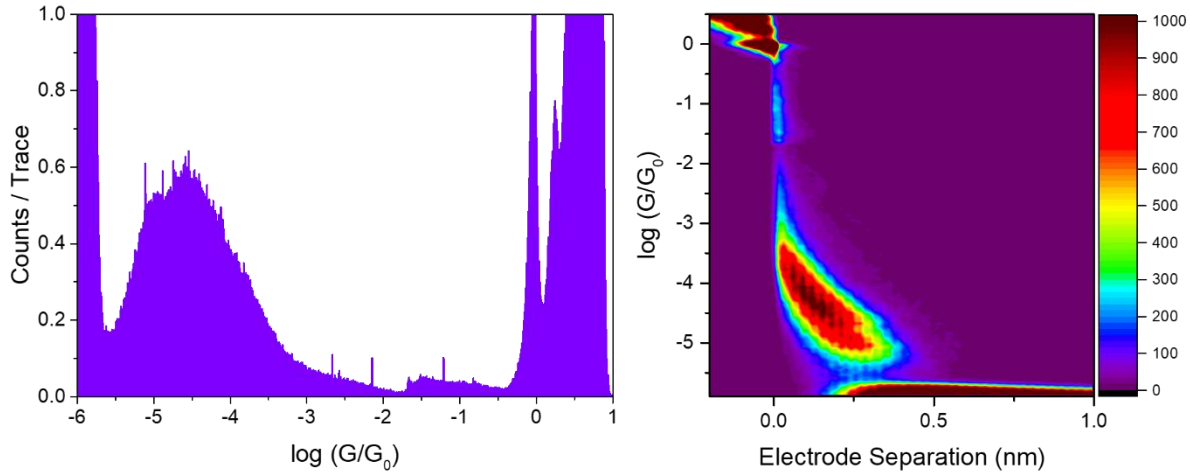

Figure A26. 1-D and 2-D conductance plots from STM-BJ measurement of DETB. 3641 traces. Bias voltage: 500 mV, solvent: 1,2,4-trichlorobenzene, concentration: 1 mM.

References

1. N. Tao, *Nature Nanotech.*, 2006, **1**, 173-181.

2. S. R. Forrest & M. E. Thompson, *Chem. Rev.*, 2007, **107**, 923-925.

3. M. A. Ratner, *Nat. Nanotechnol.*, 2013, **8**, 378-381.

4. A. Aviram & M. A. Ratner, *Chem. Phys. Lett.*, 1974, **29**, 277-283.

5. S. V. Aradhya & L. Venkataraman, *Nat. Nanotechnol.*, 2013, **8**, 399-410.

6. G. E. Moore, *Electronics*, 1965, **38**, 114-117.

7. S. E. Thompson & S. Parthasarathy, *Mater. Today*, 2006, **9**, 20-25.

8. M. A. Reed, C. Zhou, C. J. Muller, T. P. Burgin & J. M. Tour, *Science*, 1997, **278**, 252-254.

9. X. D. Cui, A. Primak, X. Zarate, J. Tomfohr, O. F. Sankey, A. L. Moore, T. A. Moore, D. Gust, G. Harris & S. M. Lindsay, *Science*, 2001, **294**, 571-574.

10. B. Xu & N. J. Tao, *Science*, 2003, **301**, 1221-1223.

11. D. Xiang, X. Wang, C. Jia, T. Lee & X. Guo, *Chem. Rev.*, 2016, **116**, 4318-4440.

12. S. Y. Quek, M. Kamenetska, M. L. Steigerwald, H. J. Choi, S. G. Louie, M. S. Hybertsen, J. B. Neaton & L. Venkataraman, *Nat. Nanotechnol.*, 2009, **4**, 230-234.

13. N. Darwish, I. Díez-Pérez, P. Da Silva, N. Tao, J. J. Gooding & M. N. Paddon-Row, *Angew. Chem. Int. Ed.*, 2012, **51**, 3203-3206.

14. B. Capozzi, J. Xia, O. Adak, E. J. Dell, Z. F. Liu, J. C. Taylor, J. B. Neaton, L. M. Campos & L. Venkataraman, *Nat. Nanotechnol.*, 2015, **10**, 522-527.

15. A. J. Bergren, L. Zeer-Wanklyn, M. Semple, N. Pekas, B. Szeto & R. L. McCreery, *J. Phys. Condens. Matter*, 2016, **8**, 094011.

16. A. Nitzan & M. A. Ratner, *Science*, 2003, **300**, 1384-1389.

17. B. Mann & H. Kuhn, *J. Appl. Phys.*, 1971, **42**, 4398-4405.

18. R. Huber, M. T. González, S. Wu, M. Langer, S. Grunder, V. Horhoiu, M. Mayor, M. R. Bryce, C. Wang, R. Jitchati, C. Schönenberger & M. Calame, *J. Am. Chem. Soc.*, 2008, **130**, 1080-1084.

19. S. H. Choi, B. Kim & C. D. Frisbie, *Science*, 2008, **320**, 1482-1486.

20. L. Venkataraman, J. E. Klare, I. W. Tam, C. Nuckolls, M. S. Hybertsen & M. L. Steigerwald, *Nano Lett.*, 2006, **6**, 458-462.

21. Q. Lu, K. Liu, H. Zhang, Z. Du, X. Wang & F. Wang, *ACS Nano*, 2009, **3**, 3861-3868.

22. X. Li, J. He, J. Hihath, B. Xu, S. M. Lindsay & N. Tao, *J. Am. Chem. Soc.*, 2006, **128**, 2135-2141.

23. J. He, F. Chen, J. Li, O. F. Sankey, Y. Terazono, C. Herrero, D. Gust, T. A. Moore, A. L. Moore & S. M. Lindsay, *J. Am. Chem. Soc.*, 2005, **127**, 1384-1385.

24. T. Hines, I. Díez-Pérez, J. Hihath, H. Liu, Z. S. Wang, J. Zhao, G. Zhou, K. Müllen & N. Tao, *J. Am. Chem. Soc.*, 2010, **132**, 11658-11664.

25. R. Yamada, H. Kumazawa, T. Noutoshi, S. Tanaka & H. Tada, *Nano Lett.*, 2008, **8**, 1237-1240.

26. L. Venkataraman, J. E. Klare, C. Nuckolls, M. S. Hybertsen & M. L. Steigerwald, *Nature*, 2006, **442**, 904-907.

27. T. A. Su, M. Neupane, M. L. Steigerwald, L. Venkataraman & C. Nuckolls, *Nat. Rev. Mater.*, 2016, **1**, 1-15.

28. B. Kim, J. M. Beebe, Y. Jun, X. Y. Zhu & C. D. Frisbie, *J. Am. Chem. Soc.*, 2006, **128**, 4970-4971.

29. Z. L. Peng, Z. B. Chen, X. Y. Zhou, Y. Y. Sun, J. H. Liang, Z. J. Niu, X. S. Zhou & B. W. Mao, *J. Phys. Chem. C*, 2012, **116**, 21699-21705.

30. Y. H. Wang, X. Y Zhou, Y. Y. Sun, D. Han, J. F. Zheng, Z. J. Niu & X. S. Zhou, *Electrochim. Acta*, 2014, **123**, 205-210.

31. J. M. Beebe, V. B. Engelkes, L. L. Miller & C. D. Frisbie, *J. Am. Chem. Soc.*, 2002, **124**, 11268-11269.

32. C. H. Ko, M. J. Huang, M. D. Fu & C. H. Chen, *J. Am. Chem. Soc.*, 2010, **132**, 756-754.

33. T. Kim, H. Vázquez, M. S. Hybertsen & L. Venkataraman, *Nano Lett.*, 2013, **13**, 3358-3364.

34. O. Adak, R. Korytár, A. Y. Joe, F. Evers & L. Venkataraman, *Nano Lett.*, 2015, **15**, 3716-3722.

35. B. Capozzi, J. Z. Low, J. Xia, Z. F. Liu, J. B. Neaton, L. M. Campos & L. Venkataraman, *Nano Lett.*, 2016, **16**, 3949-3954.

36. M. Dell'Angela, G. Kladnik, A. Cossaro, A. Verdini, M. Kamenetska, I. Tamblyn, S. Y. Quek, J. B. Neaton, D. Cvetko, A. Morgante & L. Venkataraman, *Nano Lett.*, 2010, **10**, 2470-2474.

37. A. Tan, J. Balachandran, S. Sadat, V. Gavini, B. D. Dunietz, S. Y. Jang & P. Reddy, *J. Am. Chem. Soc.*, 2011, **133**, 8838-8841.

38. F. Chen, X. Li, J. Hihath, Z. Huang & N. Tao, *J. Am. Chem. Soc.*, 2006, **128**, 15874-15881.

39. M Kamenetska, S. Y. Quek, A. C. Whalley, M. L. Steigerwald, H. J. Choi, S. G. Louie, C. Nuckolls, M. S. Hybertsen, J. B. Neaton & L. Venkataraman, *J. Am. Chem. Soc.*, 2010, **132**, 6817-6821.

40. Y. S. Park, A. C. Whalley, M. Kamenetska, M. L. Steigerwald, M. S. Hybertsen, C. Nuckolls & L. Venkataraman, *J. Am. Chem. Soc.*, 2007, **129**, 15768-15769.

41. A. Mishchenko, L. A. Zotti, D. Vonlanthen, M. Bürkle, F. Pauly, J. C. Cuevas, M. Mayor & T. Wandlowski, *J. Am. Chem. Soc.*, 2011, **133**, 184-187.

42. S. Yasuda, S. Yoshida, J. Sasaki, Y. Okutsu, T. Nakamura, A. Taninaka, O. Takeuchi & H. Shigekawa, *J. Am. Chem. Soc.*, 2006, **128**, 7746-7747.

43. C. A. Martin, D. Ding, J. K. Sørensen, T. Bjørnholm, J. M. Van Ruitenbeek & H. S. Van Der Zant, *J. Am. Chem. Soc.*, 2008, **130**, 13198-13199.

44. L. Venkataraman, Y. S. Park, A. C. Whalley, C. Nuckolls, M. S. Hybertsen & M. L. Steigerwald, *Nano Lett.*, 2007, **7**, 502-506.

45. B. Xu, X. Xiao & N. J. Tao, *J. Am. Chem. Soc.*, 2003, **125**, 16164-16165.

46. C. R. Arroyo, E. Leary, A. Castellanos-Gómez, G. Rubio-Bollinger, M. T. Gonzalez & N. Agraït, *J. Am. Chem. Soc.*, 2011, **133**, 14313-14319.

47. E. J. Dell, B. Capozzi, J. Xia, L. Venkataraman & L. M. Campos, *Nat. Chem.*, 2015, **7**, 209-214.

48. J. R. Quinn, F. W. Foss, L. Venkataraman & R. Breslow, *J. Am. Chem. Soc.*, 2007, **129**, 12376-12377.

49. V. Kaliginedi, P. Moreno-García, H. Valkenier, W. Hong, V. M. Garcia-Suarez, P. Buiter, J. L. H. Otten, J. C. Hummelen, C. J. Lambert & T. Wandlowski, *J. Am. Chem. Soc.*, 2012, **134**, 5262-5275.

50. W. Chen, H. Li, J. R. Widawsky, C. Appayee, L. Venkataraman & R. Breslow, *J. Am. Chem. Soc.*, 2014, **136**, 918-920.

51. A. Danilov, S. Kubatkin, S. Kafanov, P. Hedegård, N. Stuhr-Hansen, K. Moth-Poulsen & T. Bjørnholm, *Nano Lett.*, 2008, **8**, 1-5.

52. E. Leary, S. J. Higgins, H. van Zalinge, W. Haiss & R. J. Nichols, *Chem. Commun.*, 2007, **38**, 3939-3941.

53. T. Morita & S. Lindsay, *J. Am. Chem. Soc.*, 2007, **129**, 7262-7263.

54. G. Binnig, H. Rohrer, C. Gerber & E. Weibel, *Phys. Rev. Lett.*, 1982, **49**, 57.

55. W. Haiss, S. Martín, E. Leary, H. V. Zalinge, S. J. Higgins, L. Bouffier & R. J. Nichols, *J. Phys. Chem. C*, 2009, **113**, 5823-5833.

56. X. S. Zhou, Y. M. Wei, L. Liu, Z. B. Chen, J. Tang & B. W. Mao, *J. Am. Chem. Soc.*, 2008, **130**, 13228-13230.

57. W. Haiss, H. van Zalinge, S. J. Higgins, D. Bethell, H. Höbenreich, D. J. Schiffrin & R. J. Nichols, *J. Am. Chem. Soc.*, 2003, **125**, 15294-15295.

58. W. Haiss, R. J. Nichols, H. van Zalinge, S. J. Higgins, D. Bethell & D. J. Schiffrin, *Phys. Chem. Chem. Phys.*, 2004, **6**, 4330-4337.

59. M. H. Garner, H. Li, Y. Chen, T. A. Su, Z. Shangguan, D. W Paley, T. Liu, F. Ng, H. Li, S. Xiao, C. Nuckolls, L. Venkataraman & G. C. Solomon, *Nature*, 2018, **558**, 415-419.

60. R. Baer & D. Neuhaser, *J. Am. Chem. Soc.*, 2002, **124**, 4200-4201.

61. S. V. Aradhya, J. S. Meisner, M. Krikorian, S. Ahn, R. Parameswaran, M. L. Steigerwald, C. Nuckolls & L. Venkataraman, *Nano Lett.*, 2012, **12**, 1643-1647.

62. C. R. Arroyo, S. Tarkuc, R. Frisenda, J. S. Seldenthuis, C. H. Woerde, R. Eelkema, F. C. Grozema & H. S. Van Der Zant, *Angew. Chem. Int. Ed.*, 2013, **52**, 3152-3155.

63. T. Markussen, R. Stadler & K. S. Thygesen, *Nano Lett.*, 2010, **10**, 4260-4265.

64. H. Vazquez, R. Skouta, S. Schneebeli, M. Kamenetska, R. Breslow, L. Venkataraman & M. S. Hybertsen, *Nat. Nanotechnol.*, 2012, **7**, 663-667.

65. V. Rabache, J. Chaste, P. Petit, M. L. Dell Rocca, P. Martin, J. C. Lacroix, R. L. McCreery & P. Lafarge, *J. Am. Chem. Soc*., 2013, **135**, 10218-10221.

66. C. J. Lambert, *Chem. Soc. Rev.*, 2015, **44**, 875-888.

67. X. Liu, S. Sangtarash, D. Reber, D. Zhang, H. Sadeghi, J. Shi, Z. Y. Xiao, W. Hong, C. J. Lambert & S. X. Liu, *Angew. Chem. Int. Ed.*, 2017, **219**, 179-182.

68. C. R. Arroyo, R. Frisenda, K. Moth-Poulsen, J. S. Seldenthuis, T. Bjørnholm & H.S. Van Der Zant, *Nanoscale Res. Lett.*, 2013, **8**, 1-6.

69. D. Z. Manrique, C. Huang, M. Baghernejad, X. Zhao, O. Al-Owaedi, H. Sadeghi, V. Kaliginedi, W. Hong, M. Gulcur, T. Wandlowski, M. R. Bryce & C. J. Lambert, *Nat. Commun.*, 2015, **6**, 1-8.

70. K. Yoshizawa, *Acc. Chem. Res.*, 2012, **45**, 1612-1621.

71. Y. Yang, M. Gantenbein, A. Alqorashi, J. Wei, S. Sangtarash, D. Hu, H. Sadeghi, R. Zhang, J. Pi, L. Chen, X. Huang, R. Li, J. Liu, J. Shi, W. Hong, C. J. Lambert & M. R. Bryce, *J. Phys. Chem. C*, 2018, **122**, 14965-14970.

72. Y. Li, M. Buerkle, G. Li, A. Rostamian, H. Wang, Z. Wang, D. R. Bowler, T. Miyazaki, L. Xiang, Y. Asai, G. Zhou & N Tao, *Nat. Mater.*, 2019, **18**, 357-363.

73. J. Bai, A. Daaoub, S. Sangtarash, X. Li, Y. Tang, Q. Zou, H. Sadeghi, S. Liu, X. Huang, Z. Tan, J. Liu, Y. Yang, J. Shi, G. Mészáros, W. Chen, C. J. Lambert & W. Hong, *Nat. Mater.*, 2019, **18**, 364-369.

74. J. E. Greenwald, J. Cameron, N. J. Findlay, T. Fu, S. Gunasekaran, P. J. Skabara & L. Venkataraman, *Nat. Nanotechnol.*, 2021, **16**, 313-317.

75. G. C. Solomon, D. Q. Andrews, R. H. Goldsmith, T. Hansen, M. R. Wasielewski, R. P. Van Duyne & M. A. Ratner, *J. Am. Chem. Soc.*, 2008, **130**, 17301-17308.

76. C. M. Guédon, H. Valkenier, T. Markussen, K. S. Thygesen, J. C. Hummelen & S. J. Van Der Molen, *Nat. Nanotechnol.*, 2012, **7**, 305-309.

77. M. Baghernejad, X. Zhao, K. Baruël Ørnsø, M. Füeg, P. Moreno-García, A. V. Rudnev, V. Kaliginedi, S. Vesztergom, C. Huang, W. Hong, P.Broekmann, T. Wandlowski, K. S. Thygesen & M. R. Bryce, *J. Am. Chem. Soc.*, 2014, **136**, 17922-17925.

78. A. Alanazy, E. Leary, T. Kobatake, S. Sangtarash, M. T. González, H. W. Jiang, G. Rubio Bollinger, N. Agräit, H. Sadeghi, I. Grace, S. J. Higgins, H. L. Anderson, R. J. Nichols & C. J. Lambert, *Nanoscale*, 2019, **11**, 13720-13724.

79. C. Tang, L. Huang, S. Sangtarash, M. Noori, H. Sadeghi, H. Xia & W. Hong, *J. Am. Chem. Soc.*, 2021, **143**, 9385-9392.

80. G. Yang, S. Sangtarash, Z. Liu, X. Li, H. Sadeghi, Z. Tan, R. Li, J. Zheng, X. Dong, J. Liu, Y. Yang, J. Shi, Z. Xiao, G. Zhang, C. J. Lambert, W. Hong & D. Zhang, *Chem. Sci.*, 2017, **8,** 7505-7509.

81. Y. P. Zhang, L. C. Chen, Z. Q. Zhang, J. J. Cao, C. Tang, J. Liu, L. L Duan, Y. Huo, X. Shao, W. Hong & H. L. Zhang, *J. Am. Chem. Soc.*, 2018, **140**, 6531-6535.

82. W. Hong, D. Z. Manrique, P. Moreno-García, M. Gulcur, A. Mishchenko, C. J. Lambert, M. R. Bryce & T. Wandlowski, *J. Am. Chem. Soc.*, 2012, **134**, 2292-2304.

83. M. Frei, S V. Aradhya, M. Koentopp, M. S. Hybertsen & L. Venkataraman, *Nano Lett.*, 2011, **11**, 1518-1523.

84. Z. Li, M. Smeu, M. A. Ratner & E. Borguet, *J. Phys. Chem. C*, 2013, **117**, 14890-14898.

85. A. Bagrets, A. Arnold & F. Evers, *J. Am. Chem. Soc.*, 2008, **130**, 9013-9018.

86. J. R. Widawsky, P. Darancet, J. B. Neaton & L. Venkataraman, *Nano Lett.*, 2012, **12**, 354-358.

87. S. Y. Quek, L. Venkataraman, H. J. Choi, S. G. Louie, M. S. Hybertsen & J. B. Neaton, *Nano Lett.*, 2007, **7**, 3477-3482.

88. S. V. Aradhya, M. Frei, M. S. Hybertsen & L. Venkataraman, *Nat. Mater.*, 2012, **11**, 872-876.

89. E. S. Tam, J. J. Parks, W. W. Shum, Y. W. Zhong, M. E. B. Santiago-Berríos, X. Zheng, W. Yang, G. K. L. Chan, H. D. Abruna & D. C. Ralph, *ACS Nano*, 2011, **5**, 5115-5123.

90. C. Wang, A. S. Batsanov, M. R. Bryce, S. Martin, R. J. Nichols, S. J. Higgins, V. M. Garcia-Suarez & C. J. Lambert, *J. Am. Chem. Soc.*, 2009, **131**, 15647-15654.

91. K. A. Velizhanin, T. A. Zeidan, I. V. Alabugin & S. Smirnov, *J. Phys. Chem. B*, 2010, **114**, 14189-14193.

92. S. Naghibi, A. Ismael, A. Vezzoli, M. K. Al-Khaykanee, X. Zheng, I. M. Grace, D. Bethell, S. J. Higgins, C. J. Lambert & R. J. Nichols, *J. Phys. Chem. Lett.*, 2019, **10**, 6419-6424.

93. M. Gantenbein, L. Wang, A. A. Al-Jobory, A. K. Ismael, C. J. Lambert, W. Hong & M. R. Bryce, *Sci. Rep.*, 2017, **7**, 1-9.

94. J. Louie & J. F. Hartwig, *Tetrahedron Lett.*, 1995, **36**, 3609-3612.

95. R. S. Klausen, J. R. Widawsky, T. A. Su, H. Li, Q. Chen, M. L. Steigerwald, L. Venkataraman & C. Nuckolls, *Chem. Sci.*, 2014, **5**, 1561-1564.

96. C. Sagan, Y. Jang, F. Caban, J. Snaider, R. Amell, S. Wei & G. M. Florio, *J. Phys. Chem. C*, 2017, **121**, 24945-24953.

97. M. Kamenetska, M. Koentopp, A. C. Whalley, Y. S. Park, M. L. Steigerwald, C. Nuckolls, M. S. Hybertsen & L. Venkataraman, *Phys. Rev. Lett.*, 2009, **102**, 126803.

98. D. Q. Andrews, G. C. Solomon, R. P. Van Duyne & M. A. Ratner, *J. Am. Chem. Soc.*, 2008, **130**, 17309-17319.

99. C. Wang, M. R. Bryce, J. Gigon, G. J. Aswell, I. Grace & C. J. Lambert, *J. Org. Chem.*, 2008, **73**, 4810-4818.

100. B. Huang, X. Liu, Y. Yuan, Z. W. Hong, J. F. Zheng, L. Q. Pei, Y. Shao, J. F. Li, X. S. Zhou, J. Z. Chen, S. Jin & B. W. Mao, *J. Am. Chem. Soc.*, 2018, **140**, 17685-17690.

101. N. F. Phelan & M. Orchin, *J. Chem. Educ.*, 1968, **45**, 633.

102. G. C. Solomon, D. Q. Andrews, P. R. Van Duyne & M. A. Ratner, *J. Am. Chem. Soc.*, 2008, **130**, 7788-7789.

103. D. Vonlanthen, A. Mishchenko, M. Elbing, M. Neuburger, T. Wandlowski & M. Mayor, *Angew. Chem. Int. Ed.*, 2009, **48**, 8886-8890.

104. I. L. Herrer, A. K. Ismael, D. C. Milan, A. Vezzoli, S. Martín, A. González-Orive, I. Grace, C. J. Lambert, J. L. Serrano, R. J. Nichols & C. Pea, *J. Phys. Chem. Lett.*, 2018, **9**, 5364-5372.

105. L. Herrer, A. Ismael, S. Martín, D. C. Milan, J. L. Serrano, R. J. Nichols, C. J. Lambert & P. Cea, *Nanoscale*, 2019, **11**, 15871-15880.

106. S. Li, H. Yu, K. Schwieter, K. Chen, B. Li, Y. Liu, J. S. Moore & C. M. Schroeder, *J. Am. Chem. Soc*., 2019, **14**, 16079-16084.

107. T. Fu, S. Smith, M. Camarasa-Gómez, X. Yu, J. Xue, C. Nuckolls, F. Evers, L. Venkataraman & S. Wei, *Chem. Sci.*, 2019, **10**, 9998-10002.